Diagnostic potential of autofluorescence: an explorative study with human urine and stem cells.

Sandeep Menon Perinchery

MPhil (International School of Photonics, CUSAT, Kochi, India)

MQ Photonics Research Centre
Department of Physics & Astronomy, Faculty of Science
Macquarie University
North Ryde, NSW 2109, AUSTRALIA

Email: sandeepmenonp@gmail.com

March 31, 2011

This thesis is presented for the degree of Doctor of Philosophy

BLANK PAGE

Contents

BLANK PAGE

List of Figures

List of Tables

BLANK PAGE

Publications and Presentations

1. **S. M. Perinchery**, U. Kuzhiumparambil, S. Vemulpad, and E. M. Goldys, "The potential of autofluorescence spectroscopy to detect human urinary tract infection," Talanta 82, 912-917 (2010)

2. **S. M. Perinchery**, U. Kuzhiumparambil, S. Vemulpad, and E. M. Goldys, "The influence of indoxyl sulfate and ammonium on the autofluorescence of human urine," Talanta 80, 1269-1276 (2010).

3. A. G. Anwer, **P. M. Sandeep**, E. M. Goldys, and S. Vemulpad, "Distinctive autofluorescence of urine samples from individuals with bacteriuria compared with normals," Clinica Chimica Acta 401, 73-75 (2009).

4. **Sandeep Menon Perinchery**, Unnikrishnan Kuzhiumparambil, Subramanyam Vemulpad, Ewa M Goldys, A reagentfree method for diagnosing urinary tract infection: the potential of urine autofluorescence, SPIE Photonics West, (2011).

5. Martin E.Gosnel, **Sandeep M. Perinchery**, David Inglis, Ayad G.Anwer, Pascal vallatton, Ewa M Goldys, " Characterisation of stem cells and their differentiation using a new multi spectral imaging tools," The 11th Hunter meeting, NSW, Australia (2010).

6. **Sandeep Menon P**, A reagentfree method for diagnosing urinary tract infection: the potential of urine autofluorescence, Syntrophy, vol 11, issue 6, (2010).

7. **Sandeep Menon Perinchery**, Unnikrishnan Kuzhiumparambil, Subramanyam Vemulpad, Ewa M Goldys, Insights into autofluorescence of human urine, LILS conference, November 24-27, (2009).

8. **Perinchery M Sandeep**, K. P. Unnikrishnan, Subramanyam Vemulpad, Ewa M. Goldys, Factors influencing the UV autofluorescence of human urine, ICOP-2009, International conference on optics and photonics, India, (2009).

9. **Perinchery M Sandeep**, Subramanyam Vemulpad, Ewa M. Goldys, Diagnosis of Bacteria in Human urine, ICO-21 2008 Congress, International conference, Sydney,(2008).

Awards

1. (2010) Finalist for post graduate innovation award, Macquarie University, Sydney, Australia. http://www.mq.edu.au/researchawards/highly-commended-2010.htm.

2. (2010) Finalist for Becton Dickinson (BD) student award

BLANK PAGE

Intuition will tell the thinking mind where to look next.

Jonas Salk

Abstract

Most of the biological samples contain molecules, some of which fluoresce when excited by UV/Vis radiation of suitable wavelength (fluorophores). The fluorescence arising from these endogenous fluorophores is an intrinsic property of the sample and is called autofluorescence. In principle, autofluorescence may serve as a useful diagnostic indicator.

In the past, autofluorescence has been used to diagnose various diseases including cancer. In this study, I have investigated the autofluorescence of human urine and stem cells, two medically relevant biological materials.

With an estimated 150 million instances occurring every year globally and accounting for more than 6 billion dollars in direct health care expenditure, urinary tract infection (UTI) is one of the most common infections in the human population. UTIs can differ in severity, and are treatable if detected early. Left untreated, they can cause lasting damage, chronic kidney disease, and even death from kidney failure.

In recent years, several novel approaches have been attempted to diagnose the urinary tract infection. These include immuno-chromatography strips, real time PCR and biosensors. However, they have some limitations. For example, most of the techniques are reagent based, need sample preparation prior to diagnosis, have less sample throughput, are sensitive only to specific bacteria and are expensive.

Human urine contains a large number of fluorophores (mostly tryptophan and its metabolites) which can fluoresce under UV excitation. Due to their presence, normal urine has strong fluorescence. Although pathological and physiological changes

are known to alter the autofluorescence of urine, there is a shortage of studies investigating autofluorescence as a diagnostic tool for UTIs.

In this study, the applicability of a simple spectrofluorometric technique for rapid diagnosis of UTI, a common health condition capable of becoming a serious health problem was investigated. Excitation in the shorter UV region (250-350 nm) showed good discrimination between the normal urine and UTI samples. Specifically, excitation at 290 nm showed good discrimination between these 2 groups of samples. Principal Component Analysis (PCA) of the data revealed statistically significant differences between the fluorescence spectra for samples with UTIs as compared to the samples from normals. The synchronous scans with an offset of $\Delta\lambda$= 90 nm were also able to differentiate between normal urines and UTI samples. Three major fluorophores (tryptophan, indoxyl sulfate and 5-hydroxyindole-3-acetate) whose content in urine is strongly linked with various health conditions were further investigated. Their fluorescence was studied both individually and in combinations. It was identified that higher concentration of indoxyl sulfate produced inner filter effect and concentration quenching. Quenching of fluorophores by ammonium was also demonstrated.

These findings indicate the potential of the fluorescence spectrum of urine to be developed as a simple and rapid diagnostic tool for the urinary tract infection.

The potential of stem cells in regenerative medicine has led to an increased interest in investigating their properties. An understanding of cell differentiation process could lead to potential stem cell therapies. The reason behind using autofluorescence is that currently, most of the techniques for characterizing stem cells are reagent based and invasive. Autofluorescence can give rich insights into internal cell processes such as metabolism. The idea behind this study is that, there could be variations in the fluorophores of stem cells, for example, NADH, flavin, and col-

lagen during differentiation. These variations in fluorophores in stem cell during differentiation, in principle, could be reflected in their autofluorescence spectrum.

It was demonstrated in this preliminary study that, using a single 400 nm excitation source and PCA analysis, stem cells and osteogenic differentiated cells (osteo cells) were distinguishable within 60 hrs. In stem cell research, it is important to analyze how fast a cell differentiates. The results of this study seem promising because currently polymerase chain reaction (PCR) is the only sensitive and fast means to check for cell differentiation. However, PCR technique is known to be an 'invasive' method. On the other hand, recently some optical techniques which are noninvasive, such as lifetime measurements, have been used to study osteogenic differentiation. However, they showed a difference between undifferentiated and differentiated cells only after one week, clearly showing that the technique used in this study is more efficient and has good potential to characterize stem cells.

PCA was utilized to visualize the overall trajectory in the spectrum of stem cells undergoing differentiation in osteogenic medium. It was evident that with time, the spectrum in the 3D PCA space was spreading away from the initial point, possibly reflecting the changes happening during differentiation. Clear difference in the autofluorescence was also observed between stem cells within dense regions and sparse regions.

These preliminary results show that analyzing autofluorescence spectrum could provide a rich insight to cell metabolism and characterization.

BLANK PAGE

Statement of Originality

I, Sandeep Menon Perinchery, declare that this thesis, submitted in fulfilment of the requirements for the award of Doctor of Philosophy, in the Department of Physics & Astronomy, Macquarie University, is wholly my own work unless otherwise referenced or acknowledged. This work has not been submitted, either in whole, or in parts, for a higher degree to any other university or institution.

Sandeep Menon Perinchery

BLANK PAGE

Never express yourself more clearly than you are able to think.

Niels Bohr

Acknowledgements

Firstly, I would like to express my deep and sincere gratitude to my supervisor, Prof. Ewa M. Goldys, for her continuous support and encouragement throughout my PhD degree. Her wide knowledge and her logical way of thinking have been of great value for me. Her understanding, encouraging and personal guidance have provided a good basis for the present thesis. I have learned so much from her in so many ways, especially how to be a free thinker and an independent scientist. Her mentorship during the course of this work has motivated and inspired me to grow as an independent research scientist.

I would also like to acknowledge my Associate Supervisor A/Prof. Subramanyam Vemulpad. His assistance has been beyond my expectations, and I truly appreciate it. I am grateful to him for his detailed and constructive comments especially in my thesis writing , and for his important support throughout this work.

Special thanks to Dr. Ayad Anwer for helping me to learn stem cells culturing. I wish to thank Martin Gosnel for sharing ideas about hyperspectral imaging techniques.

I am indebted also to my many student colleagues for providing a stimulating and fun environment in which to learn and grow. Much respect to my officemates, and hopefully still friends, Ben Johnston and Martin Ams.

I also wish to extend special thanks to all the wonderful members in Biofocus group. The list includes, Associate Professor Andrei Zvyagin, Dr. David Inglis, Ms. Krystyna Tomsia, Dr. Jin Dayon, Mustaq Sobhan. I am also indebted to my officemates for providing a friendly environment to work.

Words can not express my gratitude to my parents, K Sukumara Menon and Komalam Sukumaran. Their love and unwavering support has always been the bedrock upon which every worthwhile achievement in my life has been built. Many thanks to the rest of my family, my elder sister Subha Menon, my brother Ajay. Thank you all for your support and encouragement during my studies.

I cannot end without also thanking my wife Anjana Sethumadhavan, on whose constant encouragement and love I have relied throughout my time as a PhD student. Her unflinching drive and conviction will always inspire me.

Dedicated to my parents and to my wife Anjana

BLANK PAGE

1 Introduction

1.1 Introduction

Fluorophores are molecules or chemical groups which can fluoresce when excited with light of a particular wavelength. Most of the biological samples show fluorescence due to the presence of endogenous fluorophores in them, this is known as autofluorescence. Autofluorescence is related to the relative amount, spatial distribution and micro-environment of the endogenous fluorophores. The occurrence of pathological conditions affecting histological and histochemical features of biological media such as tissues, cells, blood *etc*, can result in alteration of the autofluorescence emission properties [1]. Thus, autofluorescence has been utilized for diagnosing various diseases in the past.

For example, tissue autofluorescence is currently considered as a possible parameter for *in situ* cancer diagnosis in different tissues and organs, such as colon, bronchi, cervix and esophagus [1]. Figure 1.3 shows the typical application of autofluorescence endoscopy in diagnosing macroinvasive carcinoma [2]. In 2010, a group in Charles University in Czech Republic, has shown the applicability of using a portable preoperative optical autofluorescence diagnostic device for biopsy-verification [3]. These

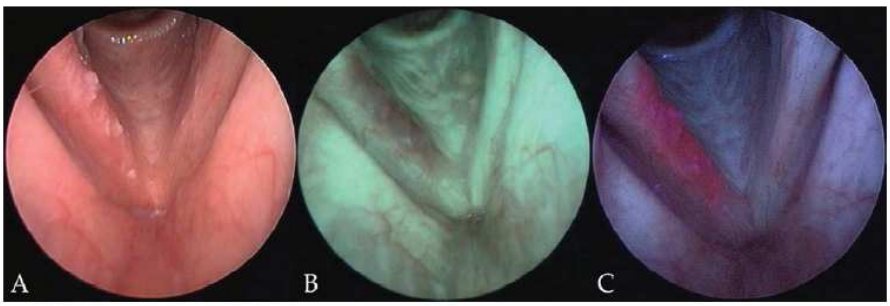

Figure 1.1: Microinvasive carcinoma. White light endoscopy (A) demonstrates an irregular leukoplakia of the right vocal fold. Autofluorescence endoscopy (B) shows a marked loss of autofluorescence, whereas induced fluorescence endoscopy (C) displays a strong protoporphyrin IX fluorescence [2].

studies clearly show the importance and significance of using autofluorescence as a diagnostic tool. However, autofluorescence has been under utilized in studying human urine or stem cells.

1.2 Motivation and Objective

Part A: Studies on autofluorescence of human urine

In the year 2000, National Institute of Health had done a comprehensive study for various urological diseases. Figure 1.2 shows the Medicare cost related to urological diseases. It is evident that compared to all other urological diseases, UTI was the highest one, around 1.4 billion dollars for direct health care [4, 5]. In addition, National Kidney and Urological Diseases Information Clearinghouse (NKUDIC), a service of NIH, has reported that the estimated number of hospital admissions among adults aged 20 or older with UTI or cystitis listed as a diagnosis in 2006 was around 479,000 [6]. The estimated number of doctor visits and outpatient hospital visits by patients aged 20 or older with UTI as the primary diagnosis in 2000 was 8.27 million visit [6].

UTIs can differ in severity and are treatable if detected early. Left untreated,

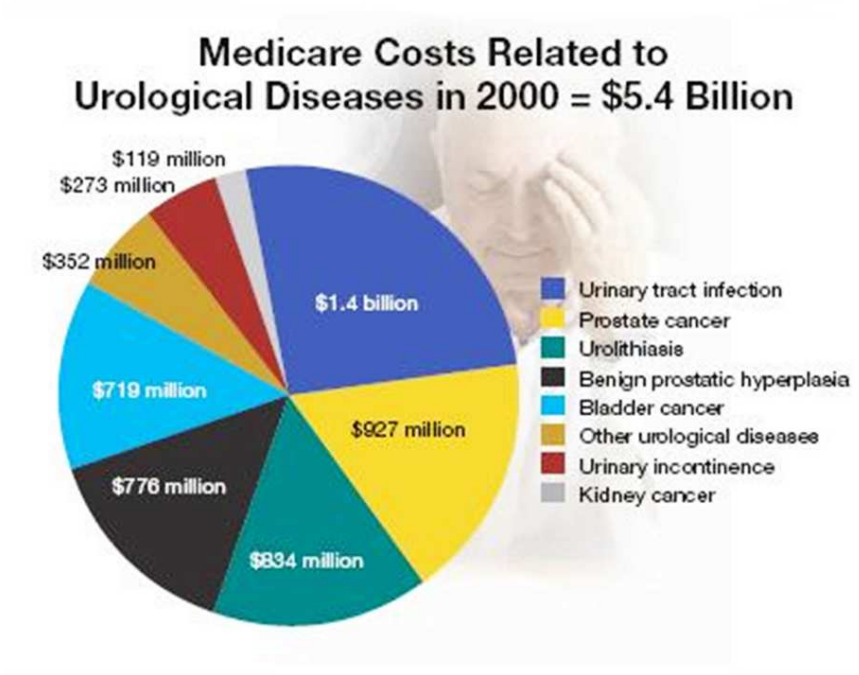

Figure 1.2: Medicare cost for urinary tract infection as compared to other urological diseases. Source: [4, 5]

they can cause lasting damage, chronic kidney disease, and even death from kidney failure. These data clearly show the overall picture of the significance of UTI. This was the primary motivation to study human urine autofluorescence.

Many microorganisms are known to cause UTI, the most common bacterial pathogen associated with UTI being *Escherichia coli*. Several tools have been developed for diagnosing UTIs. In a clinical laboratory setting, tests for UTIs include urine sediment analysis and quantitative bacterial culture. Such culture typically takes about 24 h and consequently the diagnosis is delayed. At present 'dipstick' and 'immuno-chromatography strips' are the simplest and rapid techniques available for diagnosing UTI. Dipstick urinalysis detects inter alia, leukocyte esterase (LE), nitrites, blood, and protein. LE is a polymorphic enzyme and, as such, only a surrogate marker for UTI, and not all urinary pathogens produce nitrites. On the other

hand, techniques such as real time PCR are mainly used for identifying the type of bacteria and also need sample preparation prior to detection. Other techniques such as biosensors and immuno-chromatography detection are partly based on the enzyme-linked immunosorbent (reagent based) assay system. Therefore their ability to detect different bacterial strains is limited.

It is known that human urine contains a large number of fluorophores (mostly tryptophan and its metabolites) which can fluoresce under UV excitation. Due to their presence, normal urine has strong fluorescence. Although pathological and physiological changes are known to alter the autofluorescence of urine, there is a shortage of studies investigating autofluorescence as a diagnostic tool for UTIs.

The primary objective in the study of human urine autofluorescence was to test the potential of autofluorescence as a diagnostic tool for urinary tract infection. This was done to have a simple method to detect UTI with the following advantages such as no sample preparation, no reagents, fast, cost effective and amenable to automation. Further, this technique could be utilised to design a low cost home diagnosis kit.

Part B: Studies on autofluorescence of adipose derived adult stem cells

Stem cells have the remarkable potential to develop into many different cell types in the body during early life and growth. The potential of stem cells in regenerative medicine has led to an increased interest in investigating their properties. An understanding of cell differentiation process could lead to potential stem cell therapies.

The motivation for the study was to have a noninvasive method for characterizing stem cells because all the current techniques for characterizing stem cells are invasive techniques which include using chemicals, bio-markers and by techniques such as

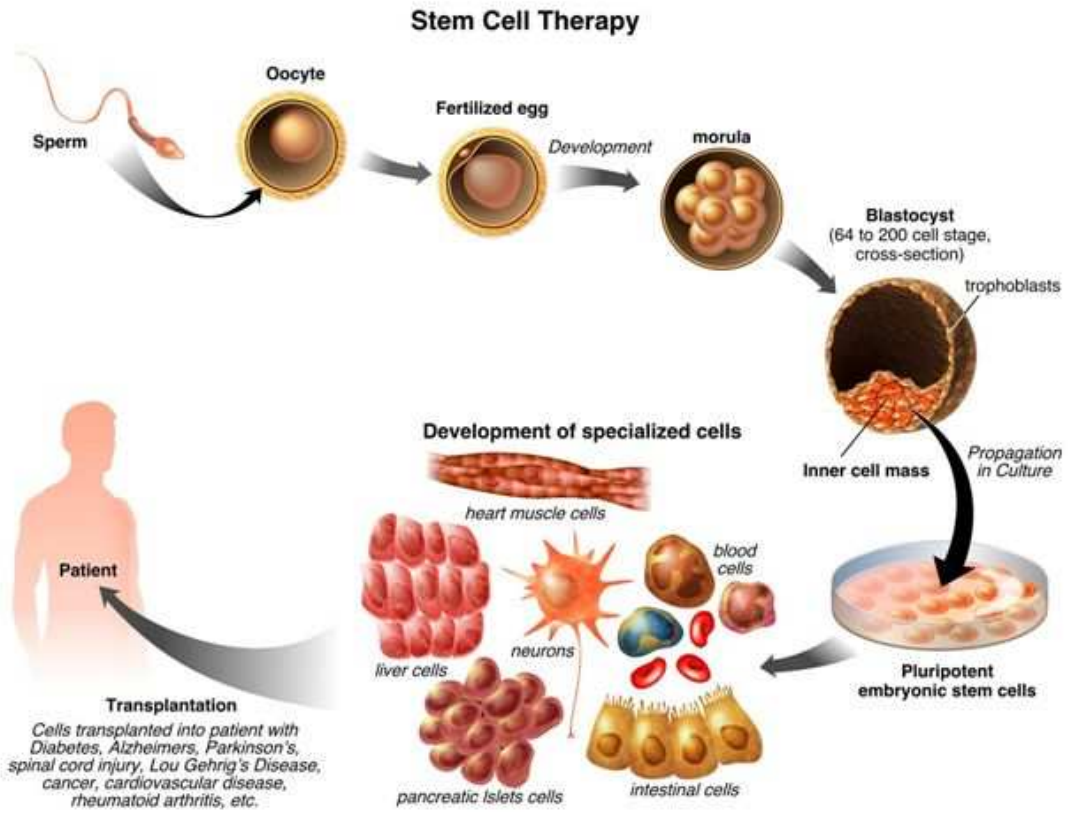

Figure 1.3: Illustration showing the potential of stem cell for therapy [7].

polymerase chain reaction (PCR).

In this study, the main objective was to test the potential of non invasive confocal imaging methods (measuring autofluorescence) for characterizing stem cells. Autofluorescence was used in this study because autofluorescence can give rich insight to cell metabolism. Another reason was autofluorescence analysis can be performed in real time (because it does not require any treatment of fixing or staining of the specimens).

1.3 Thesis structure

The thesis is divided into four chapters.

1. In Chapter 1, fluorescence of human urine (both diluted and undiluted) was explored using various fluorescence techniques which included excitation emission matrix and synchronous fluorescence spectroscopy.

2. In Chapter 2, the factors influencing UV fluorescence of human urine such as inner filter effect, concentration quenching, dimer formation and quenching were investigated.

3. In Chapter 3, fluorescence of urine from patients with urinary tract infection (UTIs) were investigated, to check the potential of using autofluorescence as a diagnostic tool for UTI.

4. Chapter 4 describes a preliminary study of stem cell autofluorescence was performed using laser scanning confocal microscopy, in an attempt to test the potential of using autofluorescence for characterizing stem cells.

The basics of fluorescence theory and various fluorescence instruments used in this study are discussed in Appendix A. The details (specifics) of the urine samples used in the study are provided as a supplementary material in a CD along with this thesis.

2

Autofluorescence of Human Urine

2.1 Introduction

In this chapter, autofluorescence of healthy human urine in the range between 250 nm to 450 nm excitation wavelength has been investigated in detail. Various techniques including emission spectra, excitation/emission matrices and synchronous fluorescence spectra was utilized to explore urine fluorescence of undiluted and diluted urine sample. This study had a particular focus on UV fluorescence because fluorophores which are excited in the range of 250 nm to 450 nm excitation such as tryptophan and its metabolites can vary with aging and certain medical conditions.

2.1.1 Composition of urine in healthy individuals

Human urine is a fluid of very complex composition. Approximately 95% volume of normal urine contains water. In addition to water, its chemical constituents are broadly classified as electrolytes, nitrogenous compounds, vitamins, hormones, organic acids and miscellaneous organic compounds [8,9]. The composition of urine varies greatly in different individuals, and in the same individual with time. The inter-individual and typically lower intra- individual variations can be due to factors

like dietary intake, physical activity, body metabolism, endocrine functions, and even body positions can influence the concentration of substances in the urine [8]. The general composition of urine is shown in Table 2.1.

Component	Amount	Comments
Organic		
Urea	25.0-35.0 g	60-90% of nitrogenous material; derived from the metabolism of amino acids into ammonia
Creatinine	1.5 g	Derived from creatine, a nitrogenous substance in muscle tissue
Uric acid	0.4-1.0 g	Common component of kidney stones; derived from the catabolism of nucleic acid in food and cell destruction
Hippuric acid	0.7 g	Benzoic acid is eliminated from the body in this form; increase with high vegetable diets
Other substances	2.9 g	Carbohydrates, pigments, fatty acids, mucin, enzymes and hormones ;may be present in small amounts depending on diet and health
Inorganic		
Sodium chloride(NaCl)	15.0 g	Principal salt; varies with intake
Potassium(K^+)	3.3 g	Occurs as chloride sulfate and phosphate salts
Sulfate(SO_4^{2-})	2.5 g	Derived from amino acids
Phosphate	2.5 g	Occurs primarily as a sodium compounds that serve as buffers in the blood
Ammonium	0.7 g	Derived from protein metabolism and from glutamine in kidneys; amount varies depending on blood and tissue fluid acidity
Magnesium	0.1 g	Occurs as chloride, sulfate and phosphate salts
Calcium	0.3 g	Occurs as chloride, sulfate and phosphate salts

Table 2.1: Composition of urine collected for 24 Hours (data from Strasinger [8]).

2.2 Autofluorescence of healthy human urine

Urine as a multicomponent biological fluid contains a number of natural fluorophores. These include tryptophan, indole, kynurenine, flavins, porphyrines, uric acid etc. A list of fluorescent species is shown in Table 2.2. Due to these fluorescing substances, human urine has broad and strong fluorescence spectra. In addition to the natural fluorophores, in some diseases which are accompanied by metabolic disorders, cer-

tain additional organic compounds, such as proteins and bilirubin may appear in the urine. These often serve as indicators in disease diagnosis [10]. For example Ohashi *et al* (1986) studied the abnormal excretion of autofluorescent lipids in urine from patients with neuronal ceroid lipofuscinosis [11].

There have been several efforts in literature to interpret autofluorescence of urine. The blue-green fluorescence of human urine on exposure to ultraviolet radiation was noted by Jaffe [12]. Squires *et al* (1928) developed a simple ultraviolet fluorophotometer to study urine fluorescence [13]. The authors described that at a certain dilution, intensity is proportional to the concentration of fluorescent substances. A correlation of fluorescence of human urine with benign and malignant growth was observed by Rabinowitz *et al* (1949). They analyzed fluorescent intensity of blue fluorescent substances and red fluorescent substances contained in human urine. The ratio of the fluorescence intensity between blue and red fluorescent substances were also analyzed for different samples like healthy human urine, proven cases of malignant growth and proven cases of benign growth including pregnancy [14].

The majority of the earlier studies in identifying fluorescent metabolites in human urine were done with the help of gel chromatography, liquid chromatography and fluorescence detection at fixed wavelengths. For example Mabuchi *et al* (1983) used high-performance liquid chromatography to profile endogenous fluorescent substances in both uremic and normal body fluids like human urine [15] and Marklova reported on screening for the variation in tryptophan metabolism in body fluids like human urine with the help of HPLC [16].

In 1987 Leiner *et al* analysed various dilutions of urine in the ultraviolet region and presented the fluorescence spectra in a 3D-form. They reported that the fluorophores which contribute to blue-green region of urine are tryptophan and its metabolites. They also demonstrated the topography of urine fluorescence and pro-

posed that pattern recognition is a useful method for studying urines [17].

In 2002 Dubayova *et al* studied the synchronous fluorescence spectrum (SFS) of urine. They were the first to report the differences in synchronous fluorescence spectra (SFS) between the urines of healthy people and patients with UTI or renal diseases. They suggested that the observed spectral variation could be due to the presence of proteins [18]. In 2004, Bukowski utilized the combination of excitation wavelength and phase resolution for minimizing autofluorescence from a specific luminophore in urine under multiphoton-excitation conditions [19]. Kusnir *et al* introduced concentration matrices for analysing autofluorescence of human urine in 2005. In their study, they also showed the difference in the spectra of healthy human urine and with various diseases, such as hepatopathy and autoimmune thrombocytopenic purpura [20].

Fluorophores species in human urine

Human urine contains a large number of fluorophores which can fluoresce under UV excitation, mostly tryptophan and its metabolites. Consequently UV fluorescence of urine, in principle should be applicable as a diagnostic tool for various diseases. However, as the literature on urine fluorescence is surprisingly scarce in spite of its easy availability, it is worthwhile to analyze spectral characteristics of urine.

Another reason for studying human urine fluorescence is that, earlier studies have mostly focused on analyzing urine after dilution, adding another step to potential diagnostic procedures and removing the possibility of monitoring fluorescence of those fluorophores which are in low concentration. The focus of the work in this Chapter will be to analyze both diluted as well as undiluted human urine, using various fluorometric techniques, to study the urine autofluorescence in detail.

Fluorophores in human urine were divided into two groups (A and B) by Leiner

Name	Excitation/ Emission (nm)	Approx daily excretion μmol	References
	GROUP A		
Melatonin	283/333		[21]
Tryptophan	280/360	50.0(+/- 27)	
Indoxyl sulphate	290/380	300.0	[17]
Indolyl-3-acetate	290/360	32.3	[17]
Skatol-5-sulphate	290/370	11.0	[17]
Skatol-6-sulphate	290/360,370	21.0	[17]
Metabolites of cathecholamines	270/290-300	-	
5-Hydroxyindole-3-acetate	300/345-355	24	[17]
5-Hydroxytryptophan	295/340	-	[17]
	GROUP B		
4-Pyridoxic acid	317-350/420-425	4.1	[17, 22]
Xanthine	315/435	40	[17]
3-Hydroxyanthranilic acid	320/415	50	[17]
5-Hydroxyanthranilic acid	340/430	-	[17]
Kynurenine	370/490	14	[17]
Biopterin	370/450	8.9	[17]
Neopterin	353/438	1.8	[17]
5-Hydroxykynurenine	375/460	-	[17]
3-Hydroxykynurenine	365/460	27	[17]
Folic acid	365/450	0.21	[17]
Xanthurenic acid	350/460)	15.0	[17]
Porphyrins			[17]
Uroporphyrins	405(596,619,653)	0.27	
Coporphyrins	400-405(595,618,652,671)	0.47	
Flavins	350-440/530-550	0.2-2.5	[17]

Table 2.2: Fluorophore species in human urine.

et al and Kusnir *et al* for easier understanding of their behaviour [17,20]. Figure 2.1 represents the distribution of fluorophores in urine. The fluorophores which get excited in the shorter UV region (250-300 nm) are grouped as group A and those which get excited in short visible region, *ie* from 300 nm excitation wavelength belong to group B.

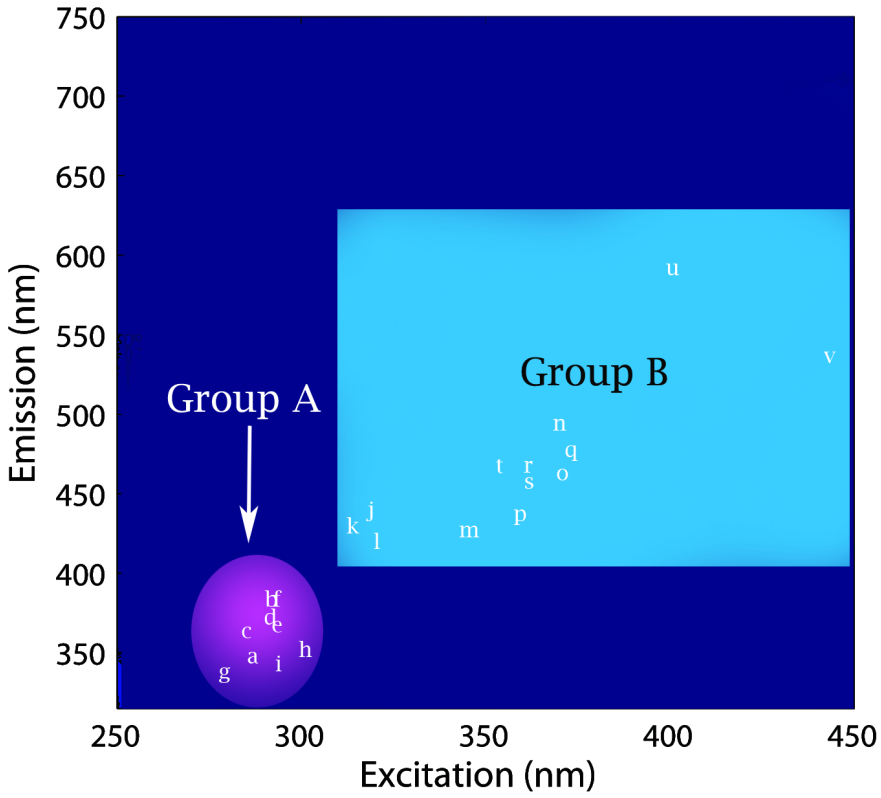

Figure 2.1: Distribution of urine fluorophores in excitation/emission matrix. (a) melatonin, (b) tryptophan, (c) indoxyl sulphate, (d) indolyl-3-acetate, (e) skatol-5-sulphate, (f) skatol-6-sulphate, (g) metabolites of cathecholamines, (h) 5-hydroxyindole-3-acetate, (i) 5-hydroxytryptophan, (j) 4-pyridoxic acid, (k) xanthine, (l) 3-hydroxyanthranilic acid, (m) 5-hydroxyanthranilic acid, (n) kynurenine, (o) biopterin, (p) neopterin, (q) 5-hydroxykynurenine, (r) 3-hydroxykynurenine, (s) folic acid, (t) xanthurenic acid, (u) porphyrins, (v) flavins, (data from Kusnir *et al* [20]).

2.3 Experimental methodology

2.3.1 Urine Samples

Urine samples were collected from a large pathology laboratory where they were analyzed for pH, protein, glucose, bilirubin, nitrate, nitrate, specific gravity, blood, ketones, urobilinogen and leukocyte esterase. The samples were also tested for the presence of red blood cells, white blood cells, casts, epithelial cells and crystals

(using iQ200 Sprint, IRIS Diagnostics Divisions, Chatsworth, California, USA). The presence of bacteria was determined by semi-quantitative culture on chromogenic agar plates. A total of 50 samples served as healthy human urines for the study. The age group from whom the samples were collected ranged from 5 to 90 years. They were chosen in such a way that they show no abnormal laboratory findings *ie* no proteins, glucose, bilirubin, blood, epithelial cells, casts, ketone, urobilinogen, leukocyte esterase and with pH 5-7.

In addition to the 50 samples, three samples were also taken from three additional healthy volunteers. Dipstick test was done on their urines, to check for abnormalities.

The samples were stored in the refrigerator (4^0C) and examined within 48 hours after collection.

2.3.2 Measurement of autofluorescence

1. Emission spectra

   The fluorescence spectra were collected at ten excitation wavelengths (250 nm, 280 nm, 290 nm, 310 nm, 340 nm, 400 nm, 450 nm, 500 nm, 550 nm and 600 nm)using a Fluorolog Tau3 system (JY Horiba, Edison, NJ) in 10 mm quartz cuvettes at room temperature. Spectral band passes were 2 nm in both excitation and emission. The spectra were corrected with respect to the optical system response. The scattering was eliminated by higher setting of emission monochromator.

2. Excitation/emission spectra

   These three dimensional plots of fluorescence intensity as a function of excitation (Ex) and emission (Em) wavelengths represent the complete fluorescence characteristic of the sample. In order to cover the broad spectral region of relevance in the most time-efficient way, four separate smaller excitation/emission

matrix EEMs were obtained and digitally integrated into a single one using MATLAB. In EEM measurements, the spectral band passes were 5 nm in both excitation and emission. The spectra were corrected for optical system response.

3. Synchronous fluorescence spectra

   Synchronous fluorescence spectra (SFS) were scanned using a Fluorolog Tau3 system in 10 mm and 4 mm quartz cuvettes at room temperature. For scanning synchronous spectra, the wavelength difference between the excitation and emission monochromators was adjusted for various $\triangle\lambda$ offset values. The excitation/emission slit was 5 nm. Scattering was eliminated by higher setting of emission monochromator.

2.3.3 Measurement of absorption

The absorption was measured using double beam CARY absorption spectrometer system (Varian Inc, USA) in 10 mm quartz cuvettes at room temperature.

2.4 Results

2.4.1 Absorption spectra of healthy human urine samples

Figure 2.2 shows example of absorption spectra of three different healthy human urine samples. The variability between the urine samples are clearly evident from Figure 2.2. However, when compared to the high absorption for healthy human urine in the UV region, there is very little absorption in the infra red area.

The absorption spectrum of urine of healthy humans over the wavelength range 190 nm to 250 nm is dependent mainly on six organic components, uric acid, urea, creatinimum, tirozinum, glicinum, and histidinum [10]. Urea, uric acid, and tirozinum are the major contributors at 250 nm [10]. Normal human urine has a strong absorption around 290 nm. This feature has been known for many years, and has been clearly mentioned in 1987 by Leiner et al [17]. The strong absorption in this region is possibly contributed by tryptophan and its metabolites.

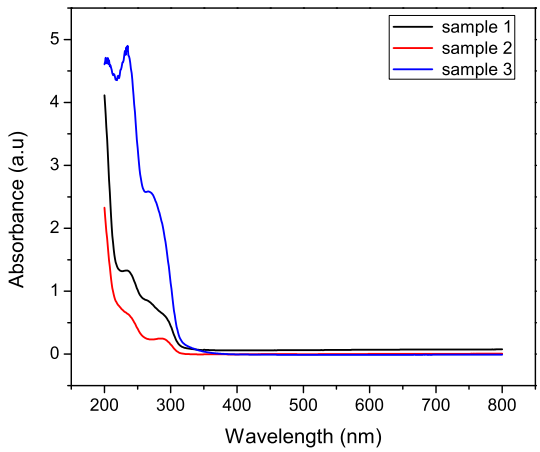

Figure 2.2: Absorption spectra of three different healthy human urines diluted 1:30 in double distilled water.

2.4.2 Excitation/emission spectra of undiluted healthy human urine

Examples of excitation/emission matrices of three different healthy human urine samples are shown in the Figures 2.3 and 2.4. It is evident from the Figures 2.3 and 2.4, that healthy human urine has a broad fluorescence spectrum. The excitation/emission matrices of samples 1 and 3 are similar and they show three distinct peaks at 360 nm, 380 nm and 450 nm excitation. In healthy sample 2.4a, two emission peaks at 360 nm and 400 nm excitation were observed. No peaks were seen in the shorter UV excitation region with any of these samples.

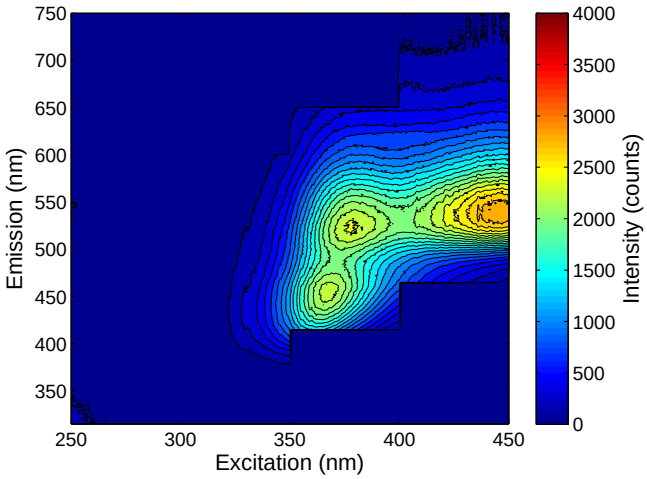

(a) Healthy urine sample 1

Figure 2.3: Excitation/emission matrices of undiluted healthy human urine sample. Note the colour scale representing intenisty.

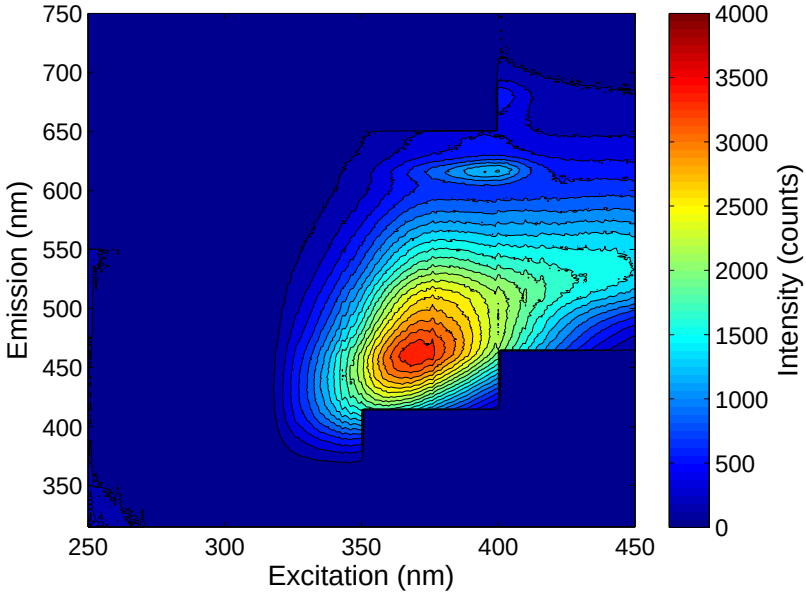

(a) Healthy urine sample 2

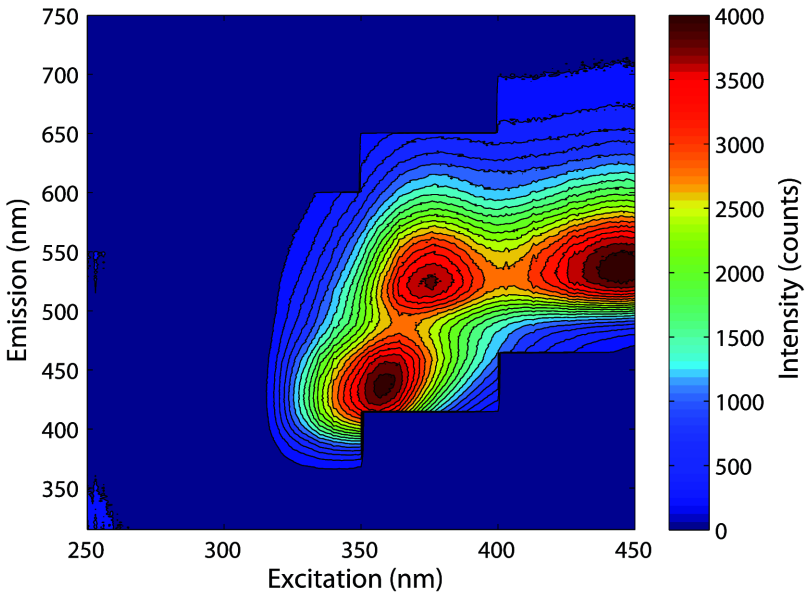

(b) Healthy urine sample 3

Figure 2.4: Excitation/emission matrices of undiluted healthy human urine sample.

Three dimensional spectra are a different way of representing the fluorescence of healthy human urine completely. Figure 2.5 depicts the three dimensional image of

a healthy urine sample. In the Figure 2.5, 'X' axis is excitation wavelength, 'Y' axis is emission wavelength and 'Z' axis represents the emission intensity.

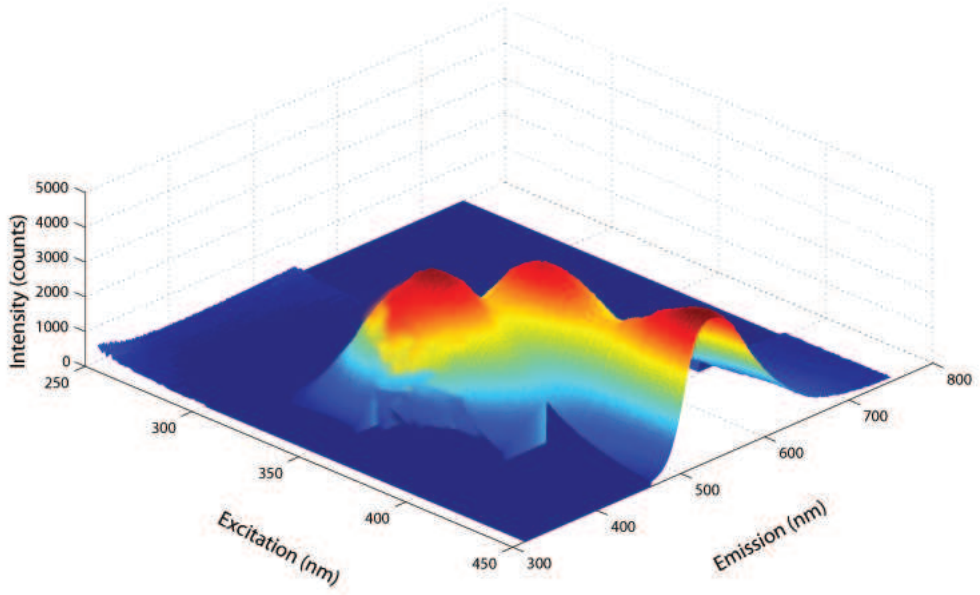

(a) Healthy urine sample 1

Figure 2.5: 3D spectrum of undiluted healthy human urine sample.

2.4.3 Effect of dilution on excitation/emission spectra of healthy human urine

The typical excitation/emission matrix of healthy human urine for dilutions 1:30, 1:300 and 1:1000 are presented in Figures 2.6 and 2.7. All the dilutions were made using double distilled water. At 1:30 dilution, an emission peak can be seen emerging at 320 nm excitation and very weak emission around 290 nm excitation. At 1:300 dilution the intensity of peak at 320 nm excitation was reduced but the peak at 290 nm became a little stronger. With 1:1000 dilution, a relatively strong emission peak could be seen at 285 ($\pm$ 10) nm excitation when compared to 1:30 and 1:300 dilutions, however the intensity of the 320 nm peak became very low.

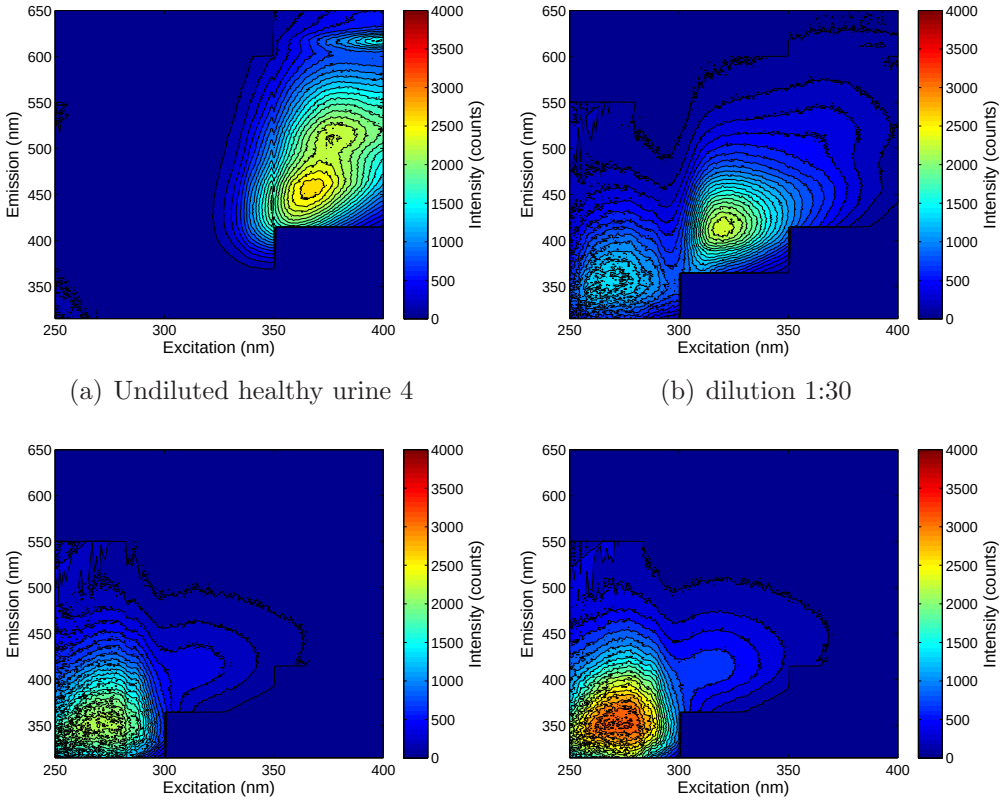

(a) Undiluted healthy urine 4

(b) dilution 1:30

(c) dilution 1:300

(d) dilution 1:1000

Figure 2.6: Excitation/emission spectrum of healthy human urine sample 4; (b),(c), (d) are at a dilution of 1:30, 1:300, 1:1000 respectively.

It is thus evident that with higher dilutions the group A fluorophores (tryptohan and its metabolites) show high intensity of fluorescence, and the intensity of fluorescence due to group B fluorophores drops. At lower dilutions group A fluorophores are quenched and group B fluorescence dominates.

2.4.4 Emission spectra of undiluted healthy human urine

Since it takes half an hour to scan the entire spectrum of excitation/emission matrix, we decided to use simple emission scan. Ten excitation wavelengths (250, 280, 290, 310, 350, 400, 450, 500, 550 and 600 nm) were explored for three different healthy human urine samples, as shown in Figures 2.8 and 2.9. All the three urine samples

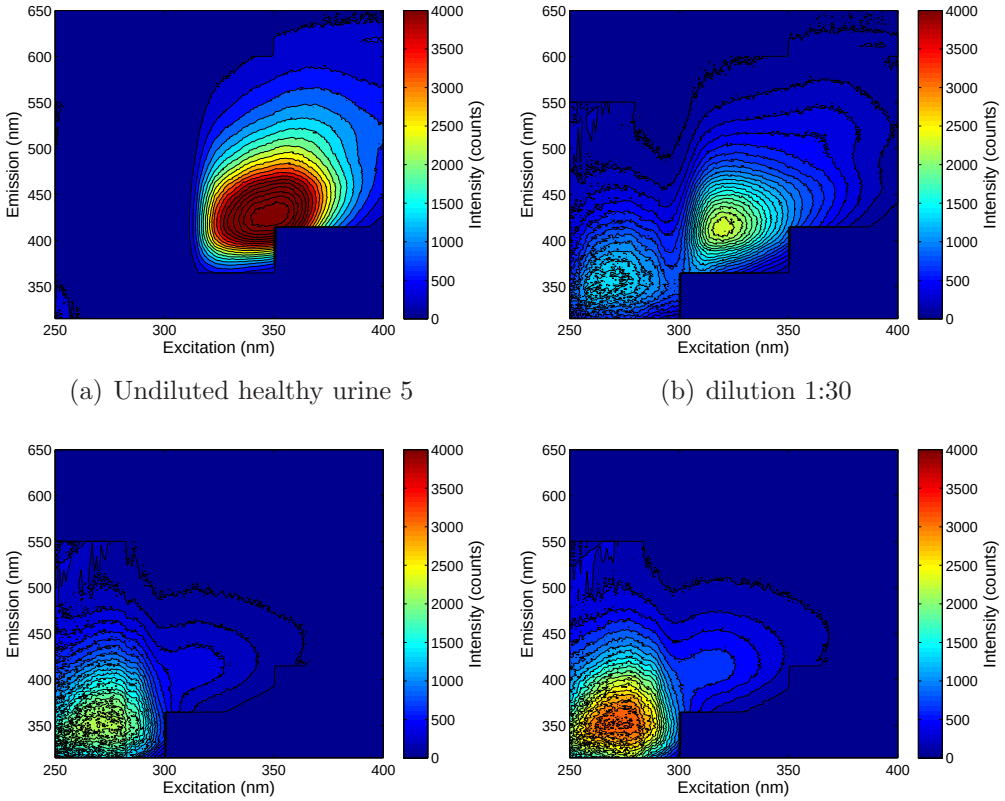

(a) Undiluted healthy urine 5

(b) dilution 1:30

(c) dilution 1:300

(d) dilution 1:1000

Figure 2.7: Excitation/emission spectrum of healthy urine sample 5; (b),(c), (d) are at a dilution of 1:30, 1:300, 1:1000 respectively.

showed similar spectral features.

For excitations at 250 nm, 280 nm and 290 nm, the emission peak was very weak. At the same time, excitations at 310 nm, 340 nm, 400 nm and 450 nm showed high intensity of fluorescence. The highest emission intensity for the three healthy urines was seen at 340 nm excitation. A very weak fluorescence peak was seen around 415 nm when excited at 250 nm. For excitations at 280 and 290 nm, peak emission for healthy human urine was observed around 425 ($\pm$10) nm. For excitation at 310 nm and 340 nm, emission peak was near 440 nm ($\pm$10) nm. For 450 nm excitation a clear emission maxima was seen at 550 nm. For 500 nm, 550 nm, 600 nm excitations,

a small emission peak at 620 nm could be seen.

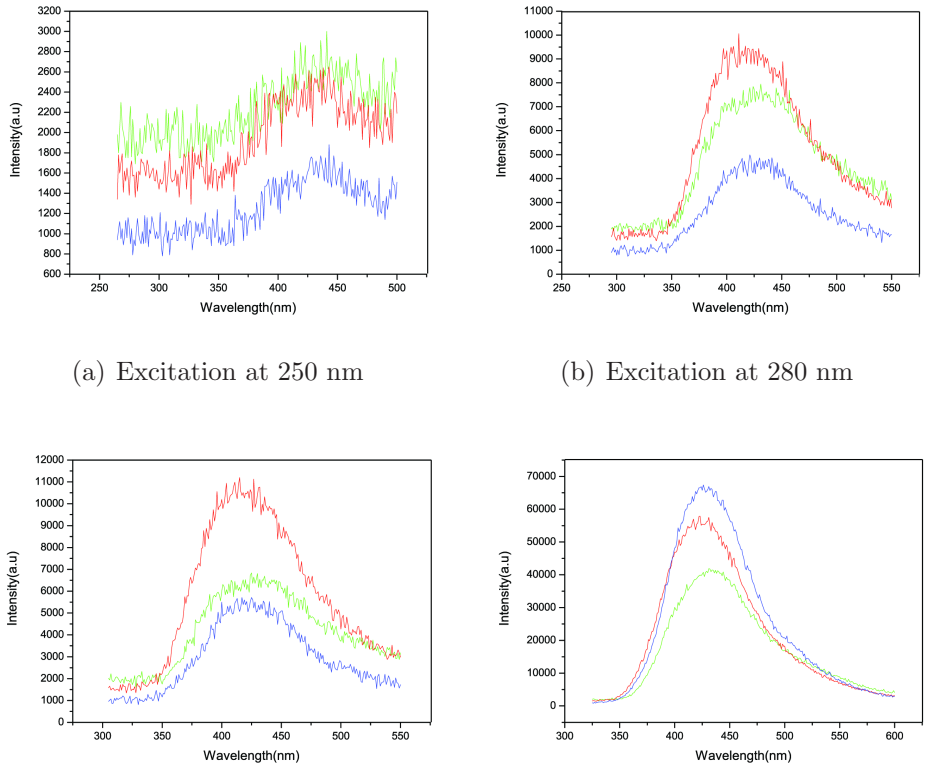

(a) Excitation at 250 nm

(b) Excitation at 280 nm

(c) Excitation at 290 nm

(d) Excitation at 310 nm

Figure 2.8: Fluorescence spectrum of undiluted healthy urine samples for excitations at 250 nm, 280 nm, 290 nm and 310 nm.

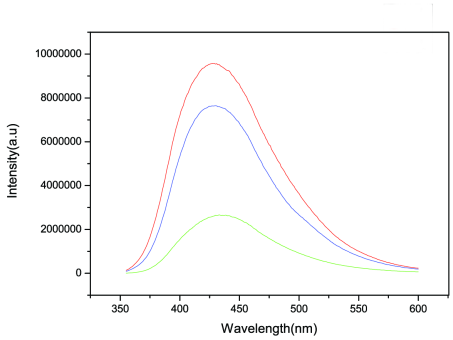

(a) Excitation at 350 nm

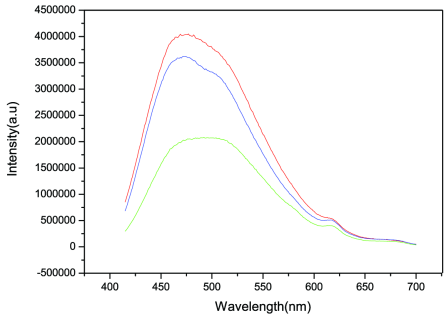

(b) Excitation at 400 nm

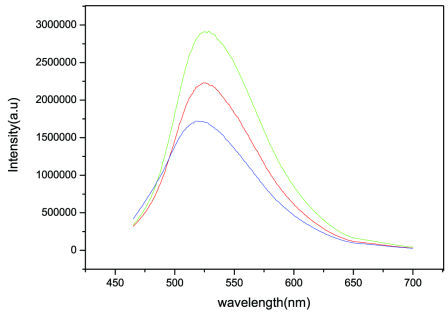

(c) Excitation at 450 nm

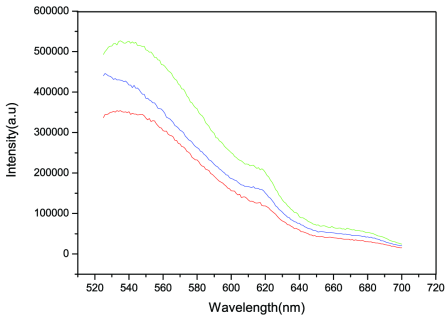

(d) Excitation at 500 nm

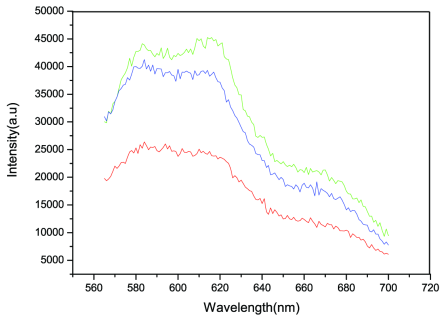

(e) Excitation at 550 nm

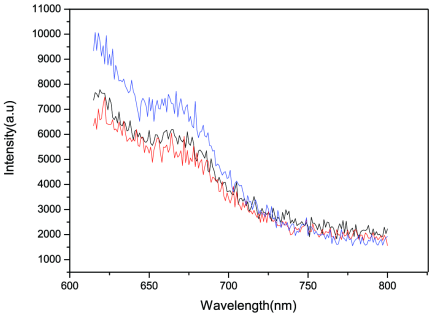

(f) Excitation at 600 nm

Figure 2.9: Fluorescence spectrum of undiluted healthy human urine samples for excitations at 340 nm, 400 nm, 450 nm, 500 nm, 550 nm and 600 nm.

2.4.5 Effect of dilution on the emission spectra of healthy human urines

Figures 2.10 and 2.11, represent both non-normalized and normalized graphs (dividing by maximum intensity) of fluorescence emission spectra of diluted and undiluted healthy urine (sample 9) measured at different excitation wavelengths. For the excitation wavelengths 290, 310 and 340 nm, the peak emission wavelengths for diluted samples showed clear shifts compared with the emission peak of the undiluted urine samples. It was also clear that the peak shift was greater with the higher dilutions (ie 1:1000>1:300>1:10). The peak shift was highest when the diluted samples were excited with shorter wavelength (290 nm). For normalized graphs, a narrow and sharp peak was seen in double distilled water. This is due to "Raman scattering".

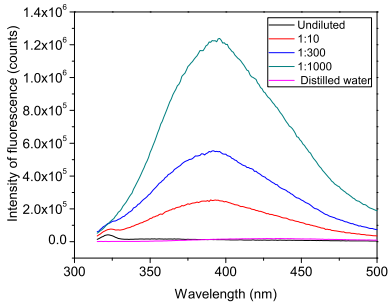

(a) excitation at 290 nm

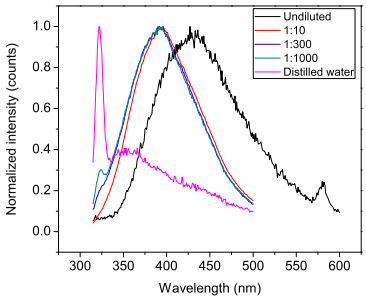

(b) normalized graph for 290 nm excitation

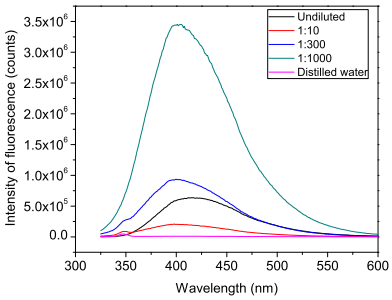

(c) excitation at 310 nm

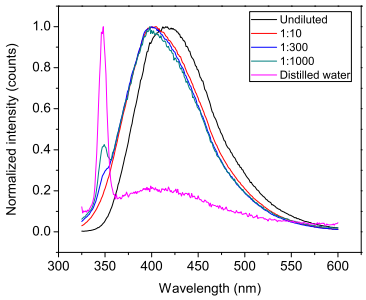

(d) normalized graph for 310 nm excitation

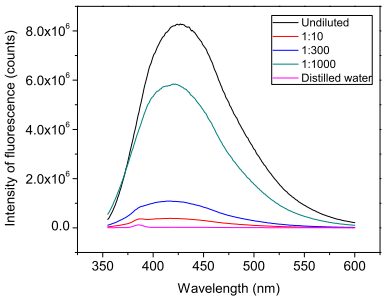

(e) excitation at 350 nm

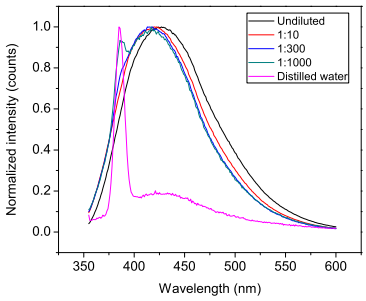

(f) normalized graph for 350 nm excitation

Figure 2.10: Fluorescence emission spectra of a diluted and undiluted healthy human urine (sample 9) for excitation wavelengths 290 nm, 310 nm, 340 nm. The various dilutions tested were 1:30, 1:300 and 1:1000. (The normalized graphs were plotted for the above spectra to observe the peaks clearly).

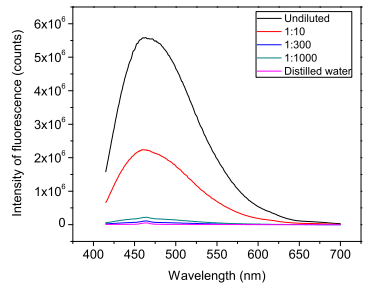

(a) excitation at 400 nm

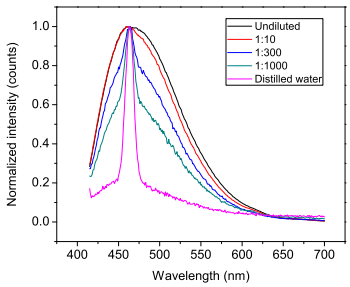

(b) normalized graph for 400 nm excitation

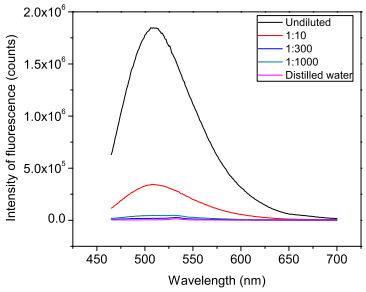

(c) excitation at 450 nm

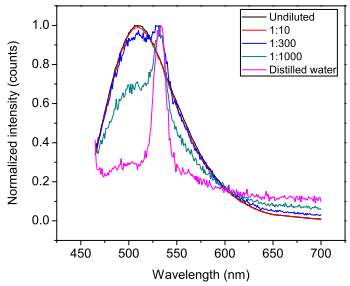

(d) normalized graph for 450 nm excitation

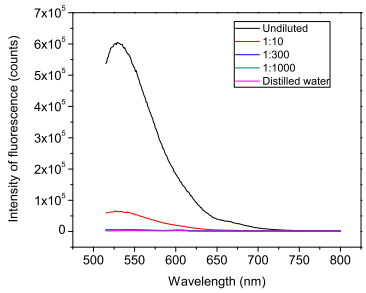

(e) excitation at 500 nm

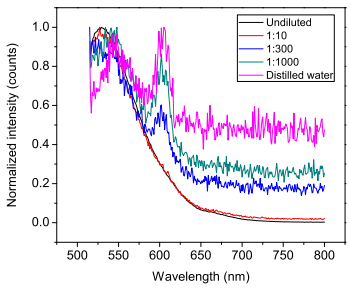

(f) normalized graph for 500 nm excitation

Figure 2.11: Fluorescence emission spectra of a diluted and undiluted healthy human urine (sample 9) for excitation wavelengths 400 nm, 450 nm, 500 nm. The various dilutions tested were 1:30, 1:300 and 1:1000. (The normalized graphs were plotted for the above spectra to observe the peaks clearly).

2.4.6 Emission spectra of undiluted healthy human urines at 290 nm excitation

In order to establish the level of individual variability at the short UV excitation, 40 samples were taken from a mixed age/gender population. The fluorescence spectra

for all these samples excited at 290 nm had a similar spectral pattern, but with variations in intensity.

Emission spectra of healthy human urine taken at 290 nm excitation wavelength are shown in Figure 2.12. The peak fluorescence was observed at 420 ±15 nm and the mean peak intensity varied by ±50% (Figure 2.13). A sharp peak seen at 580 nm is the "second order affect" from monochromator grating.

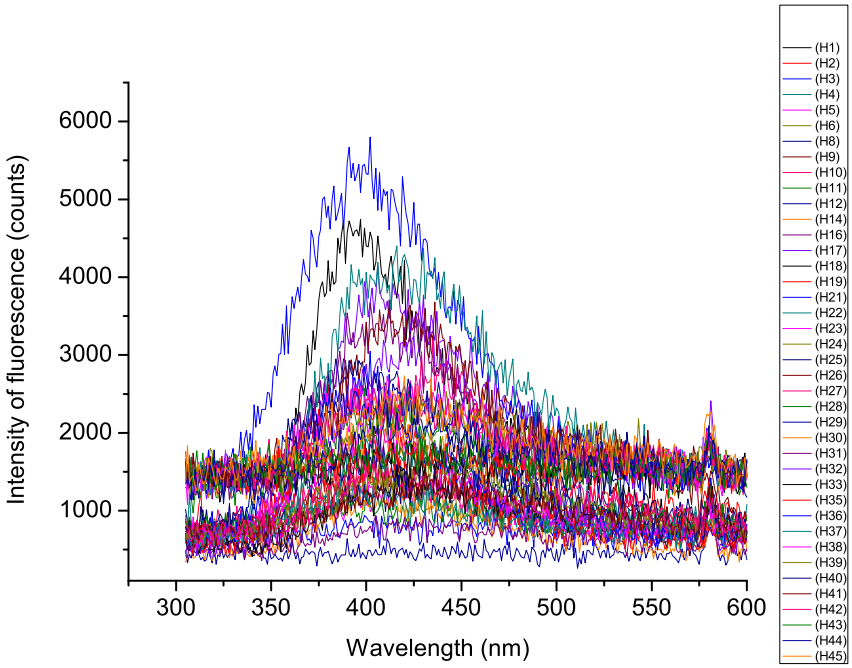

Figure 2.12: Emission spectra for 40 undiluted healthy urine samples at 290 nm excitation.

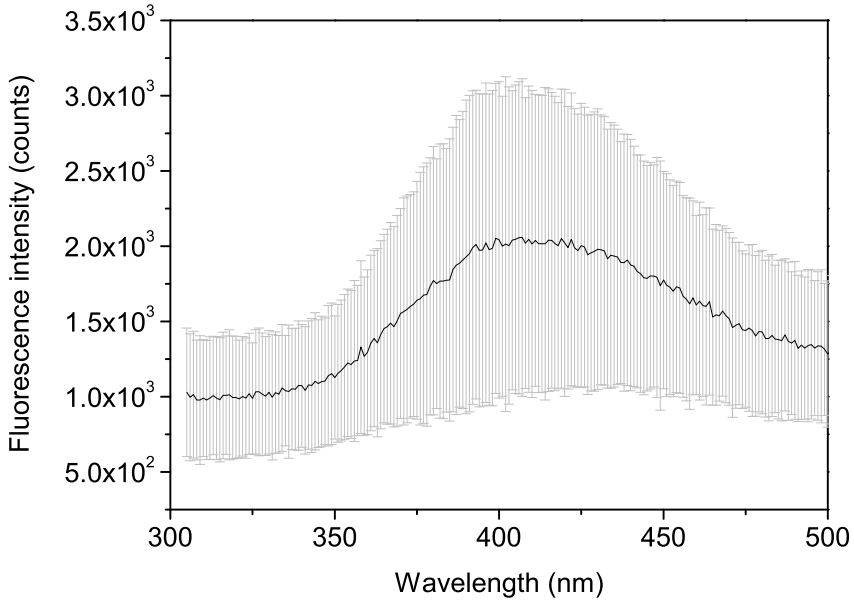

Figure 2.13: Mean emission peak intensity for 40 undiluted healthy urine samples excited at 290 nm [mean=2075].

2.4.7 Variation in the fluorescence emission of undiluted healthy urine excited at 290 nm with age and gender

Since the urine samples tested were from the age group 5 to 90 years and with mixed gender, it is possible that the samples could vary in their metabolite composition. Therefore, the focus was to on analyze the urine spectra for 290 nm excitation wavelength where the major fluorophores in urine (for example indoxyl sulfate and tryptophan) are distributed. To test this, 43 healthy urine samples were divided into two arbitrary age groups, 5 - 49 years (24 samples) and 50 - 90 years (19 samples).

The sample groups were analyzed by two sample independent t-test. The result indicated that there in no significant difference in the fluorescence intensities between the two groups (P=0.5311), suggesting that the intensity of emission spectra of healthy human urine at 290 nm excitation may not be related to age.

The t-test analysis for any gender difference (33 male and 10 female samples) showed no significant difference (P=0.1317) in fluorescence emission intensity at 290 nm excitation. It is thus clear that age and gender do not significantly influence the intensity of emission spectra at 290 nm for healthy human urine. Any discussion of spectral variation due to diet is beyond the scope of this study.

2.4.8 Synchronous fluorescence spectra (SFS) of healthy human urine

The synchronous fluorescence spectra were measured using a single healthy human urine, without dilution as well as at a dilution of 300 in double distilled water. SFS technique was used, as it is known to produce a spectrum with less overlapping as compared to the emission spectra. The synchronous fluorescence spectra were obtained in the emission wavelength range of 250- 630 nm for various $\Delta\lambda$ offset values. Excitation and emission slits were 2 nm and 5 nm respectively. The results are shown in Figures 2.14 and 2.15.

It is evident from the synchronous spectra that, the diluted sample shows fluorescence peak at shorter UV. The first peak was observed around 280-290 nm and the second peak at 340 nm excitation. When compared to emission at 340 nm excitation for the undiluted samples, emission of the diluted sample is very less. The undiluted sample did not have any peaks in between 250-310 nm excitation. The shoulders, near 370 and 440 were not seen for the diluted sample.

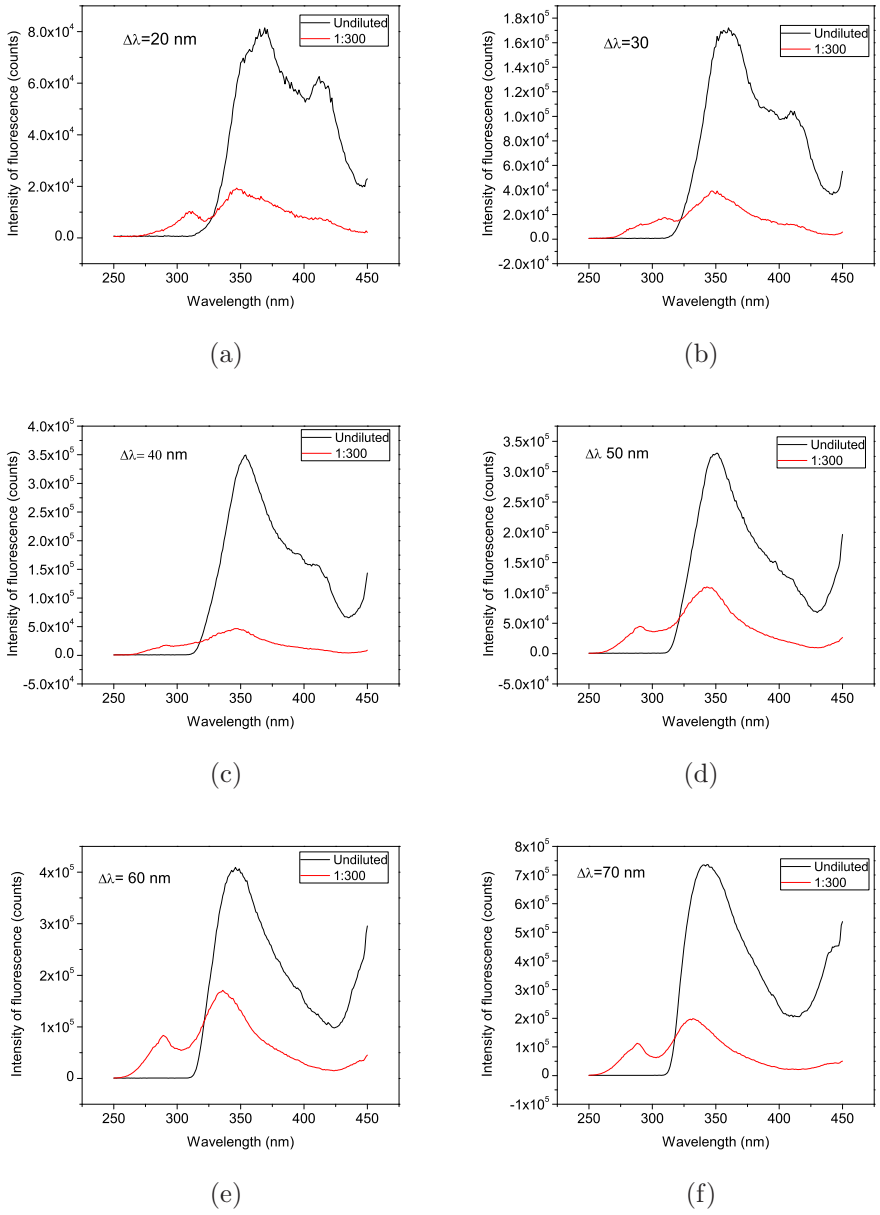

Figure 2.14: SFS of a healthy human urine (sample S) for 20, 30, 40, 50, 60 and 70 $\Delta\lambda$ offset values respectively. (−) undiluted urine and (−) urine diluted at 1:300 with double distilled water.

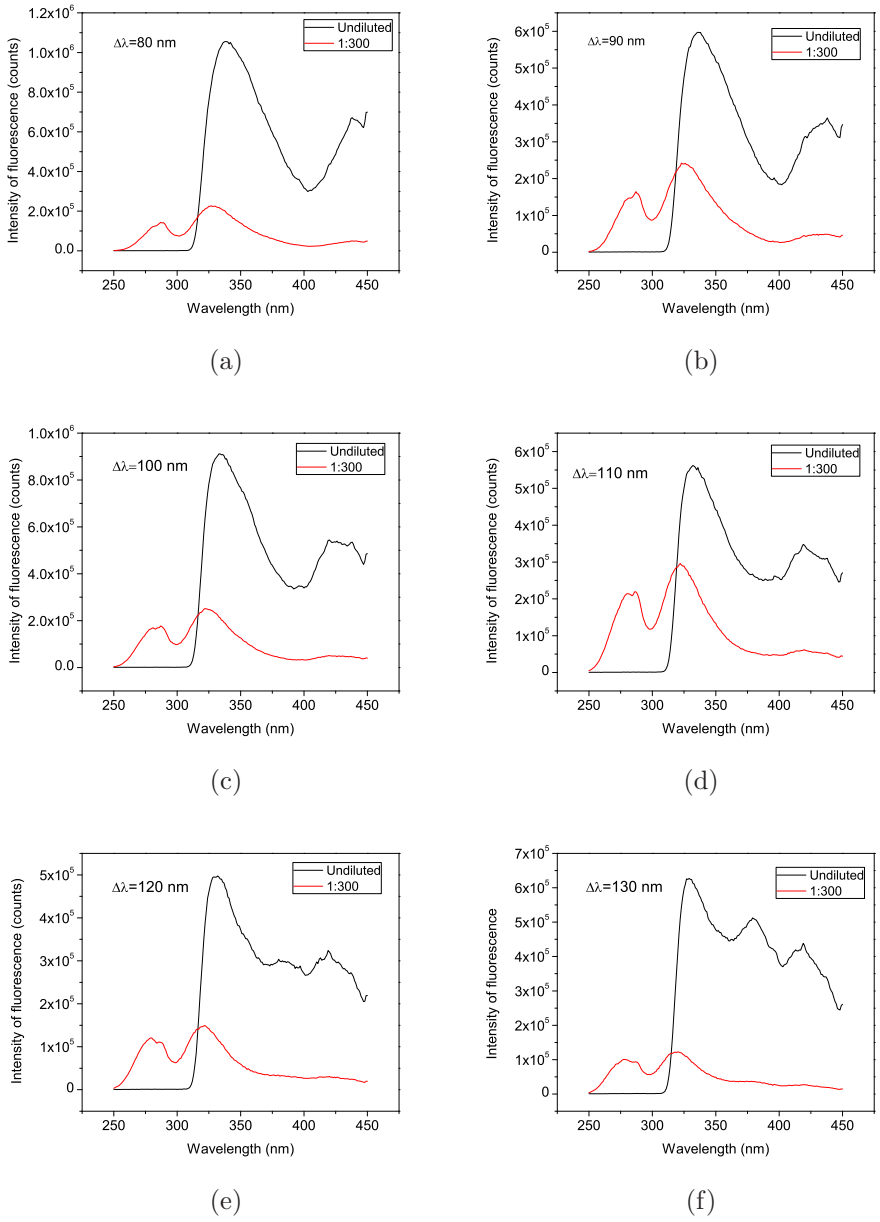

Figure 2.15: SFS of a healthy human urine (sample S) for 80, 90, 100, 110, 120 and 130 $\Delta\lambda$ offset values respectively. (−) undiluted urine and (−) urine diluted at 1:300 with double distilled water.

2.4.9 The effect of storage at 4^0C on the fluorescence in undiluted healthy human urine

Two undiluted healthy human urine samples (a and b) were analyzed for the effect of storage at 4^0C, on their fluorescence spectrum. The excitation/emission matrix of both samples were measured initially. The samples were then stored in the refrigerator (4^0C) and examined after 96 hours. The results are given in Figure 2.16.

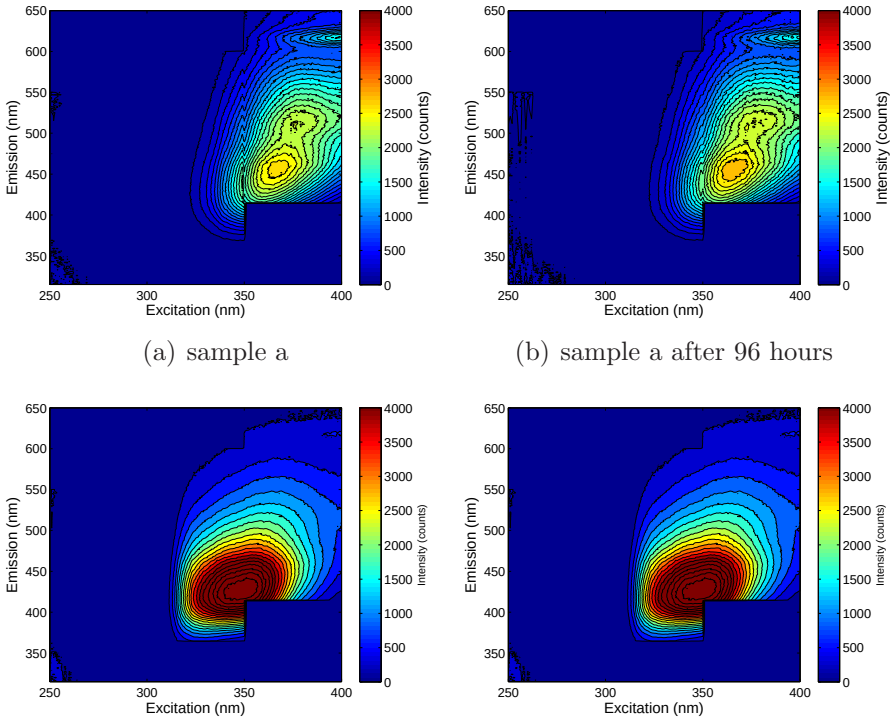

(a) sample a

(b) sample a after 96 hours

(c) sample b

(d) sample b after 96 hours

Figure 2.16: Illustration of the effect of storage at 4^0C on the fluorescence in undiluted healthy human urine samples (a and b).

There was no appreciable spectral variation of fluorescence for the undiluted healthy urine samples after storage at 4^0C for 96 hours.

2.5 Discussion

Overview

To analyze fluorescence spectra of undiluted human urine sample is always a challenging task for the following reasons. Firstly, urine has a large number of known and perhaps some unknown fluorophores. Secondly, most of the urine fluorophores have similar properties and in a complex mixture, it is highly likely that the fluorescence characteristics of individual fluorophores can be influenced by other fluorophores. Finally, the concentration of fluorophores vary in different individuals [20].

In this study, three different spectroscopic measurement techniques were utilised to analyze fluorescence spectra of healthy human urine samples. The techniques used were emission spectra, excitation/emission matrices and synchronous fluorescence spectra (SFS).

2.5.1 Fluorescence characteristics of undiluted healthy urine samples

Tentative identification of peaks from excitation/emission matrix

Two examples of excitation/emission matrices of undiluted healthy samples with different spectral features are shown in Figure 2.17 and 2.18. The observed differences can be due to variations in the fluorophores in the urine composition. From Figures 2.17 and 2.18, four major peaks were clearly seen. Properties of the various fluorophores are shown in Table 2.2. The information from Table 2.2 has been extrapolated to the Figure 2.17 and 2.18 for inferring the contribution by different fluorophores. The possible contributors to the various peaks are given below.

1. Peak 1: 360/450 nm (excitation/emission) : This peak is mainly contributed by a number of endogenous fluorescent metabolites such as xanthurenic acid, neopterin, 5-hydroxyanthranilic acid, 4-pyridoxic acid, folic acid, 5-hydroxy

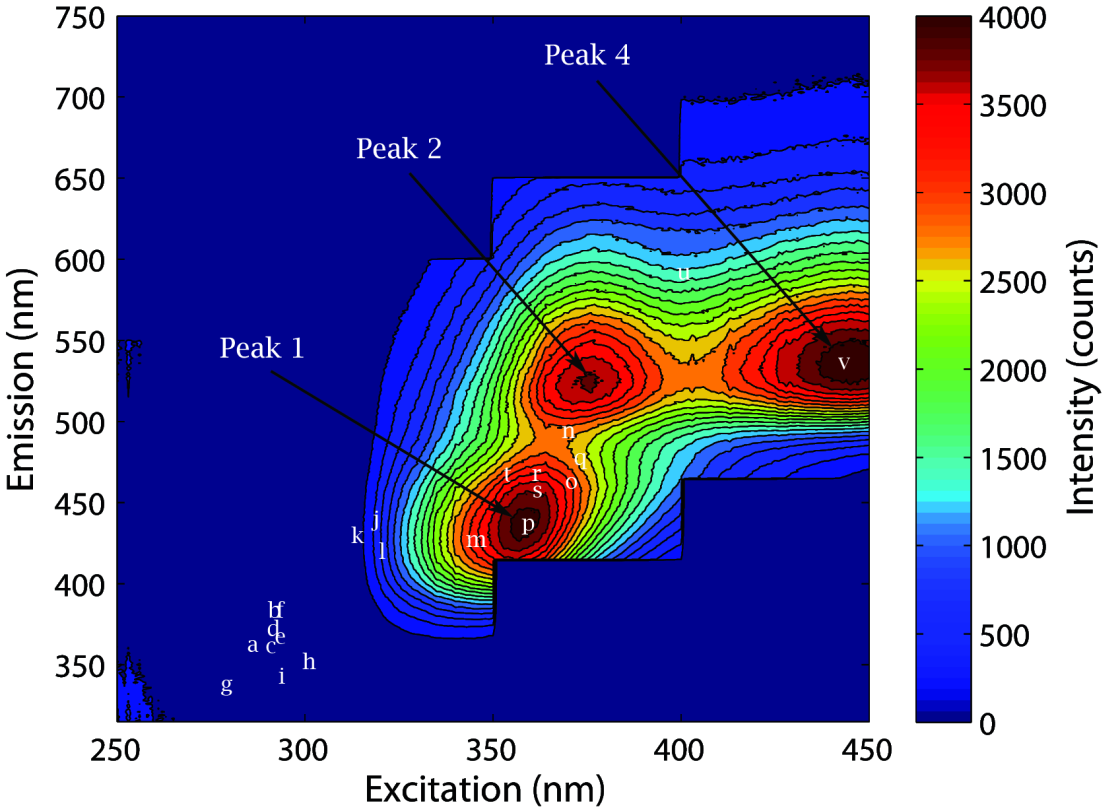

Figure 2.17: Tentative identification of emission peaks in urine: (a) melatonin, (b) tryptophan, (c) indoxyl sulphate, (d) indolyl-3-acetate, (e) skatol-5-sulphate, (f) skatol-6-sulphate, (g) metabolites of cathecholamines, (h)5-hydroxyindole-3-acetate, (i) 5-hydroxytryptophan, (j) 4-pyridoxic acid, (k)xanthine, (l) 3-hydroxyanthranilic acid, (m) 5-hydroxyanthranilic acid, (n) kynurenine, (o) biopterin, (p) neopterin, (q) 5-hydroxykynurenine, (r) 3-hydroxykynurenine, (s) folic acid, (t) xanthurenic acid, (u) porphyrins, (v) flavins. Note: The information from Table 2.2 has been extrapolated to the Figure 2.17 and 2.18 for inferring the contribution by different fluorophores.

kynurenine, 3-hydroxy kynurenine and biopterin.

2. Peak 2: 375/530 nm (excitation/emission) : The possible contributors for this peak could be kynurenine and flavins.

3. Peak 3: 400/620 nm (excitation/emission) : Porphyrins could be responsible

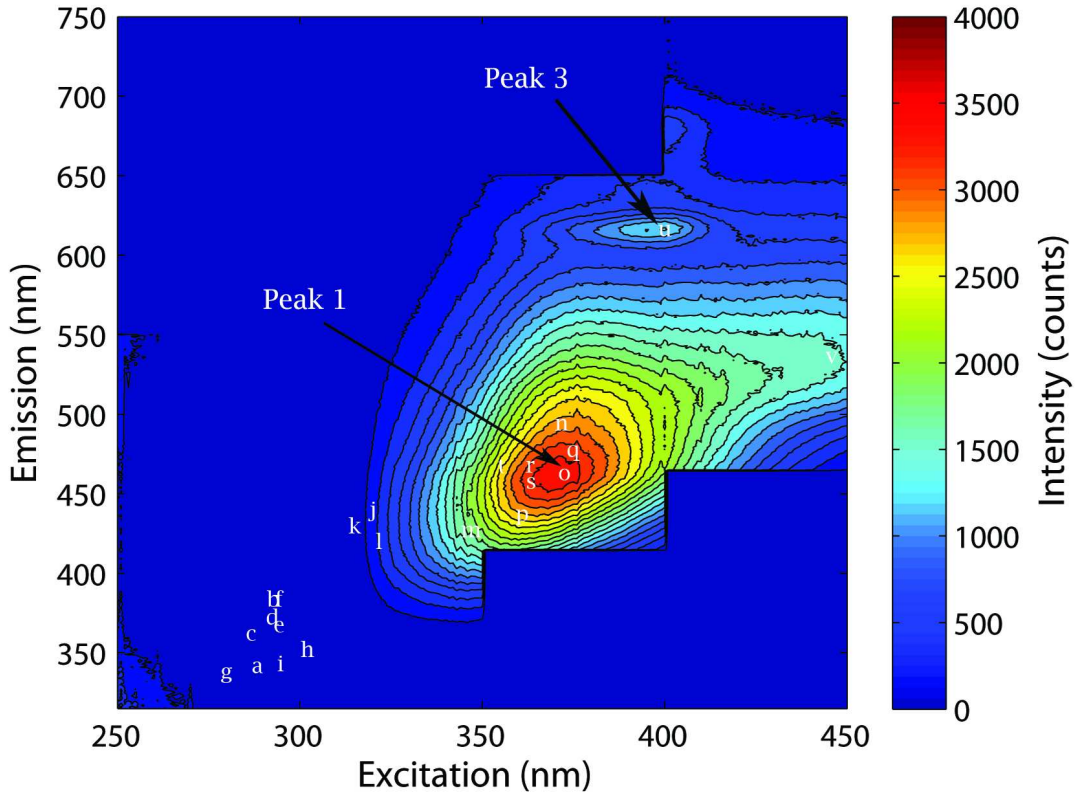

Figure 2.18: Tentative identification of emission peaks in urine: (a)melatonin, (b)tryptophan, (c) indoxyl sulphate, (d) indolyl-3-acetate, (e) skatol-5-sulphate, (f) skatol-6-sulphate, (g) metabolites of cathecholamines, (h)5-hydroxyindole-3-acetate, (i) 5-hydroxytryptophan, (j) 4-pyridoxic acid, (k)xanthine, (l) 3-hydroxyanthranilic acid, (m) 5-hydroxyanthranilic acid, (n) kynurenine, (o) biopterin, (p) neopterin, (q) 5-hydroxykynurenine, (r) 3-hydroxykynurenine, (s) folic acid, (t) xanthurenic acid, (u) porphyrins, (v) flavins. Note: The information from Table 2.2 has been extrapolated to the Figure 2.17 and 2.18 for inferring the contribution by different fluorophores.

for this peak.

4. Peak 4: 450/550 nm (excitation/emission) : Riboflavin and its metabolites could be the major contributors to this peak.

It is apparent from the Figures 2.17 and 2.18, that the autofluorescence of undiluted human urine excited in 250 nm-300 nm range is very weak when compared to

longer UV (300-450 nm) excitation. The reduced fluorescence emission of group A fluorophores has been reported in earlier papers [17, 18], but no proper explanation with experimental evidence has been offered so far. Chapter 3 has more detailed discussion of this issue.

Comparison of excitation/emission matrix results obtained with those of earlier studies

There is limited information in literature on the excitation/emission matrix for undiluted healthy human urine. Kusnir *et al* [20] have shown a typical example of excitation/emission matrix for an undiluted healthy human urine sample (Figure 2.20). Two different spectral patterns were noted in the present study for undiluted healthy human urine (Figures 2.19 a and b). One of the sample patterns (Figure 2.19 a) observed was similar to that reported by Kusnir *et al* (Figure 2.20) [20].

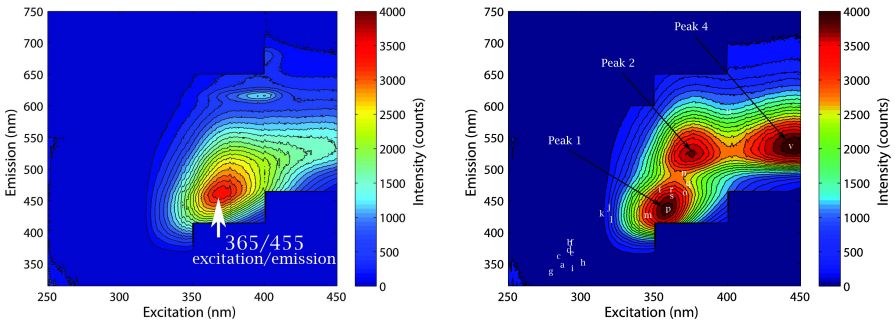

(a) Healthy urine sample 2 (b) Healthy urine sample 3

Figure 2.19: Excitation/emission matrices of undiluted healthy urine samples.

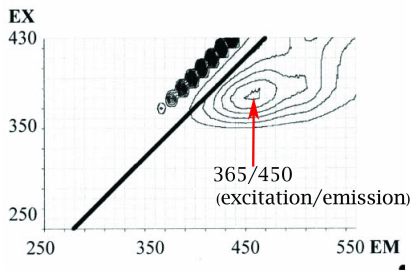

(a)

Figure 2.20: Excitation/emission matrices of undiluted healthy urine sample. Data from Kusnir *et al* [20]

Emission spectra of undiluted healthy human urine samples

After analyzing the excitation/emission spectra of urine, a few selective excitation wavelengths (250, 280, 290, 310, 350, 400, 450, 500, 550 and 600 nm) were chosen to analyze urine. This was done to reduce measurement time.

Excitation/emission matrix from the emission spectra of the three samples were plotted to compare with our previous result. This is given in Figure 2.21. Even though the resolution for the contour of the three samples was less, it is clear that emission spectral measurements were in agreement with the earlier excitation/emission matrix results (Figure 2.21 a, Figures 2.3 and 2.4).

The results of emission spectra are given in Figures 2.8 and 2.9. The intensity of the three samples varied from one another for various excitations. This may be due to inter-individual and typically lower intra-individual variations in urine metabolites. But the spectral patterns (peak positions) of all the three healthy human urine samples were similar.

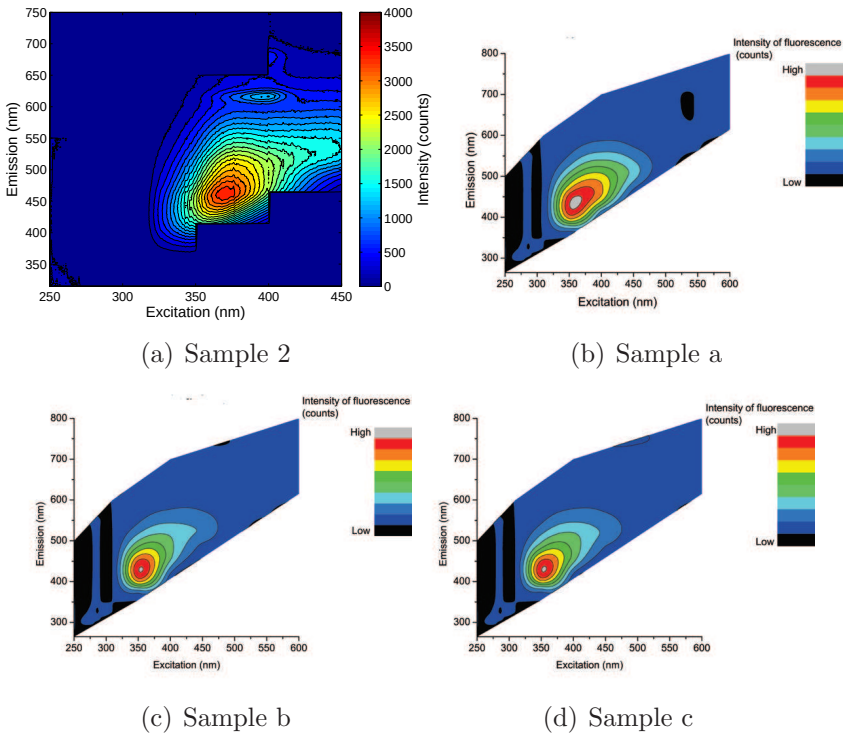

(a) Sample 2 (b) Sample a

(c) Sample b (d) Sample c

Figure 2.21: Comparison of emission spectra of healthy undiluted human urine with our earlier results of excitation/emission spectra. Note Figures b, c and d are excitation/emission matrices obtained from emission spectra.

SFS of undiluted healthy human urine

Synchronous fluorescence spectra are strongly dependent on the wavelength offset, $\Delta\lambda$ [18]. In the earlier works by Kusnir *et al* and Dubayova et al, $\Delta\lambda = 30$ nm was used as the offset, because it is very sensitive to pathological changes [18]. Here, in the study many spectra were acquired in the emission wavelength range of 250- 630 nm for various $\Delta\lambda$ offsets (from 20 nm through to 130 nm, with 10 nm increments).

The undiluted healthy human urine samples had a major peak around 340 - 350 nm excitation, irrespective of the $\Delta\lambda$ offset. This is evident from the results of spectra shown in Figures 2.14 and 2.15. The possible fluorophores contributing to this peak are 4- pyridoxic acid, 5-hydroxyanthranilic acid, neopterin and uric acid

(Table 2.2).

For the $\Delta\lambda$ 80 nm offset, the peak at 340 nm excitation showed the maximum intensity in undiluted sample (Figure 2.22). According to earlier studies, this peak at 340 nm excitation is mainly attributable to 4-pyridoxic acid [17, 18, 22].

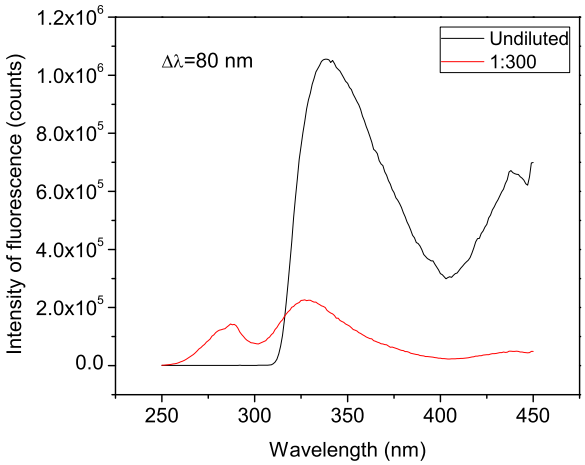

Figure 2.22: SFS for $\Delta\lambda$ 80 nm offset. (−) undiluted urine and (−) urine diluted at 1:300 with double distilled water.

For the $\Delta\lambda$ offsets 80 to 130 nm, more peaks were observed in undiluted healthy urine, as shown in Figures 2.14 and 2.15. At $\Delta\lambda$ 30 nm offset, three peaks could be seen at 320, 375 and 440 nm excitation (Figure 2.23). The peak at 440 nm excitation could be mainly contributed by flavins, which have excitation and emission at 350-440 nm and 530-550 nm respectively [23–25]. Porphyrins could also be contributing to this peak. The peak seen around 375 nm excitation for $\Delta\lambda$ 130 nm (Figure 2.14) could be contributed by 5- hydroxykynurenine, 3- hydroxykynurenine, kynurenine and biopterin. No fluorescence emission corresponding to group A fluorophores was detected by SFS in undiluted healthy human urine. The reason for this will be explained in Chapter 3.

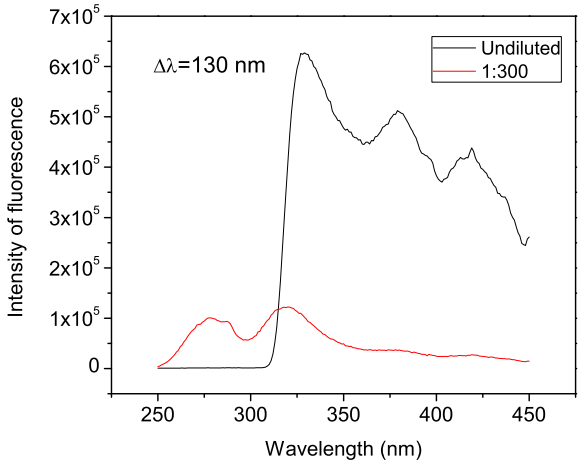

Figure 2.23: SFS for $\Delta\lambda$ 130 nm offset. (−) undiluted urine and (−) urine diluted at 1:300 with double distilled water.

Comparison of SFS obtained with those of earlier studies

Synchronous spectra of undiluted healthy human urine for $\Delta\lambda$ 30 offset was earlier reported by Kusnir *et al* [20]. Their results are similar to the synchronous measurement results for $\Delta\lambda$ 30, as plotted in Figure 2.24b of this study. Both spectra had a dominant emission near 360 nm excitation.

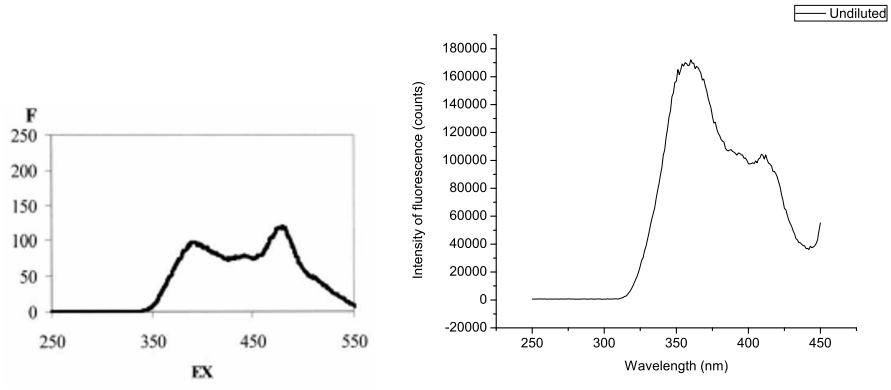

(a) SFS for undiluted healthy human urine, kusnir et al [20]

(b) SFS data from the study for undiluted healthy human urine

Figure 2.24: Excitation/emission matrices of healthy urine sample.

2.5.2 Effect of dilution on the fluorescence characteristics of healthy urine samples

Identification of peaks from excitation/emission matrix for diluted healthy human urine samples

Diluting human urine with any solvent is perhaps not ideal from a diagnostic point of view because it could affect the sample condition and it introduces an additional assay step. The dilution factor is an important aspect to be considered as significant variations occur in fluorescence spectra with different dilutions. By diluting the concentration of fluorophores, the pH and viscosity are altered, which can have a net effect on the observed fluorescence. The fluorescence spectra of diluted healthy human urine are therefore totally different from the undiluted ones.

The majority of previous studies on the fluorescence of human urine were with diluted samples. In this study, double distilled water was used for for diluting healthy human urine. The dilution factors were 1:30, 1:300 and 1:1000. As can be seen in Figure 2.25, with higher dilutions, all the peaks observed for undiluted healthy samples (ie peaks at 360 nm, 375 nm, 400 nm and 450 nm) disappeared. For 1: 30 dilution two emissions *ie* one at 435 nm and 365 nm were seen at 320 nm and 270 nm excitations respectively. The intensity of peak 2 increased with dilution (maximum at 1:1000 dilution). Peak 1 emission decreased with dilution and disappeared completely at 1: 1000 dilution.

1. peak 5: The possible contributor for this peak could be 4-pyridoxic acid [17,18]. Pyridoxinic compounds are of a great interest in biological studies as they are constituents of vitamin B_6. Spectral properties of 4-pyridoxic acid are pH sensitive [22].

2. peak 6: Group A fluorophores are the principal contributors to this peak.

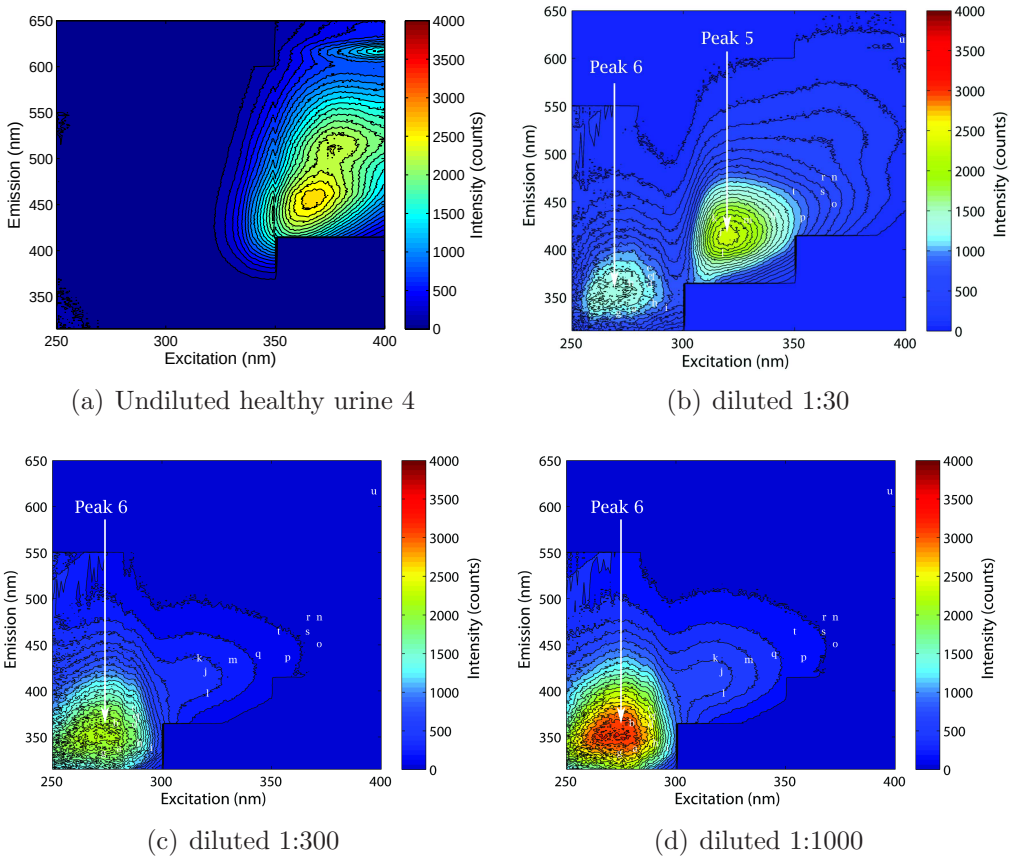

(a) Undiluted healthy urine 4

(b) diluted 1:30

(c) diluted 1:300

(d) diluted 1:1000

Figure 2.25: Excitation/emission matrices of healthy urine sample 4. (a) undiluted, (b)-(d) urine diluted 1:30, 1:300, and 1:1000, respectively.

Comparison of excitation/emission matrix results obtained with those of earlier studies

The SFS data in this study, can only be compared with the work done by Kusnir *et al*, where they had presented excitation/emission matrix of healthy human urine for various dilutions (1:30 and 1:500) [20]. The emission excitation matrix by Kusnir *et al* is shown in Figure 2.26 and the data from this study Figure 2.25. A comparison of both results shows that at 1:30 dilution, two peaks were seen, one each at 270 nm and 320 nm excitation with 365 nm and 435 nm emission respectively. It was evident that with higher dilution (1:1000), group A fluorophore emission peaks became more

intense. At the same time, group B fluorophore, peak was reduced. The reason for this is explained in the later part of discussion.

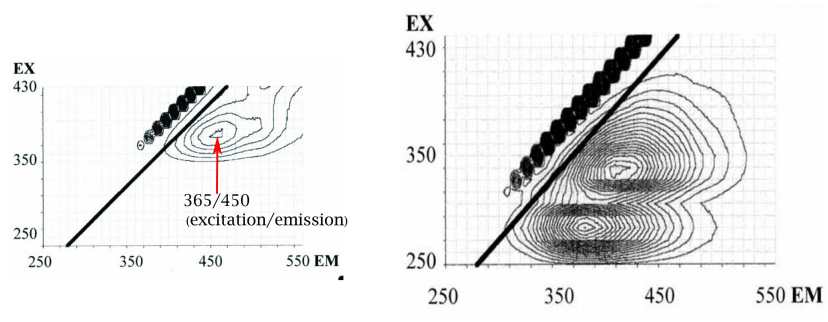

(a) Excitation/emission of healthy urine at 1:300 dilution

(b) Excitation/emission of healthy urine at 1:30 dilution

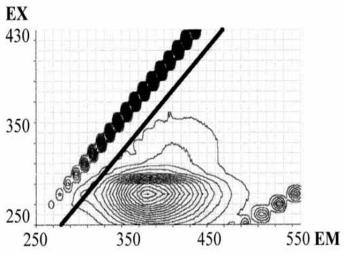

(c) Excitation/emission of healthy urine for 1:500 dilution

Figure 2.26: Urine excitation/emission matrix taken from Kusnir *et al* (2005).

Thus spectral pattern observed in the study is in agreement with the result of Kusnir *et al* (2005).

SFS of diluted healthy human urine

A 1:300 dilution was used for recording the SFS. 1:300 dilution was an optimum dilution, so as to observe the emission of both group A and group B fluorophores. The results of synchronous measurements of this study are shown in the Figure 2.14 and 2.15. Compared to the SFS spectra of undiluted healthy human urine, the spectra of diluted samples were different. Irrespective of the $\Delta\lambda$ offset, the intensity of fluorescence due to group B fluorophores reduced drastically as compared to that

in undiluted samples (Figure 2.27 c).

For $\Delta\lambda$ 60 and $\Delta\lambda$ 70, clear sharp peaks at 280 nm, which may be contributed mostly by tryptophan and other group A fluorophores (Figure 2.27 a and b). The emission with 320 nm excitation was also prominent, were observed irrespective of the offset value (Figure 2.14 and 2.15). The behavior of spectral pattern observed by SFS is in total agreement with the excitation/emission matrix results which have been previously discussed for healthy human urine.

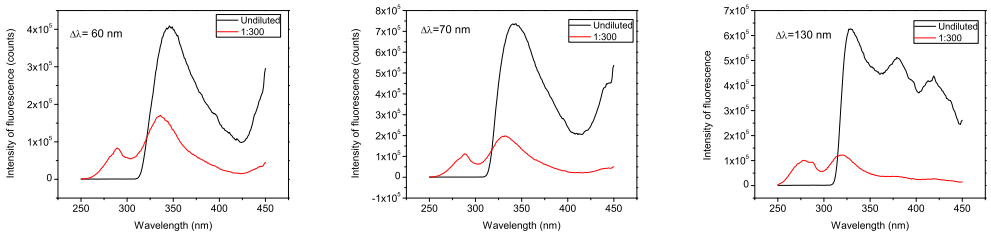

(a) (b) (c)

Figure 2.27: Comparison of SFS for different offset and dilutions. (a), (b) and (c) are $\Delta\lambda$ offset values 60, 70 and 130 respectively. (−) undiluted urine and (−) urine diluted at 1:300 with double distilled water.

Comparison of SFS results of this study to that of earlier studies

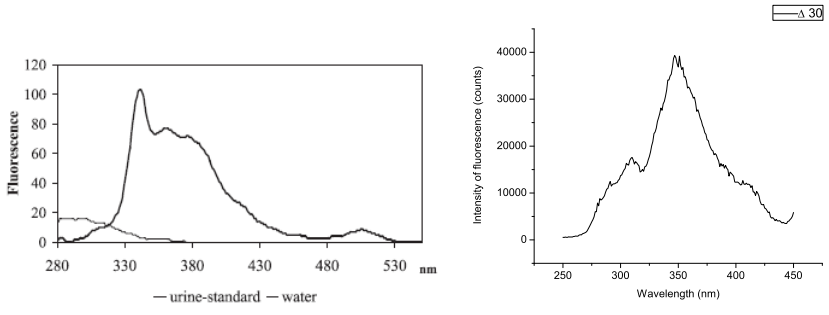

(a) (b)

Figure 2.28: Comparison of the SFS result with findings of Dubayova *et al* for $\Delta\lambda$ = 30 nm offset. a: data from Dubayova *et al*; b: SFS data of this study.

Dubayova *et al* statistically represented urine composition of a healthy child for $\Delta\lambda$ of 30 nm offset (1:300 dilution). Data from this study for $\Delta\lambda$ of 30 nm offset (1:300 dilution) is shown in Figure 2.28. The features of both spectra were similar, having a dominant peak near 350 nm excitation.

2.6 Summary

In this Chapter, autofluorescence of undiluted as well as diluted human urine with UV excitation is described. Various techniques including emission spectra, excitation/emission matrices and SFS were utilized to explore urine fluorescence. Two different spectral patterns were observed for undiluted healthy human urine. Despite the biological variability, the spectral characteristics of undiluted urine showed relatively low autofluorescence at shorter UV (250-300 nm) excitation when compared with 300-450 nm excitation. However, with dilution, the fluorescence intensity increased remarkably (this is further discussed in Chapter 3).

This study had a particular focus on group A fluorophores (excited at 250-300 nm). This is because group A fluorophores such as tryptophan and its metabolites can vary with aging and certain medical conditions. In order to establish the level of individual variability with the shorter UV excitation wavelengths (290 nm) in this study, a larger set of samples taken from a mixed age and gender population were analysed. At 290 nm, the fluorescence spectra for all the healthy urine sample samples had a similar spectral pattern with some intensity variations.

It was also observed that storing the urine sample in the refrigerator (4^0C) for 96 hrs, did not affect its fluorescence.

3

Factors influencing fluorescence quenching of human urine

3.1 Introduction

This Chapter describes the human urine fluorescence by identifying and quantifying the factors responsible for low intensity of fluorescence when excited at 250-300 nm (vide, Chapter 2). In addition, due to the significant role of indoxyl sulfate in health, the contribution of its fluorescence in human urine is a major focus of this Chapter. In this study, it has been identified that the three most abundant, high quantum yield fluorophores excited at 250-300 nm, indoxyl sulfate, tryptophan and 5-hydroxyindole-3-acetate and the abundant non-fluorescent urine component ammonium, play a significant role in the quenching of urine fluorescence when excited at 250-300 nm. A clearer understanding of the interactions between the key fluorophores and other components in urine is essential to broaden the potential of fluorescence as a diagnostic tool.

3.1.1 Basic concepts of fluorescence quenching

The phenomenon of fluorescence involves the absorption of photons from a primary exciting light beam to produce an atom (or molecule) in an excited state. It is possible for an excited species to be de-excited by a non-radiative process as a result of collisional interactions with other species present in the environment. The resultant reduction in observed fluorescence intensity is generally referred to as quenching of the fluorescence.

Fluorescence quenching can be brought about in many ways such as (refer, Appendix for more details):

1. **Fluorescence quenching by inner filter effect**

   The recorded fluorescence intensity may not be proportional to the fluorophore concentration due to a well known phenomenon known as the inner filter effect. This can be due to high absorption of excitation light by the sample (primary inner filter effect) and or by reabsorption of emitted light (secondary inner filter effect) [26, 27].

2. **Fluorescence quenching by energy degradation**

   The quencher can reduce the energy of the excited state by several ways, such as by conversion of the excited molecule into the triplet state, by electron transfer, or by energy transfer.

3. **Fluorescence quenching by chemical change**

   If a fluorescent compound (fluorophore) undergoes a chemical change as a result of the presence of a second compound, it could be converted into a non-fluorescent product [28].

3.1.2 Fluorescence quenching in human urine

As mentioned in the Chapter 2, human urine contains large number of fluorophores which can become excited in the UV. However, a reduced fluorescence observed for undiluted human urine under UV excitation. Similar finding was also observed by Leiner *et al* [17]). This phenomenon in human urine is generally attributed to the quenching effect.

Since human urine is a complex and highly variable medium, it is difficult to attribute the fluorescence quenching to a single mechanism as there could be many possible influencing factors such as energy transfer, concentration quenching and inner filter effect [20].

As the major fluorophores excited in the UV in the human urine are tryptophan and its metabolites (refer to Table 3.1), efforts to understand the fluorescence properties of a mixture of these compounds will provide a good foundation to understand the urine fluorescence.

3.1.3 Significance of indole, tryptophan and their derivatives in human urine fluorescence

Name	Excitation/ Emission (nm)	Approx daily excretion μmol	References
Melatonin	283/333		[21]
Tryptophan	280/360	50.0($\pm$ 27)	
Indoxyl sulphate	290/380	300.0	[17]
Indolyl-3-acetate	290/360	32.3	[17]
5-Hydroxyindole-3-acetate	300/345-355	24	[17]
5-Hydroxytryptophan	295/340	-	[17]
Kynurenine	370/490	14	[17]
5-Hydroxykynurenine	375/460	-	[17]
3-Hydroxykynurenine	365/460	27	[17]

Table 3.1: List of indole, tryptophan and its derivative fluorophores in human urine.

Table 3.1 shows the list of indole, tryptophan and their derivatives in human urine. It is apparent from Table 3.1 that fluorescence of human urine excited at UV

has major contributions from indole, tryptophan and their derivatives.

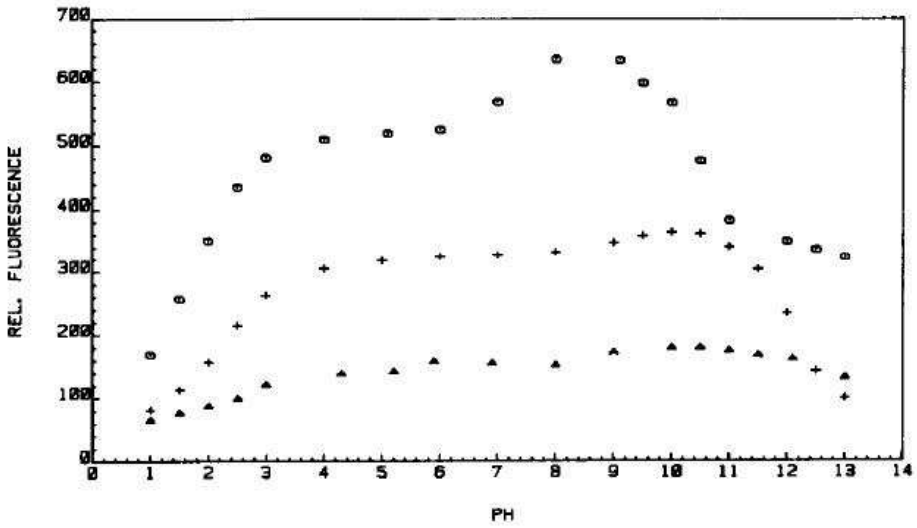

Figure 3.1: Plot of fluorescence intensity of human urine vs pH at various excitations and emissions; (+) at 290/380 nm; (△) at 325/420 nm.

Indeed, earlier literature assigned the fluorescence peak observed in human urine at 370 nm and 420 nm when excited at 290 nm and 325 nm, respectively to indole derived species. This is supported by the pH dependence curve which is typical of indole compounds (refer Figure 3.1) [17].

Fluorescence properties of indole, tryptophan and their derivatives

Indole, tryptophan and their derivatives are known to be highly sensitive to the local molecular environment [29]. In 1961 Van Duuren *et al* demonstrated that pronounced changes are observed in the fluorescence emission spectra of indole and substituted indoles with a change of the solvent. The authors stated that dielectric constants of solvents and hydrogen bond formation account for the change in spectral properties of indole fluorescence [30].

The temperature dependence of indole quantum yield in water has been explained by Edward *et al* in 1970 in terms of two non radiative de-excitation processes. They

proposed that the temperature dependent process may be associated with electron ejection from the excited indole [31].

Fluorescence decay of indole in different solvents was analysed in 1971 by Lauder *et al* [32]. The authors mentioned that the solvent effect of indole fluorescence is complex with fluorescence maximum shifting to higher wavelengths in more polar solvent [32].

In 1995 Lipinski *et al* [33], adapted a semiempirical all-valence method together with a virtual charge method to represent solvent effect on the spectroscopic properties of indole. The authors concluded that in the non-polar solvents fluorescence of indole originates from the L_b state whereas in the polar solvents the L_a emission occurs (L_b and L_a represent the state of energy level). The other finding was that the large shift observed in polar solvents can be explained as a combination of normal solvent effect and specific interactions between the excited indole ring and solvent molecule via charge transfer mechanism [33].

Later in 1999, Lakowicz mentioned that the fluorophores that are sensitive to the solvent polarity are typically those that display a large charge separation in the excited state. But its spectral properties cannot be totally explained by the change in dipole moment in the excited state [29].

Lakowicz explained that the complex formation of indole and tryptophan are due to presence of two overlapping transition to the $1L_a$ and $1L_b$ states of indole. In case of tryptophan, indole and their derivatives the long wavelength absorption (240 nm - 300 nm) consist of two overlapping transitions to $1L_a$ and $1L_b$ excited states. These states have similar energies; depending on the environment either state can have lower energy. It has to be noted that emission occurs from the lowest energy state (Kasha's rule). The $1L_a$ and $1L_b$ have different direction in the molecules. Since each state has different dipole moment so that $1L_a$ and $1L_b$ respond differently to

solvent polarity [29].

Due to the above mentioned facts, interpretation of fluorescence of indole and its derivatives, especially in human urine is a challenging task. However, in the study it was decided to primarily focus on those regions of human urine fluorescence spectra which could at least tentatively be attributed to specific indole fluorophores due to their comparatively high concentration. One such example is indoxyl sulfate.

3.1.4 Indoxyl sulfate

Indoxyl sulfate is the major metabolite of indole [34]. In the body it originates from the dietary protein-derived tryptophan which is metabolized into indole by tryptophanase produced by intestinal bacteria. Indole is absorbed into the blood from the intestine, and is metabolized to indoxyl sulfate in the liver. Indoxyl sulfate is normally excreted into urine (Figure 3.2). Its daily excretion is 300 μmol, and in urine it is the most abundant fluorophore [17, 18].

Indoxyl sulfate (IS) is also known to be a uraemic toxin that accelerates the progression of chronic kidney disease (CKD) [35]. Serum IS levels are increased in patients with CKD [36]. Indoxyl sulfate is known to stimulate glomerular sclerosis and interstitial fibrosis [37]. Some studies suggest that indoxyl sulfate is also involved in oxidative stress in endothelial cells [38].

3.2 Experimental methodology

3.2.1 Urine Samples

Urine samples were collected from a local pathology laboratory where they were analyzed for pH, protein, glucose, bilirubin, nitrate, specific gravity, blood, ketones, urobilinogen and leukocyte esterase. The presence of red blood cells, white blood cells, casts, epithelial cells and crystals was also tested for these samples (using iQ200

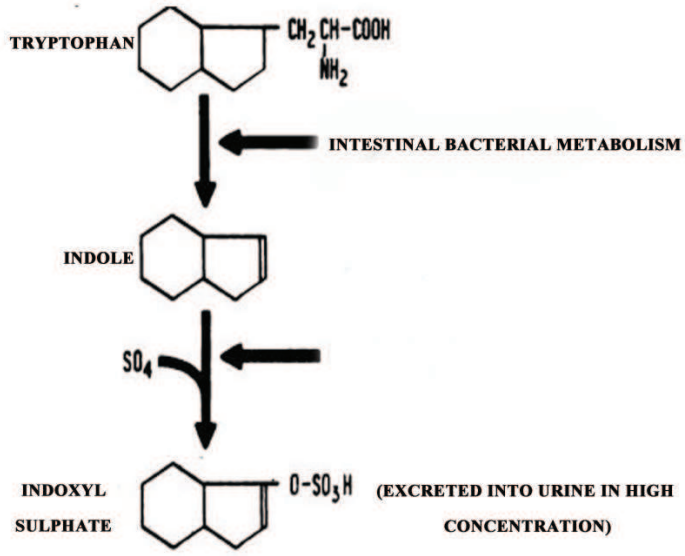

Figure 3.2: Pathway of indoxyl sulfate formation in the body [39].

Sprint, IRIS Diagnostics Division, Chatsworth, CA). Semi-quantitative culture on chromogenic agar plates was also carried out to test for the presence of bacteria. A total of 46 human urine samples were used in this study, including samples from 35 males (age 2-90 years) and 11 females (age 5-90 years). These samples showed no abnormal laboratory findings, i.e., they were culture-negative as well as negative for other abnormal findings such as protein, glucose, bilirubin, nitrate, specific gravity, blood, ketones, urobilinogen, leukocyte esterase and they had pH within the range of 5-7. They are referred to as healthy human samples. All the urine samples were stored in the refrigerator (4^0C) and examined within 48 hours after collection. Urine dilutions when required were made using double distilled water.

3.2.2 Other materials and reagents

l-Tryptophan, indoxyl sulfate and 5-hydroxyindole-3-acetate were obtained from SigmaAldrich (Sydney, Australia). Stock solutions of 300 μmol indoxyl sulfate, 50 μmol of l-tryptophan and 24 μmol of 5-hydroxyindole-3-acetate were prepared in deionised

water. The required dilutions of ammonia (Unilab, Sydney, 28%, v/v) were made in milli-Q water. In addition, simulated urine that consisted of a mixture of 300 μmol indoxyl sulfate, 50 μmol of l-tryptophan and 24 μmol of 5-hydroxyindole-3-acetate (at approximately physiological concentrations) with a pH of 5.1 was also utilised in this study.

3.2.3 Measurement of autofluorescence

The fluorescence was measured using a Fluorolog Tau3 system (JY Horiba, Edison, NJ) in 10mm quartz cuvettes at room temperature. The fluorescence emission spectra after excitation at various wavelengths as well as the excitation/emission matrices (EEMs) were obtained. These three-dimensional plots of fluorescence intensity as a function of excitation and emission wavelengths represent the complete fluorescence characteristics of the sample. In order to cover the broad spectral region of relevance in the most time-efficient way, four separate smaller EEMs were obtained and digitally integrated into a single one using MATLAB. In EEM measurements the spectral band passes were 5 nm in both excitation and emission. The spectra were corrected for optical system response.

3.2.4 Measurement of absorption

The absorption was measured using double beam CARY absorption spectrometer system (Varian Inc., USA) in 10mm quartz cuvettes at room temperature.

3.2.5 Liquid chromatography-mass spectrometry analysis

The mass spectrum was obtained using a Shimadzu LCMS 2010 EV system with an SIL 20 AL autosampler. The mobile phase was water:acetonitrile (9:1, v/v) in the isocratic mode, with a flow rate of 0.2 mL/min. The analysis was performed with the Electron Spray Ionisation (ESI) probe.

3.3 Results

3.3.1 Absorbance spectra of human urine and various fluorophores in urine

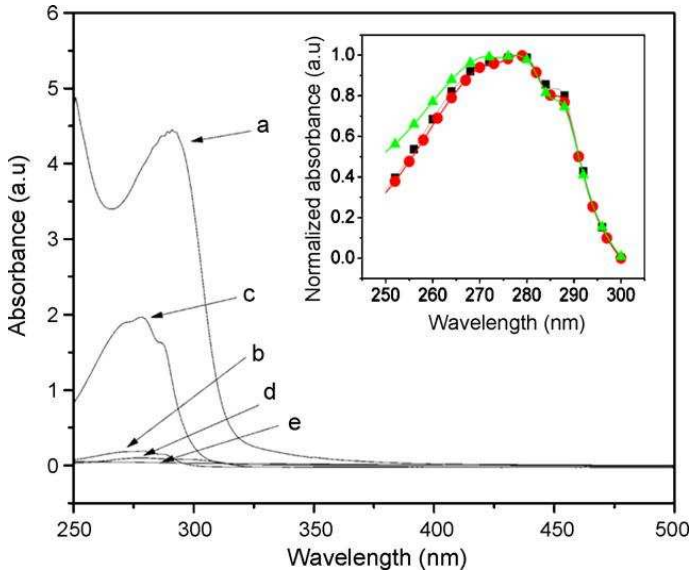

Figure 3.3: Comparison of optical absorption spectra.(a) Healthy human urine, (b) tryptophan 50 μmol, (c) indoxyl sulfate 300 μmol, (d) 5-hydroxyindole-3-acetate 24 μmol, which were all diluted 1:10 in double distilled water and (e) 19 mol of ammonium in distilled water. The inset shows the absorption spectra of 300 μmol of indoxyl sulfate. (−) undiluted, (−) diluted 1:1, (−) diluted 1:30.

The absorption spectrum of healthy human urine (Figure 3.3a) indicates that the absorption, especially in the region 250-350 nm, is quite high (note that the absorption spectra in Figure 3.3 were taken at 1:10 dilution as compared to physiological conditions). Thus, Figure 3.3a indicates that the primary inner filter effect will be a significant effect in the range below 300 nm (due to high absorption), especially for undiluted urine. At the same time, the absorption in 300-500nm range is negligible; hence, the secondary inner filter effect is not critical.

From Figure 3.3c, it is evident that indoxyl sulfate at physiological concentration contributes significantly to the total absorption of undiluted urine. The absorption

maximum of indoxyl sulfate was observed at 280 nm. However, tryptophan and 5-hydroxyindole-3-acetate did not show significant absorption compared to indoxyl sulfate. In addition, the almost identical absorption for indoxyl sulfate at physiological concentration (300 μmol) and at two dilutions (1:1 and 1:30) suggests there is less possibility of aggregation (Figure 3.3 inset).

3.3.2 Excitation/emission matrices of indoxyl sulfate at 300 μmol concentration

The Figure 3.4 shows the excitation/emission matrix of 300 μmol indoxyl sulfate. It is evident that indoxyl sulfate has a broad fluorescence spectrum, with the maximum emission peak at 380 nm when excited at 300 nm.

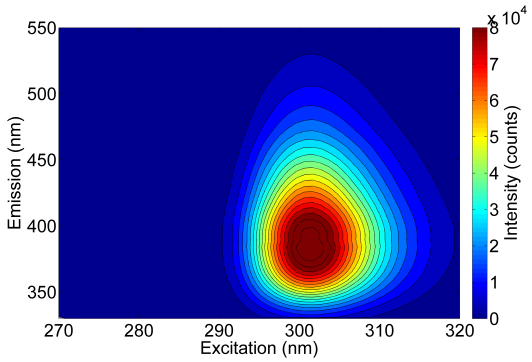

Figure 3.4: Excitation/emission matrices of 300 μmol indoxyl sulfate (pH 5.1).

3.3.3 Effect of dilution on excitation/emission matrices of indoxyl sulfate

The typical excitation/emission matrices of indoxyl sulfate for dilutions 1:10 and 1:1000 are presented in Figure 3.5. All the dilutions were made using double distilled water. At 1:10 dilution, an emission peak can be clearly seen at 380 $\pm$10 nm when excited at 275 $\pm$10 nm. A similar spectral patter with a distinct peak at 380 nm when excited at 280 $\pm$5 nm was also observed at 1:1000 dilution with lower

fluorescence intensity. It is also evident that the EEMs of indoxyl sulfate at the dilutions 1:10 and 1:1000 are different as compared to the EEM of indoxyl sulfate at physiological concentration of 300 μmol, the latter showing a peak at 300 nm/380 nm) (Figure 3.4).

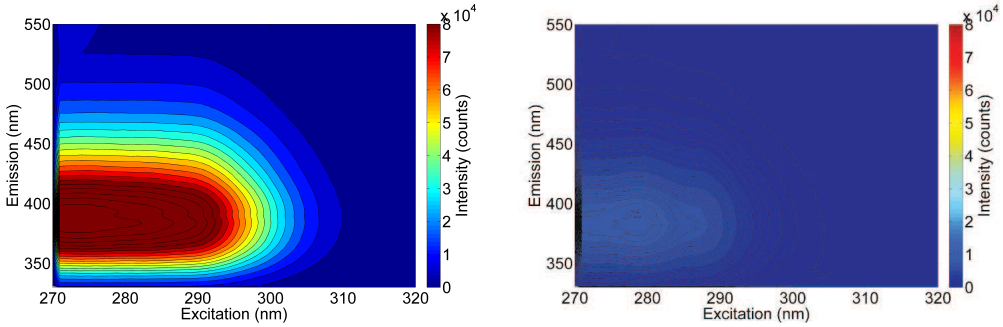

(a) Indoxyl sulfate at 1:10 (pH 5.3) (b) Indoxyl sulfate at 1:1000 (pH 5.5)

Figure 3.5: Excitation/emission matrices of indoxyl sulfate at 1:10 and 1:1000 dilution.

3.3.4 Inner filter corrected excitation/emission matrices of indoxyl sulfate

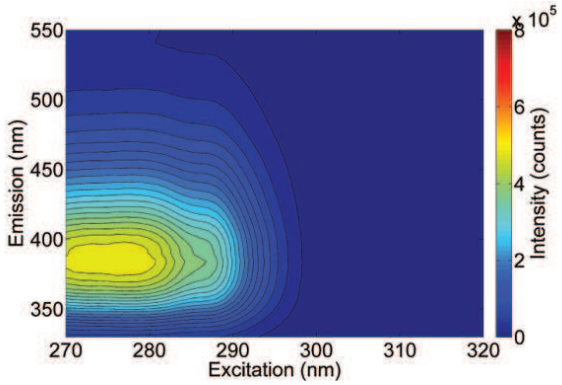

Figure 3.6: Inner filter corrected excitation/emission matrices of 300 μmol indoxyl sulfate (pH 5.1).

Figure 3.6 shows the inner filter corrected excitation/emission matrices of 300 μmol indoxyl sulfate. The peak emission was observed at 380 $\pm$10 nm when excited

at 275 ±5 nm. The inner filter corrected spectrum of 300 μmol indoxyl sulfate (physiological concentration)(Figure 3.6) as compared to its uncorrected spectrum (Figure 3.4) shows that there is a blue shift of 15 nm in the peak excitation. In addition, there is also a change in the emission spectra with higher intensity. These results show that spectral variation in indoxyl sulfate at physiological concentration is due to concentration quenching (high inner filter effect).

Similar spectral features were observed when a comparison of corrected EEM spectra of indoxyl sulfate with EEMs of uncorrected indoxyl sulfate dilutions (1:10 and 1:1000, Figure 3.5) was made. This result shows that at higher dilution the inner filter effect is no longer present.

3.3.5 Indoxyl sulfate fluorescence as a function of concentration

Figure 3.7 shows the peak fluorescence intensity at 280 nm/380 nm, of indoxyl sulfate at various concentrations, before and after correcting for the inner filter effect. It shows that the fluorescence intensity at 300 μmol concentration after correcting for the inner filter effect is lower than that of the 30 μmol concentration, confirming that at physiological concentration (300 μmol), indoxyl sulfate exhibits concentration quenching.

3.3.6 Dimer formation of Indoxyl sulfate at Physiological concentration

Electron Spray Ionisation- Mass Spectroscopy (ESI-MS) analysis using Liquid chromatography/mass spectrometry (LCMS) was carried out in negative ion mode for indoxyl sulfate at physiological concentration (Figure 3.8). The atomic weight of indoxyl sulfate potassium salt is 251 [40]. The atomic weight of potassium is 39. In the mass spectrometer, the potassium part of indoxyl sulfate is separated. Therefore

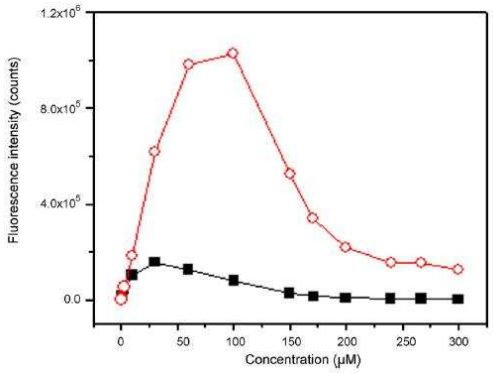

Figure 3.7: Fluorescence intensity at 280 nm/380nm versus concentration of indoxyl sulfate; (−) uncorrected data; (−) data corrected for the inner filter effect.

the total weight reduces to 212 (ie 251-39=212). The peak 212 in the Figure 3.8, represents the monomer and peak 463 (2x212+39) corresponds to its dimer (Figure 3.8).

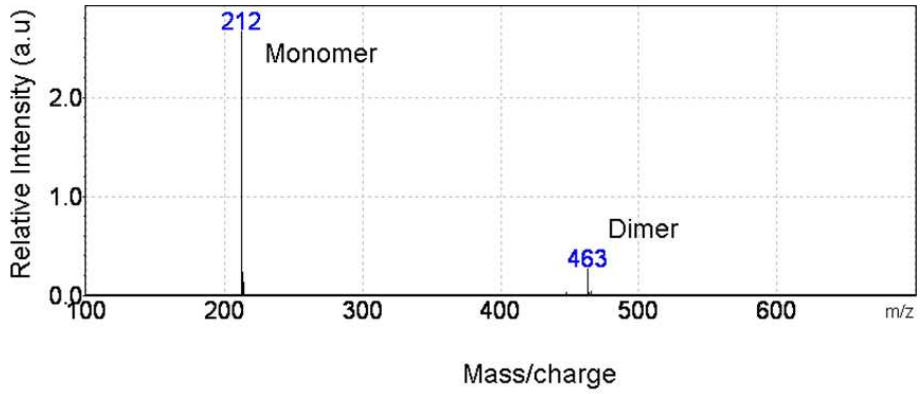

Figure 3.8: Liquid chromatography/mass spectrometry (LCMS) plot showing dimer formation in 300 μmol of indoxyl sulfate.

3.3.7 Excitation/emission matrices of 'simulated urine'

'Simulated urine' consisted of a mixture of 300 μmol indoxyl sulfate, 50 μmol of l-tryptophan and 24 μmol of 5-hydroxyindole-3-acetate (at approximately physiological concentrations) with a pH of 5.1. The Figure 3.9 shows the excitation/emission

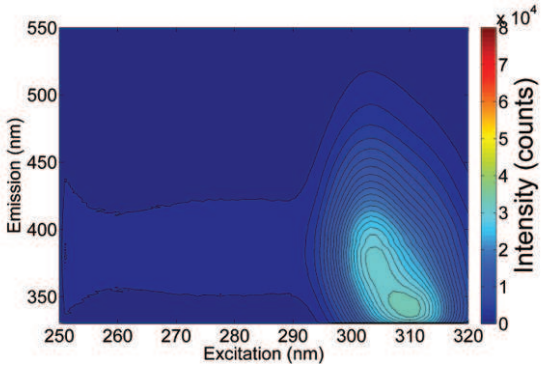

Figure 3.9: Inner filter corrected excitation/emission matrices of 'simulated urine' (pH 5.1).

matrices of 'simulated urine'. The fluorescence intensity of the 'simulated urine' was very weak, with a peak at 340 nm when excited at 310 nm.

3.3.8 Effect of dilution on excitation/emission matrices of 'simulated urine'

The typical excitation/emission matrices of 'simulated urine' for dilutions 1:10 and 1:1000 are presented in Figure 3.10. All the dilutions were using double distilled water. At 1:10 dilution, an emission peak can be clearly seen at 380 ±10 nm when excited at 280 ±10 nm. A similar spectral patter was also observed at 1:1000 dilution with lower fluorescence intensity.

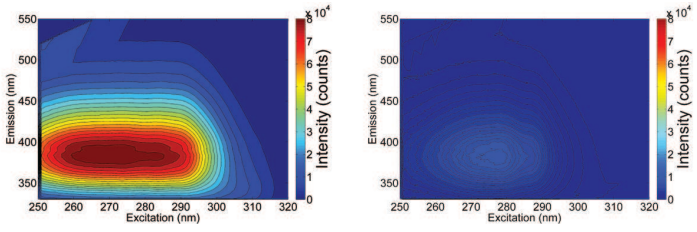

(a) Simulated urine at 1:10 (b) Simulated urine at 1:1000

Figure 3.10: Excitation/emission matrices of simulated urine at 1:10 and 1:1000 dilution.

It is also evident that the EEMs of simulated urine at dilutions 1:10 and 1:1000

are different as compared to the EEM of undiluted simulated urine (Figure 3.9). The fluorescence intensity of the simulated urine was very weak, with a peak at 340 nm when excited at 310 nm (Figure 3.9) as compared to its dilutions (1:10 and 1:1000), having peak emission at 380 ±10 nm at 280 ±10 nm (Figure 3.10).

3.3.9 Inner filter corrected excitation/emission matrices of simulated urine

The Figure 3.11 shows the excitation/emission matrices of 'simulated urine'. The peak emission was observed at 380 ±10 nm when excited at 275 ±5 nm. Inner filter corrected spectrum of simulated urine (Figure 3.11) as compared to its uncorrected spectrum (Figure 3.9), shows that there is a blue shift of 30 nm in the peak excitation with a change in peak emission from 340 nm to 380 nm. In addition, the fluorescence intensity for the corrected simulated urine was much higher than the uncorrected simulated urine. These results show that spectral variation in simulated urine is due to concentration quenching (high inner filter effect).

However, similar spectral features were observed when a comparison of corrected EEM spectrum of simulated urine to its dilutions (1:10 and 1:1000, uncorrected)(Figure 3.5). This result shows that with higher dilution the inner filter effect is no longer present.

3.3.10 Simulated urine fluorescence as a function of concentration

Figure 3.12 shows the peak fluorescence intensity at 280 nm/380 nm, of simulated urine at various concentrations, before and after correcting for the inner filter effect. Confirming that simulated urine exhibits concentration quenching at physiological concentartion (self-quenching).

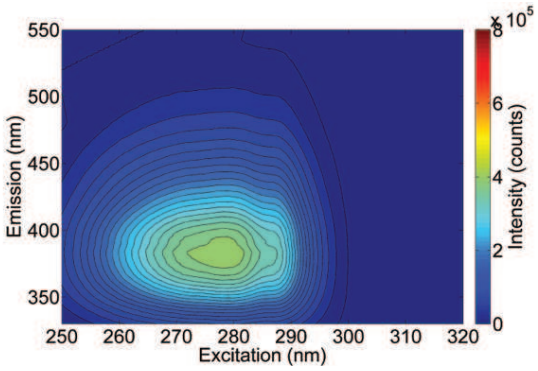

Figure 3.11: Excitation/emission matrix of simulated urine (pH 5.1) after inner filter correction.

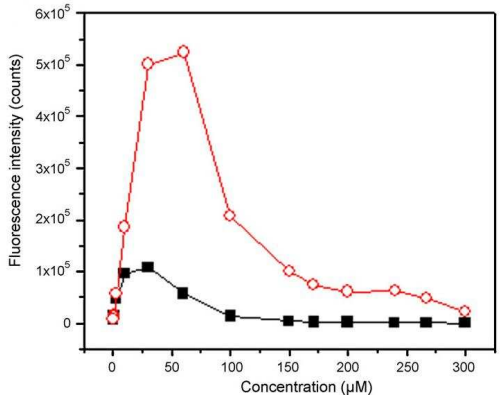

Figure 3.12: fluorescence intensity at 280 nm/380nm versus concentration of simulated urine; (−) uncorrected data; (−) data corrected for the inner filter effect note the different colour scale in.

3.3.11 Quenching of the fluorescence spectra of simulated urine by ammonium

Figure 3.13 shows that the addition of a physiological amount of ammonium lowers the fluorescence of the simulated urine by a factor of two. From Figure 3.13, it is also evident that, not only does the quenching disappear, but the fluorescence increases drammatically when the sample is diluted by a factor of 1:10. This result clearly indicate that the quenching mechanism by ammonium on simulated urine is a reversible process.

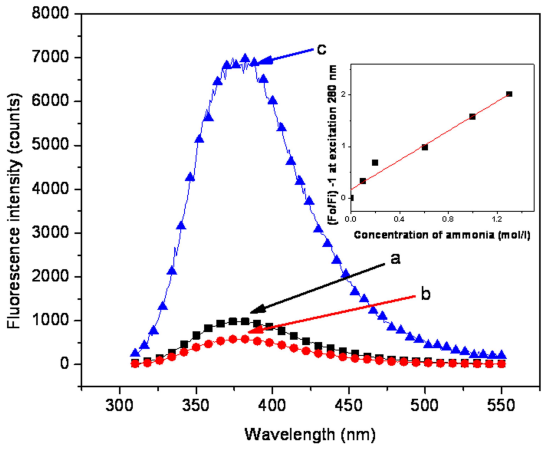

Figure 3.13: Effect of the addition of varying amounts of ammonium on the fluorescence spectra of simulated urine containing tryptophan (50 mol), indoxyl sulfate (300 μmol) and 5-hydroxyindole-3-acetate (24 μmol), at 280 nm excitation.(a) Simulated urine, without any ammonium, (b) simulated urine with 19 mmol of ammonium and (c) simulated urine with 19 mmol of ammonium, diluted 1:10 with double distilled water. The inset shows the Stern-Volmer plot representing the fluorescence quenching of the simulated urine by ammonium (fluorescence intensity at 380 nm for excitation at 280 nm as a function of ammonium concentration).

The Stern-Volmer plot is shown in Figure 3.13(inset). The SternVolmer quenching constant was calculated using the following equation

$$F_0/F = 1 + K[Q] \tag{3.1}$$

where F_0 and F are the fluorescence intensities in the absence and presence of quencher (ammonium), [Q] is the concentration of quencher and K is the Stern-Volmer constant. The K value was calculated to be approximately 1.4 L/mol.

3.4 Discussion

3.4.1 Spectral characteristics of undiluted healthy human urine

As mentioned in Chapter 2, fluorescence characteristics of urine are variable and strongly sample-dependent. Two examples of excitation/emission matrices of undiluted healthy samples with different spectral features are shown in Figure 3.14 (a and b). The observed differences are due possibly to variations in the relative composition of fluorophores in the urine. The fluorescence is observed mainly at 300-450 nm excitation wavelength range. The identification of the fluorescence features is difficult due to the similarities in the spectral properties of the component fluorophores and large spectral widths. However, the spreading of the spectral features in a two-dimensional EEM makes the task easier. The major fluorophores which are likely to contribute to urine fluorescence at 300-450 nm excitation are 4-pyridoxic acid, pterins, flavins and porphyrins [17, 18].

4-pyridoxic acid is a strong fluorescent compound which has emission maximum at 420 nm at 317 nm excitation [18]. In addition, 3-hydroxynthranilic acid (320 nm/415 nm) and xanthine (315 nm/435 nm) also likely to contribute when excited in this region [18]. Riboflavin is also known to contribute to urine fluorescence spectra, with emission maxima ranging from 510 to 531 nm for excitation in the range of 436 to 455 nm.

It is apparent from Figure 3.14 (a and b) that the autofluorescence of urine excited in 250-300 nm range is very weak when compared to longer UV (300-450 nm) excitation. This property was consistently observed in all samples examined in this study and in the earlier work (Chapter 2). In order to establish the level of individual variability at the short UV excitation wavelengths a larger set of 40 samples taken from a mixed age/gender population (Figure 3.14 c) were used. The

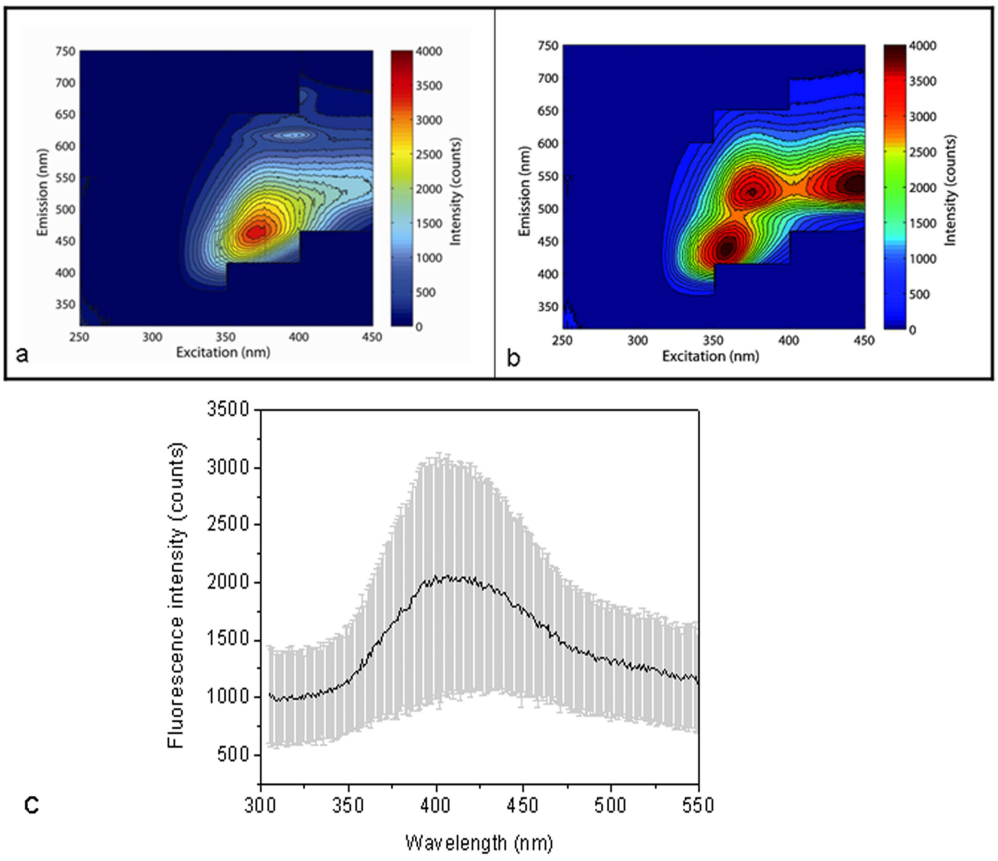

Figure 3.14: (a and b) Excitation/emission matrices of two representative undiluted healthy human urine samples. (c) The mean emission spectrum for 40 undiluted healthy human urine samples at 290 nm excitation (−). The error bars represent standard deviation.

fluorescence spectra when excited at 290 nm for all these samples have a similar pattern with some intensity variations. The peak fluorescence was observed at 420 ±15 nm and the peak intensity varied by ±50%. It was unable to identify any sub-classes in these spectra based on gender or age, by using the Principal Component Analysis.

Thus, it was established that the key fluorescence features of undiluted healthy human urine are observed at 300-450 nm excitation and are highly variable, while shorter UV excitation produces only very weak fluorescence that is much more con-

sistent. This finding is in agreement with the earlier literature that introduced the terms group A and group B fluorophores excited at 250-300 nm, and 300-450 nm, respectively [17, 18]. Accordingly, the EEM in Figure 3.14 (a and b) shows very prominent but less abundant group B fluorophores, some of which are of direct dietary origin and highly variable, while the group A fluorophores, which are more abundant, are barely observed. Such low intensity of group A fluorophores is generally attributed to fluorescence quenching [17, 18].

3.4.2 Spectral characteristics of diluted healthy human urine

The dilution of the urine profoundly affects the excitation/emission matrices. This is shown in Figure 3.15 where the EEMs for healthy human urine at various dilutions (1:30, 1:300 and 1:1000) are compared. In undiluted urine observed features at 365 nm/470 nm (where 365 nm refers to peak excitation wavelength and 470 nm to peak emission wavelength), 380 nm/520 nm and at 400 nm/625 nm (attributable to group B fluorophores). These disappear at 1:30 dilution, and a moderately intense emission peak at 325 nm/425 nm emerges (tentatively attributed to 4-pyridoxic acid [17]) and also a very weak 290 nm/350 nm feature attributable to one of group A fluorophores. At 1:300 dilution, the peak at 325 nm/425 nm practically disappears but the 290 nm/350 nm peak becomes more intense. With 1:1000 dilution, this peak dominates the spectrum. This result shows that by adjusting the dilution, especially in the range from 1:30 to 1:1000, it is possible to enhance the emission of various fluorophores that are not observable without dilution. This is because the undesired absorption of excitation light at lower dilutions that underpins the inner filter effect is reduced or eliminated at higher dilutions [26]. Thus, high dilution expands the spectral window available for fluorescence observation. Consequently, high dilution makes it possible to start observing group A fluorophores (Figure 3.15 b and c).

As the dilution is increased, at some point, the quenching starts to be reduced as well, and this additionally enhances the fluorescence from group A fluorophores (Figure 3.15 2d). The details of these two effects and the influence they have on the EEMs of urine will be discussed now.

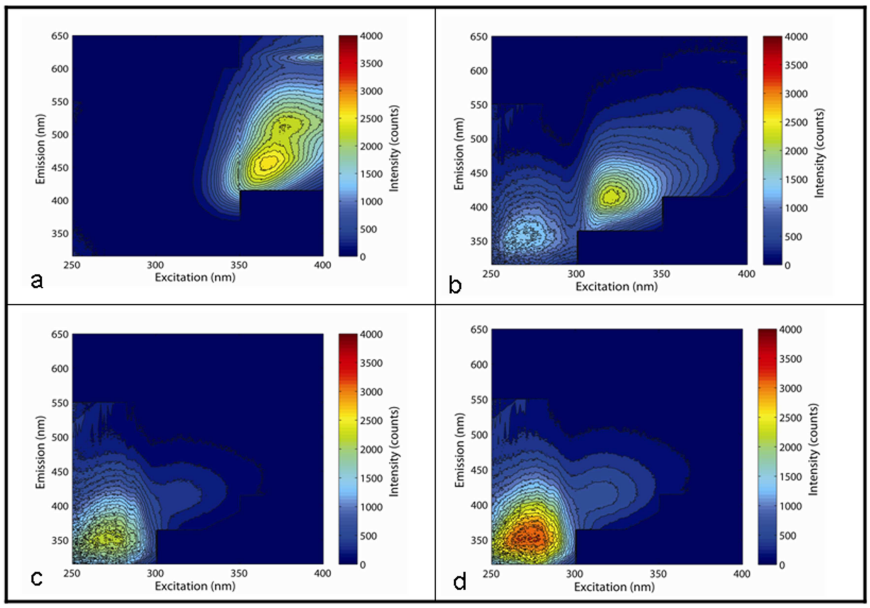

Figure 3.15: Excitation/emission matrices of healthy urine sample.(a) Undiluted urine and (b-d) diluted 1:30, 1:300 and 1:1000, respectively.

3.4.3 Inner filter correction for the EEMs

The absorption spectrum of human urine (Figure 3.16a) indicates that the absorbance, especially in the region 250-350 nm, is quite high (note that the absorption spectra in Figure 3.16 were taken at 1:10 dilution as compared to physiological conditions). It is well known that in order to avoid the inner filter effect, the optical density of the sample for fluorescence measurement should be less than 0.05

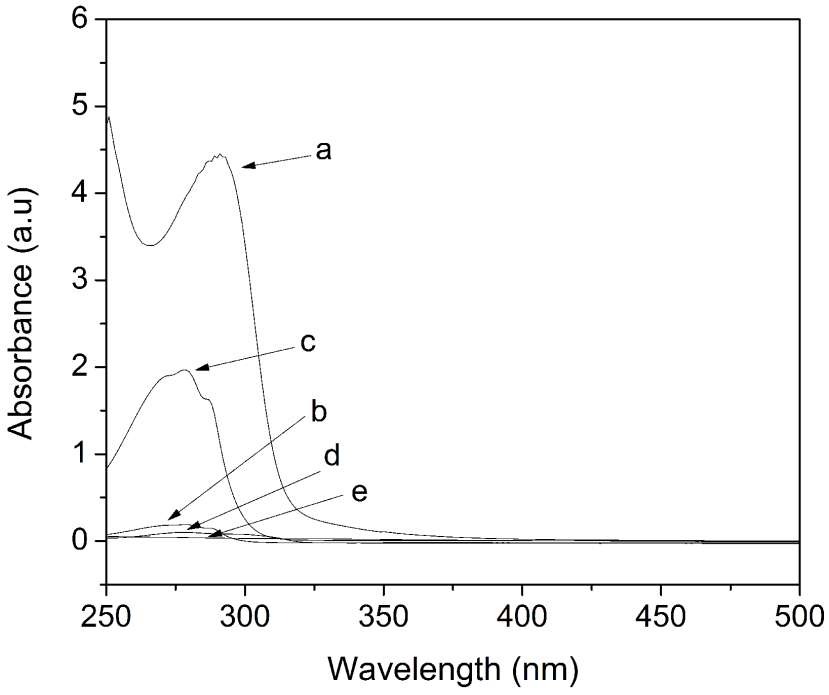

Figure 3.16: Comparison of optical absorption spectra. (a) Healthy human urine, (b) tryptophan (50μmol), (c) indoxyl sulfate (300μmol), (d) 5-hydroxyindole-3-acetate (24μmol), which were all diluted 1:10 in double distilled water and (e) 19 mmol of ammonium in distilled water.

[26,29,41]. Thus, Figure 3.16a indicates that the primary inner filter correction factors are significant in the range below 300 nm, especially for undiluted urine. At the same time, the absorbance in 300-500 nm range is negligible; hence, the secondary inner filter correction (equation not shown) is not required. On these grounds EEMs of this study and the underlying spectra have been corrected by using Equation 3.2 so that the issue of quenching can be addressed.

$$\beta_i = (\alpha_i L_l)/1 - exp(-\alpha_i L_l) \tag{3.2}$$

where β_i is the inner filter correction factor by which the spectra need to be

multiplied, α_i is the optical density for the sample at the excitation wavelength and Li is the cuvette dimension. In deriving this equation, two assumptions are made that the optical density for the emitted light is negligible and the fluorescence is collected from the full length of the cuvette. This correction requires the knowledge of the absorption spectra that are presented in Figure 3.16.

It is illustrative to see the influence of the inner filter effect in the EEM matrices of a selected component of urine, indoxyl sulfate (Figure 3.17), which produces dramatically varying spectral features as the dilution is varied. The EEM of indoxyl sulfate at physiological concentration of 300 μmol shows a peak at 300 nm/380 nm. At 1:10 and 1:1000 dilutions, the peak excitation changes to 280 nm but the emission maximum remains the same, i.e., 380 ($\pm$10) nm. This result shows that interpreting peaks in emission spectra or excitation/emission matrices should to be done with a great deal of caution, as major shifts and spectral shape changes can be observed at higher fluorophore concentration, when the inner filter effect is operational. Indeed, Figure 3.16 c indicates that indoxyl sulfate at physiological concentration contributes significantly to the total absorption of undiluted urine (OD = 17 at peak) and that the fluorescence data for indoxyl sulfate must be corrected for the inner filter effect. However, these matrices can be corrected, by using the inner filter correction Equation 3.2, provided the inner filter effect does not reduce fluorescence to unobservable levels. Figure 3.17 d shows an EEM corrected for the inner filter effect, and note that the corrected EEM shows a close similarity with the EEM for a highly diluted fluorophore (Figure 3.17 c).

3.4.4 Fluorescence quenching in urine

With the inner filter effect fully accounted for, it was able to establish the extent of fluorescence quenching in this complex fluid. In order to capture the key features of

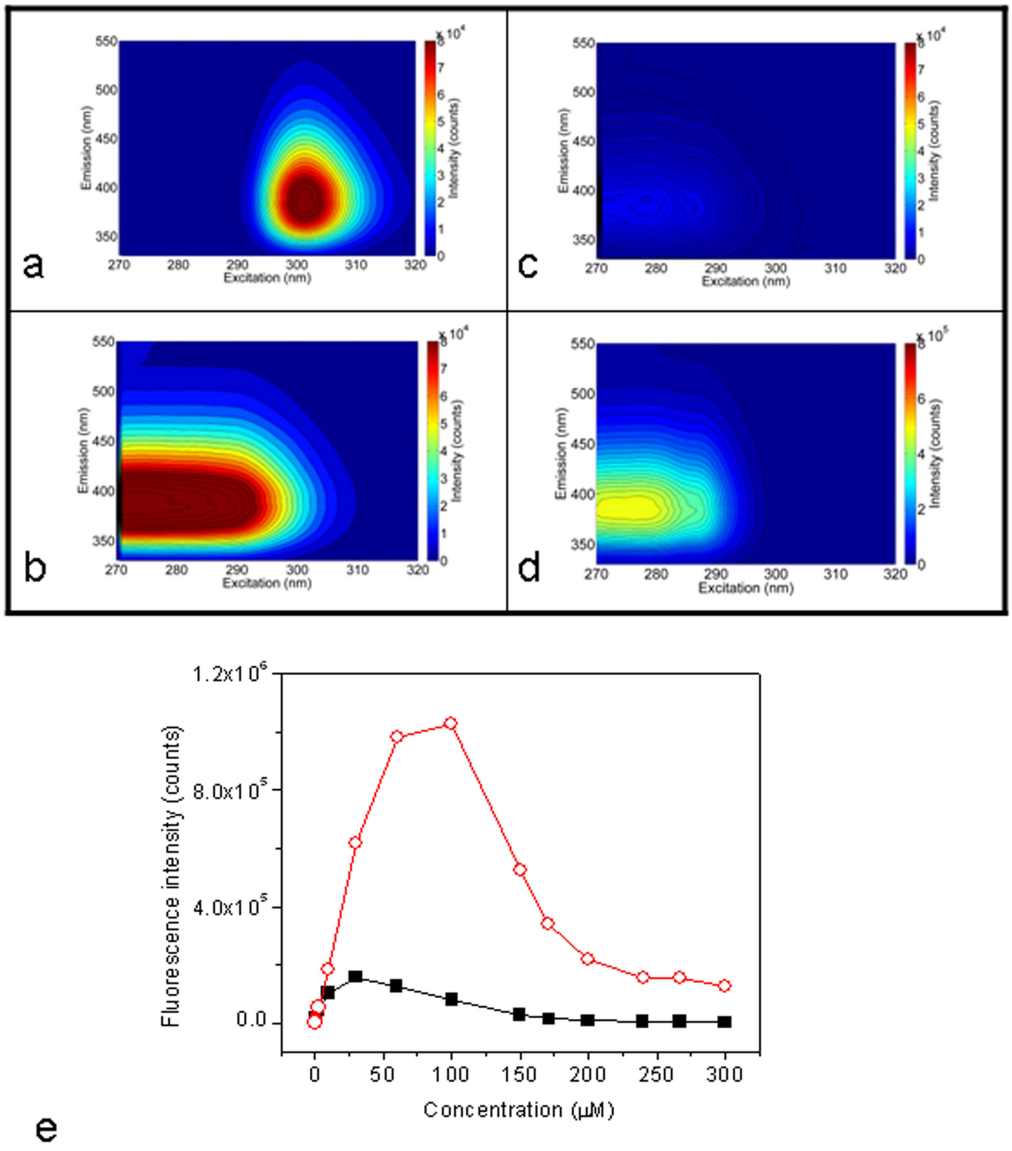

Figure 3.17: Excitation/emission matrices of indoxyl sulfate. (a) Indoxyl sulfate at a concentration of 300μmol, (b) diluted 1:1000 in double distilled water, (c) diluted 1:10 in double distilled water, (d) 1:10 dilution corrected for the inner filter effect and (e) fluorescence intensity at 280 nm/380nm versus concentration of indoxyl sulfate; (−) uncorrected data; (−) data corrected for the inner filter effect; note the different colour scale in (d).

all quenching processes, the most abundant group A fluorophores, indoxyl sulfate, tryptophan and 5-hydroxyindole-3-acetate were focused [7]. The fluorescence of

these three fluorophores was studied in isolation as well as in mixtures, including a representative simulated urine with selected urine components (indoxyl sulfate, tryptophan and 5-hydroxyindole-3-acetate) at typical physiological concentrations of 300, 50 and 24 μmol, respectively. In order to establish the significance of the inner filter effect the absorbance of these three fluorophores (see Figure 3.16 where a 1:10 dilution was used to obtain measurable values) were also measured. As indicated earlier, the absorbance of indoxyl sulfate at physiological concentration is high, and the other two fluorophores did not show significant absorption in the examined region.

Fluorescence of indoxyl sulfate was measured as a function of dilution. Figure 3.17 e shows the peak fluorescence intensity at 280 nm/380 nm, of indoxyl sulfate at various concentrations, before and after correcting for the inner filter effect. It shows that the fluorescence intensity at 300 μmol concentration after correcting for the inner filter effect is lower than that of the 30 μmol concentration, confirming that at physiological concentration (300 μmol), indoxyl sulfate exhibits concentration quenching. Consequently, indoxyl sulfate in undiluted healthy human urine must also be subject to concentration quenching (self-quenching). The other two fluorophores were examined, tryptophan and 5-hydroxyindole-3-acetate below and at physiological concentrations. These did not show the self-quenching effect (data not presented).

Common mechanisms behind concentration quenching include collisional quenching and dimer formation. The dimers are known to show a relatively weak fluorescence compared with fluorescent monomers [42]. In order to test this possibility, liquid chromatography/mass spectrometry (LCMS) to detect the presence of indoxyl sulfate dimers at physiological concentration. The peak at 463 (mass/charge) in the LCMS (Figure 3.8) indicates that dimers are indeed formed, but at a low relative

concentration of 10 % compared with the monomers. Also, aggregate formation if significant, could change the shape and shift the maxima of absorption bands [43]. The absorption spectra of urine as well as its key fluorescent component at varying dilutions, do not suggest much influence of aggregate formation, as seen by the almost identical absorption of indoxyl sulfate at physiological concentration and at two dilutions (Figure 3.3 inset). Thus it is infered that the fluorescence reduction due to dimer or aggregate formation is very minimal. Therefore it is proposed that collisional quenching as the major mechanism of concentration quenching by indoxyl sulfate at physiological concentrations.

The mutual interactions between the three key group A fluorophores (tryptophan, 5-hydroxyindole-3-acetate and indoxyl sulfate) at physiological concentrations and at various dilutions was also studied. In the presence of indoxyl sulfate, the fluorescence of tryptophan as well as 5-hydroxyindole-3-acetate showed reduced fluorescence (data not shown). The fluorescence intensity of the simulated urine (a combination of these three fluorophores) was also very weak, with a peak at 310 nm/340 nm (Figure 3.18 a-c). This is consistent with the spectral position for the 5-hydroxyindole-3-acetate peak (Table 2.2), although in light of a very strong inner filter effect, an unambiguous assignment is not possible. Overall, the trend observed in Figure 3.18 with dilution is similar to that in Figure 3.17, i.e., a deformed peak at 1:10 dilution which, after correction for the inner filter effect, reveals a pure indoxyl sulfate feature, more clearly observed at 1:1000 dilution. This is an indication that indoxyl sulfate reduces the fluorescence of tryptophan and 5-hydroxyindole-3-acetate when these are in combination. Moreover, the maximum fluorescence intensity at physiological concentration of the simulated urine (Figure 3.18 a) is significantly lower than that of indoxyl sulfate alone (Figure 3.18 a), confirming energy transfer between these fluorophores and indoxyl sulfate. Similar to the case of pure indoxyl

sulfate, the concentration quenching was confirmed by observing the concentration trends in peak fluorescence intensity of the simulated urine before and after correcting for inner filter effect (Figure 3.18 e).

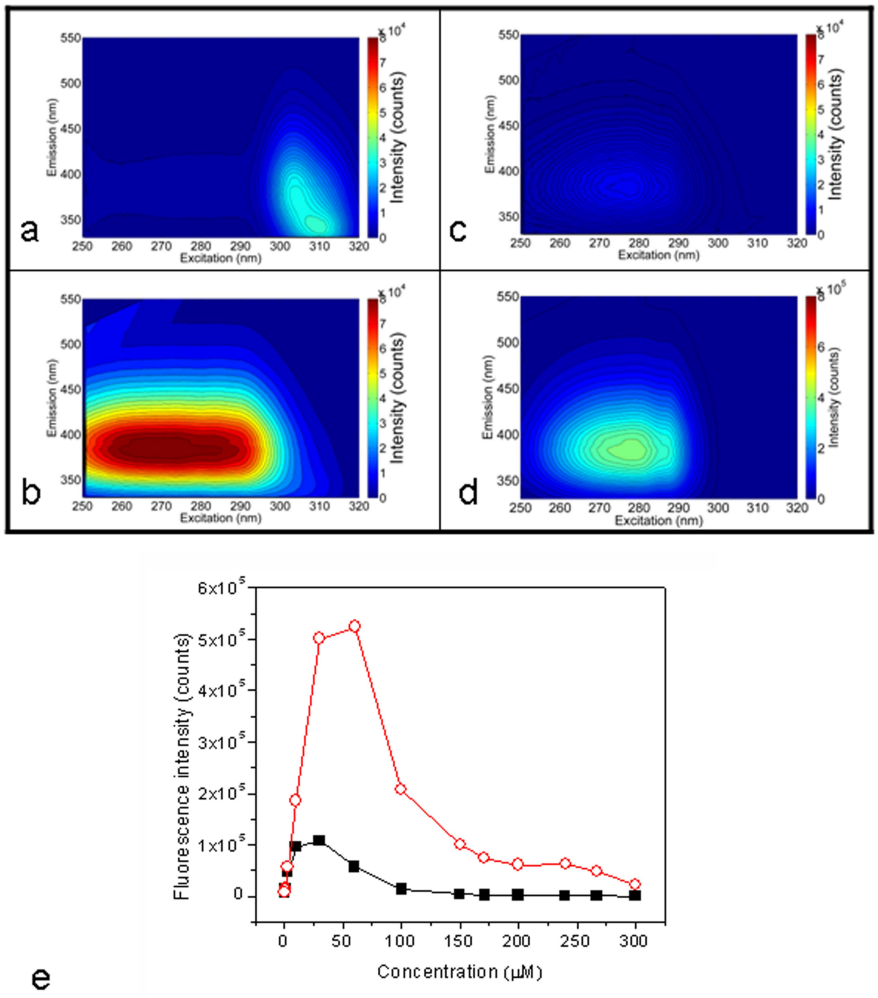

Figure 3.18: Excitation/emission matrices of simulated urine containing indoxyl sulfate (300μmol), tryptophan (50μmol) and 5-hydroxyindole-3-acetate (24μmol). (a) Undiluted;(b) diluted 1:1000; (c) diluted 1:10; (d) diluted 1:10, with spectra corrected for inner filter effect. Note the different colour scale in (d). All dilutions were made in double distilled water. (e) Fluorescence intensity at 280 nm/380nm of simulated urine as a function of indoxyl sulfate concentration. (−) uncorrected data; (−) data corrected for the inner filter effect.

Finally, the effect of other non-fluorescent components in urine, on its fluores-

cence was explored. As previously, the key group A fluorophores was focused, indoxyl sulfate, tryptophan and 5-hydroxyindole-3-acetate and their interaction with a major non-fluorescent component ammonium. Ammonium was selected because it is reported to be an efficient quencher of indole fluorophores [44], and this behaviour is confirmed in this study. Moreover, its physiological concentration tends to be high, and a 24 h sample of normal human urine contains 19 mmol (0.7 g) of ammonium, derived from protein metabolism and from glutamine in kidneys. The concentration of ammonium varies depending on blood and tissue fluid acidity [8]. Figure 3.13 shows that the addition of a physiological amount of ammonium lowers the fluorescence of the simulated urine by a factor of two. To understand the quenching effect in detail, the SternVolmer quenching constant was calculated using the following equation [29]:

$$F_0/F = 1 + K[Q] \tag{3.3}$$

where F_0 and F are the fluorescence intensities in the absence and presence of quencher (ammonium), [Q] is the concentration of quencher and K is the Stern-Volmer constant. The K value was calculated to be approximately 1.4 L/mol. The SternVolmer plot is shown in Figure 3.13(inset).

Additional quenching studies, with each of the three fluorophores independently, showed that ammonium quenched the fluorescence of all the three examined fluorophores, tryptophan, indoxyl sulfate and 5-hydroxyindole-3-acetate. Figure 3.13 also shows that dilution reduces the quenching of simulated urine by ammonium, as expected. However, the fact that in Figure 3.13 the emission peak of simulated urine does not change with dilution indicates that the concentration quenching is not due to reabsorption. This result is consistent with the increased intensity observed for the human urine at shorter UV region with dilution (Figure 3.15). Separately, it was

observed that ammonium also reduced the fluorescence of each of the three examined fluorophores in a concentration dependent way (data not shown). The overall conclusion from this study is that the key indole fluorophores in healthy human urine are quenched by the presence of ammonium. The mechanism behind this quenching is the sensitivity of indole fluorophores to the local environment [29,31,33,45]. The electron transfer from excited fluorophores to ammonium has been reported to be the cause of this quenching [44].

A survey of the literature indicates that the fluorescence properties of human urine are also affected by factors other than those examined here. For example, the pH can rebalance the fluorescence intensities of component fluorophores in favour of certain components such as, pterin and 4-pyridoxic acid [17, 32, 46]. Undiluted healthy human urine has a pH between 5 and 7.5. As the pH is increased from 8 to 10, the quantum yield and mean life time of the indole fluorophores increases three-fold as compared with that at pH between 3 and 7.5 [29]. This means that the quantum yield of indole fluorophores in normal urine is suboptimal. Pterin and 4-pyridoxic acid contribute significantly to the fluorescence of undiluted healthy human urine at 300-450 nm excitation. The 4-pyridoxic acid and pterins have high fluorescence intensity in an acidic medium (pH 4-7) as compared to a basic medium [22, 47]. These fluorophores therefore exhibit optimal fluorescence at the pH of undiluted normal human urine. This is in contrast to the indole fluorophores whose quantum yield is not at their peak in healthy human urine. The overall picture of fluorescence quenching in urine is also more complex. In addition to ammonium, urine contains other known quenchers. A 24 h sample of human urine contains hippuric acid, whose carboxyl group is able to quench the indole fluorophores in urine. All these effects additionally contribute to the main quenching mechanisms discussed here, *i.e.*, the autoquenching of indoxyl sulfate, quenching of tryptophan and 5-hydroxyindole-3-

acetate by indoxyl sulfate and the quenching of indole fluorophores by ammonium.

3.5 Summary

Despite high concentration of UV excitable (250-300 nm) fluorophores, the fluorescence of undiluted healthy human urine is weak. However, with dilution, the fluorescence intensity increases substantially. Although this is generally attributed to fluorescence quenching and/or inner filter effect, the existing literature does not provide any explanation concerning the factors contributing to the relatively low UV fluorescence of undiluted healthy human urine. A detailed understanding of the factors influencing UV fluorescence of human urine could contribute to harnessing fluorescence as a diagnostic tool.

In this work, fluorescence of undiluted healthy human urine samples as well as three major UV-excitable fluorophores in urine: tryptophan, indoxyl sulfate and 5-hydroxyindole-3-acetate was analysed, in order to understand the key fluorescence features in this complex biological fluid. Both undiluted (physiological concentration) as well as various dilutions were studied. The effect of physiological concentration of another major component of urine, ammonium, on the fluorescence of key urine fluorophores and their mixtures was also established.

The findings indicate that the key factors contributing to the reduction of fluorescence observed in the undiluted healthy human urine samples excited in the shorter UV wavelength include high concentration of indoxyl sulfate contributing to the inner filter effect and the concentration quenching of fluorophores by ammonium. This work fills a gap in the existing literature concerning the factors influencing UV fluorescence of human urine.

4

Autofluorescence of bacteriuria samples

4.1 Introduction

In this Chapter, fluorescence spectra of bacteriuria samples (presence of bacteria in urine), in the range between 250 nm to 450 nm wavelength (excitation) are studied in detail, to identify the potential of using fluorescence measurement as a diagnostic tool for urinary tract infections.

4.1.1 Urinary tract infections (UTIs)

Definition

Although urine contains a variety of salts and metabolic waste products, it usually does not have bacteria in it. When bacteria get into the bladder or kidney and multiply in the urinary tract, it results in a UTI. There are two types of UTI:

1. Lower UTI: this is an infection of the lower part of the urinary tract that includes the bladder and the urethra. An infection/inflammation of the bladder is called *cystitis*, while an infection/inflammation of the urethra is known as *urethritis*.

2. Upper UTI: this is an infection/inflammation of the upper part of the urinary

tract that includes the kidneys (pyelonephritis) and the ureters (ureteritis). Upper UTIs are potentially more serious than lower UTIs because there is a possibility of kidney damage.

Urinary tract infections (UTIs) are common in general population. Although a variety of microbes can cause UTI, bacteria are the most common etiologic agents [48]. "Significant bacteriuria" is defined as the presence of 10^5 colony forming units (c.f.u.) of bacteria per ml of urine [49].

Causes, Prevalence and Risk factors

Escherichia coli is the most common bacterium associated with UTI [50]. In addition to *Escherichia coli*, many other pathogens have been found as the cause of UTIs, which include gram negative bacteria (Klebsiella, Enterobacter, *Pseudomonas aeruginosa* and *Proteus mirabilis*), gram positive bacteria (*Staphylococci* and *Enterococci*) as well as fungal pathogens [51].

It is estimated that, nearly 150 million UTIs occur per year on a global basis, causing more than 6 billion dollars in direct health care expenditure [52, 53]. There are many factors that increase the risk of developing urinary tract infection, for example sex, age, pregnancy, catheterization, kidney stones, tumors, urethral strictures, neurological diseases, congenital/acquired anomalies of bladder, vesicoureteric reflex, suppressed immune system, diabetes mellitus, enlarged prostrate and ureteric stresses [54–57].

Kidney Health Australia estimated that one in three adult women and one in twenty for men will get UTIs in their lifetime [58]. Women tend to get them more often because their urethra is shorter and its opening is located closer to the anus in women. Faecal bacteria from the anus can easily travel up the urethra and cause infections. Adult women are more vulnerable to UTI [50]. Menopause also increases

the risk of a UTI.

Complicated UTIs

Complicated urinary tract infections are those that occur in a patient who has a functionally, metabolically, or anatomically abnormal urinary tract or those that are caused by pathogens that are resistant to antibiotics. The clinical spectrum ranges from mild cystitis to life-threatening urosepsis. In addition, there may be long periods of asymptomatic bacteriuria. A broad range of bacteria can cause complicated infections (for example *E coli*, Proteus species, Klebsiella species, Pseudomonas species, Serratia species, Enterococci and Staphylococci), and many are resistant to multiple antimicrobial agents [57].

Diagnosis

Several tools have been developed for diagnosing UTIs. Near patient tests in primary care are most widely done using dipsticks [51]. Urinalysis tests for UTIs in the clinical laboratories include urine sediment analysis (i.e., examining for cells, microorganisms, casts and crystals) and quantitative bacterial culture [59–61]. In recent years, to diagnose UTIs, several novel approaches have been attempted which include real time PCR, biosensors, immuno-chromatography strips and capillary electrophoresis [62–64].

Limitations of the current diagnostic techniques

First of all, most of the current diagnostic techniques are reagent based (Dipsticks, biosensores, immunochromatogrphy etc) [62–64]. Urinalysis using dipsticks detects inter alia, leukocyte esterase (LE), nitrites, blood, and protein. LE is a polymorphic enzyme and as such, is only a surrogate marker for UTI [65]. Similarly, not all urinary pathogens produce nitrites (for example enterococci and *Staphylococcus* .

saprophyticus). False-negative results may also occur due to frequent urination, which lowers the exposure of the microorganisms to nitrate; this can also occur with a diet poor in vegetables (a source of nitrates) [49, 66]. Proteinuria or hematuria can be caused by other disorders besides UTI [65]. Due to these reasons, dipsticks are not always accurate for UTI diagnosis.

PCR has been successfully used to detect bacterial DNA in clinical samples and has improved the rate of microbial detection [67]. In addition to the reproducibility of PCR, it is extremely sensitive, requiring only a small number of organisms for analysis. This sensitivity has been exploited as the basis for a number of tests, including tests for detecting pathogens [68] and for detecting the mechanism of resistance to specific therapeutic agents. The contamination of PCR reagents with bacterial DNA, e.g., contamination with the bacterium-derived polymerases, is a major problem that can detract from the sensitivity provided by PCR technology [69,70]. Techniques like PCR and biosensors are expensive and they also need sample preparations prior to measurement.

Urine contains a variety of organic and inorganic chemicals dissolved in water, including a number of natural fluorophores, most of which are tryptophan metabolites. Due to these substances, normal urine has strong fluorescence. Variations in the concentration of these substances can occur due to the dietary intake, body metabolism and age. Investigators have identified high inter-individual and typically lower intra-individual variations in urine metabolites. In some diseases which are accompanied by metabolic disorders, certain additional organic compounds may appear in the urine, such as proteins and bilirubin. These often serve as additional indicators in disease diagnosis.

Although pathological and physiological changes are known to alter the autofluorescence of urine, there is a paucity of studies investigating autofluorescence as a

diagnostic tool for UTIs [14, 18, 20, 71, 72].

4.2 Experimental methodology

4.2.1 Urine Samples

Urine samples were collected from Douglass Hanly Moir, a large pathology laboratory where they were analysed for pH, protein, glucose, bilirubin, nitrate, specific gravity, blood, ketones, urobilinogen and leukocyte esterase. The samples were also tested for the presence of red blood cells, white blood cells, casts, epithelial cells and crystals (using iQ200 Sprint, IRIS Diagnostics Division, Chatsworth, CA) and semi-quantitative culture on chromogenic agar plates for the presence of bacteria was also carried out routinely in the pathology laboratory.

A total of 154 samples were chosen for the study. They were chosen in such a way that 87 urine samples which showed no abnormal laboratory findings (ie, culture negative as well as negative for other abnormal findings), served as a control group of normal samples. The remaining 67 samples with $\geq 10^5$ colony forming units of *Escherichia coli* per ml, served as bacteriuria samples. All the urine samples were stored in the refrigerator (4^0C) and examined within 48 hours after collection. Urine dilutions when required were made using double distilled water.

4.2.2 Measurement of autofluorescence

Excitation/emission matrices: Whole uncentrifuged urine (3 ml) was used for measuring autofluorescence using a Fluorolog Tau3 system (JY Horiba, Edison, NJ) in 10 mm quartz cuvettes at room temperature. The fluorescence emission spectra after excitation at various wavelengths, *i.e.* excitation/emission matrices (EEMs), were obtained in the following ranges, for excitation (Ex) 250-450 nm and 310-750 nm for emission (Em). These three-dimensional plots of fluorescence

intensity as a function of excitation and emission wavelengths represent the complete fluorescence characteristics of the sample. In order to cover the broad spectral region of relevance in the most time-efficient way, separate smaller EEMs focused on regions of particular interest were obtained and digitally integrated into a single one using MATLAB software.

Synchronous fluorescence spectra: (SFS) SFS measurements were made for undiluted and diluted (1:30) urine samples using Fluorolog Tau3 system. SFS of urine samples were analysed using two different offset wavelengths of $\triangle\lambda$ 90 nm and $\triangle\lambda$ 30 nm and cuvettes with two different path lengths i.e. 10 mm and 4 mm.

For EEM and SFS measurements, the spectral band passes were 2 nm in both excitation and emission. The spectra were corrected for optical system response.

4.2.3 HPLC analysis of the concentration of indoxyl sulfate and tryptophan in normal and bacteriuria samples

Urine samples were prepared as per a previously reported method [19]. Stock solutions (1 mg/mL) of tryptophan and indoxyl sulfate standards were prepared in the mobile phase.

A Shimadzu HPLC system consisting of a LC-10 AVP pump with a SPD M10AVP photodiode array detector and an autosampler was used. Chromatographic separations were performed at ambient temperature (23-25^{o}C) on a Waters 4.6 150 mm (particle size - 3.5 m), SunFire C18 column connected with a guard column. The mobile phase consisted of 0.04 M acetate buffer at pH 4.5 with 5 % acetonitrile. The total run time was 60 min at a flow rate of 0.8 ml/min [19]. Indoxyl sulfate and tryptophan were detected by using absorption at 280 nm.

4.3 Results

4.3.1 Comparison of excitation/emission matrices (EEMs) of normal human urines with bacteriuria samples

A comparison of the excitation/emission matrices of thirteen each of undiluted normal human urines and bacteriuria samples clearly showed that undiluted normal urine samples had an emission peak around 440 ±15 nm when excited at 355 ±15 nm, whereas undiluted bacteriuria samples had a dominant emission peak around 425 ±10 nm when excited at much shorter wavelength (blue shift) i.e. at 330 20 nm excitation (Figure 4.1a). One example each of excitation/emission matrices of undiluted normal urine sample and undiluted bacteriuria sample with different spectral features are shown in Figure 4.1(b, c).

In addition, the bacteriuria samples showed a weak fluorescence emission peak emerging at 380 ±15 nm with 280 ±10 nm excitation which was not observed for the normal samples (Figure 4.1(b, c)).

4.3.2 Comparison of emission maxima at 290 nm excitation for undiluted normal human urines with undiluted bacteriuria samples

Figure 4.2 shows that at 290 nm excitation wavelength the normal urine samples showed very low intensity of fluorescence emission compared with the bacteriuria samples.

Figure 4.2 also reveals very large variations of fluorescence intensity between individual samples, and thus required statistical analysis. With this in mind, when the average fluorescence intensities of the two groups of urine samples were plotted, a significant difference between the fluorescence emission peak intensities for the two sample sets was clearly seen Figure 4.3. A two sample t test showed a statistically significant difference between the two groups ($P = 4.3\text{x}10^{-12}$ for 0.05% error). This

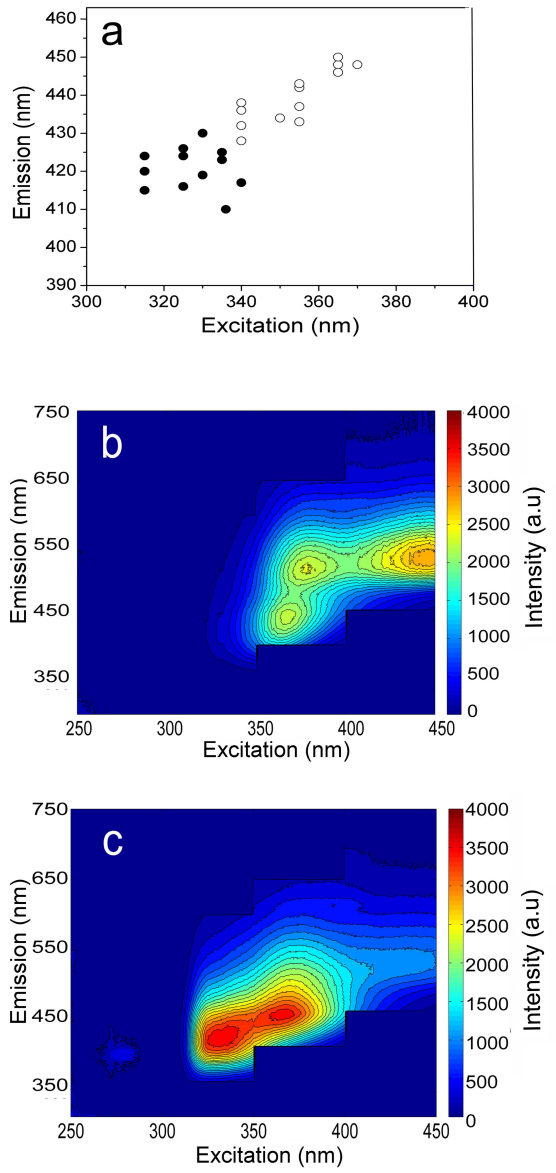

Figure 4.1: (a) Localisation of highest excitation/emission peak of thirteen each of undiluted normal urine (○) and undiluted bacteriuria samples (●); (b) Example EEM of an undiluted normal human urine sample; (c) Example EEM of an undiluted bacteriuria sample. Note: the region between 250-300 nm excitations is not visible in the matrix due to intensity scale being adjusted to show the main feature.

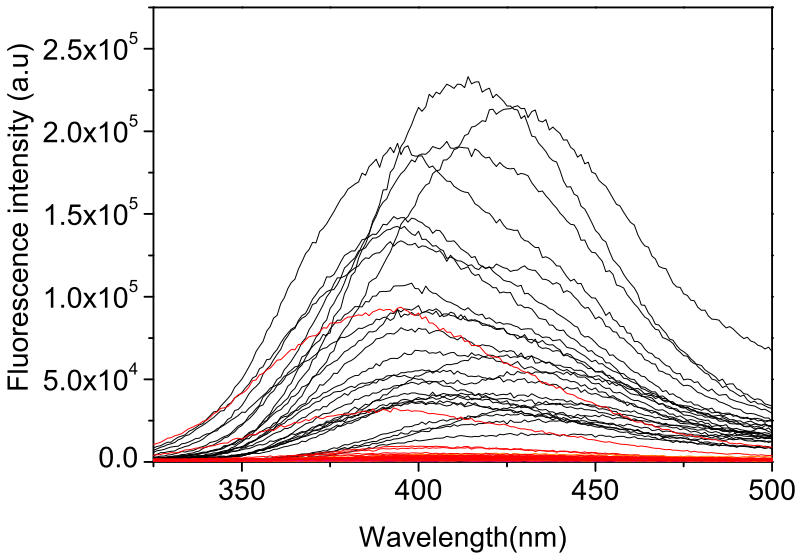

Figure 4.2: Emission spectra of autofluorescence of urine (25 bacteriuria and 45 normal) samples when excited at 290 nm.

indicates that at 290 nm excitation the fluorescence intensities of bacteriuria samples and normal urine samples are different. Note that scanning speed of SFS for a single sample is approximately 1 minute.

However, Figure 4.4 shows that there is no correlation between bacterial count and fluorescence intensity or the type of bacteria and fluorescence intensity

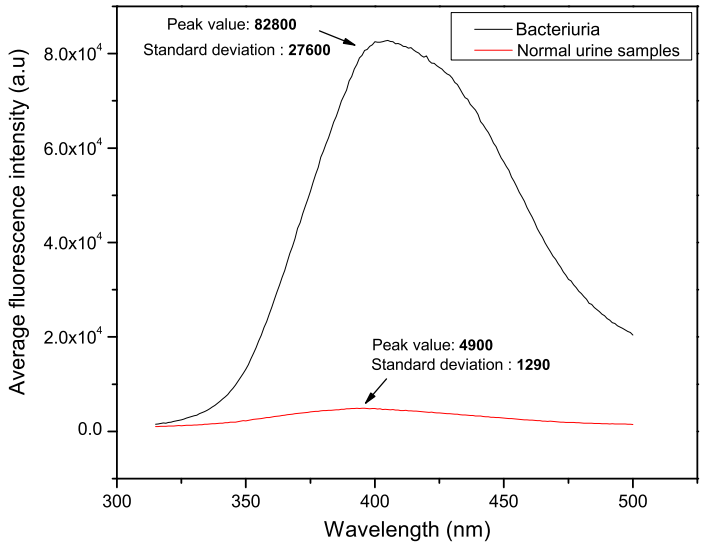

Figure 4.3: Average emission spectra of autofluorescence of urine (25 bacteriuria and 45 normal) samples when excited at 290 nm.

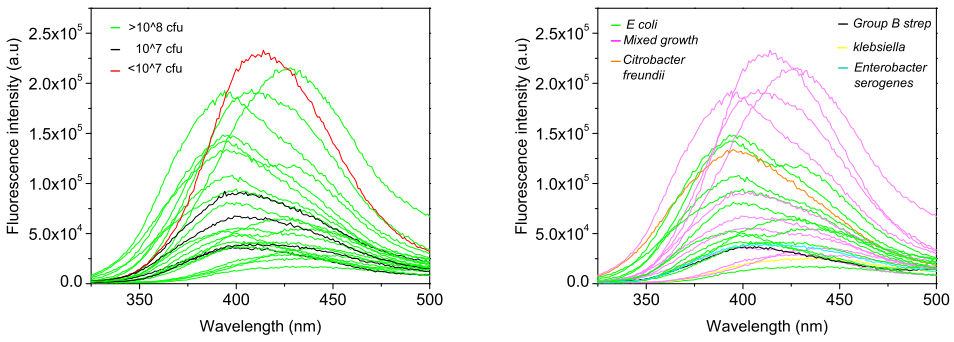

(a) (b)

Figure 4.4: (a) Bacterial count and fluorescence intensity at 290 nm excitation (b) Bacterial type and fluorescence intensity at 290 nm excitation.

4.3.3 Principal component analysis (PCA) for checking spectral pattern in the autofluorescence of urine samples at 290 nm excitation

Figure 4.5 shows the principal components analysis (PCA) for the autofluorescence emission spectra of urine samples at 290 nm. All the normal samples except two were grouped in a close cluster, indicating a very similar pattern of autofluorescence spectrum. The points representing the 25 bacteriuria samples although spread widely over an area, were clearly separated from the cluster of the normal samples.

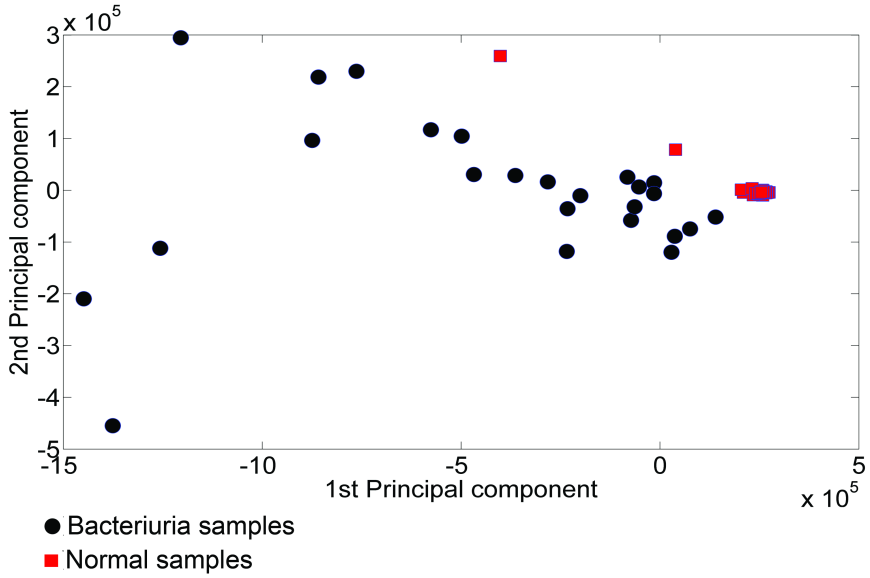

Figure 4.5: PCA for the autofluorescence emission spectra of undiluted human urine samples (45 normal and 25 bacteriuria samples) at 290 nm.

4.3.4 Comparison of synchronous fluorescence spectra (SFS) of undiluted normal human urines with bacteriuria samples with offset $\Delta\lambda$ 90 nm wavelength

Figure 4.6 shows that undiluted bacteriuria samples have higher fluorescence intensity when excited at 280 ±5 nm with an emission peak at around 375 ±10 nm compared to undiluted normal human urine samples. A 2 sample "t test" showed a statistically significant difference between the 2 groups (P = 9.4768 x 10^{-10} for 0.05% error). This result indicates that $\Delta\lambda$=90 nm offset for SFS can be used effectively to differentiate undiluted bacteriuria samples from normal urines.

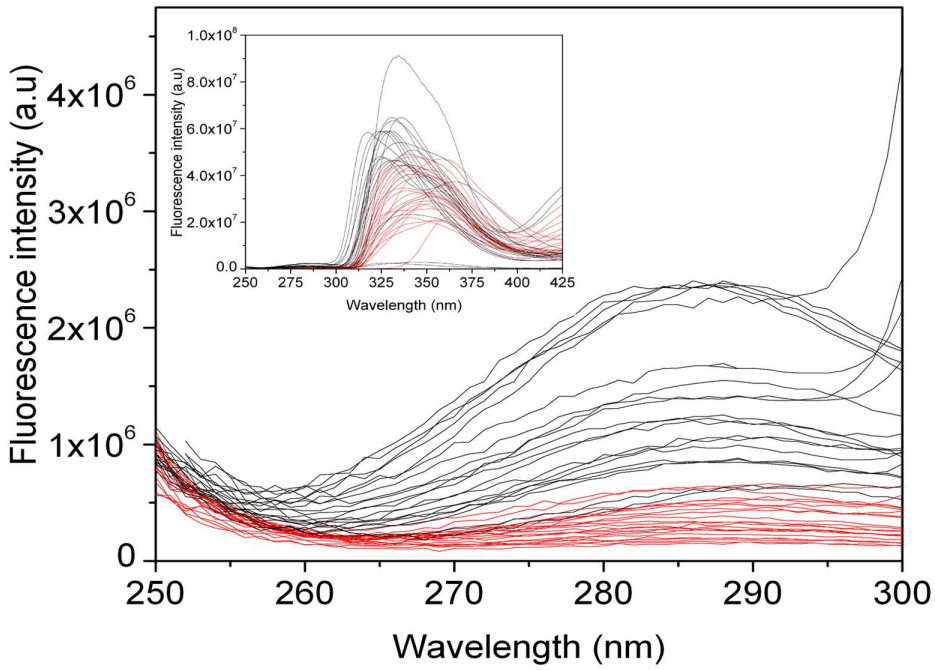

Figure 4.6: Comparison of SFS ($\Delta\lambda$=90 nm) of undiluted normal human urines with undiluted bacteriuria samples measured in 10 mm cuvette. The inset shows the SFS ($\Delta\lambda$=90 nm) of the same samples for 250 to 425 nm excitation. Each curve represents a different urine sample.

4.3.5 A comparison of the SFS ($\Delta\lambda$=90 nm) of undiluted urines measured using 10 mm and 4 mm cuvette

A comparison of the SFS ($\Delta\lambda$=90 nm) of undiluted urines measured using 10 mm (Figure 4.6 inset) and 4 mm (Figure 4.7) cuvette clearly showed that spectra obtained by measuring with these cuvettes were different. With the 4 mm cuvette, both undiluted normal and bacteriuria samples showed higher emission intensity in the shorter UV (250 -300 nm) relative to the emission in the 300-450 nm range. This feature was not observed for urine samples measured with 10 mm cuvette.

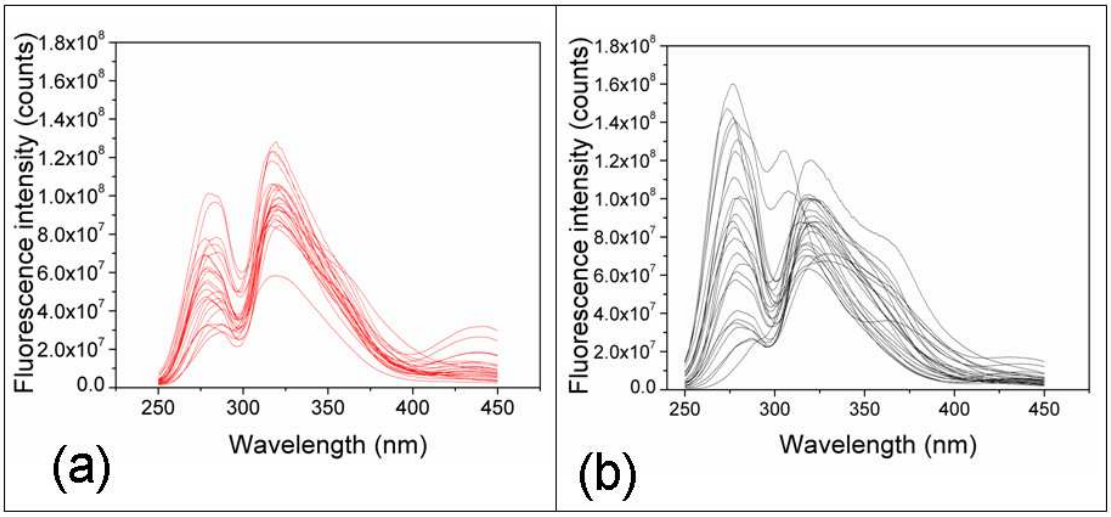

Figure 4.7: Comparison of SFS ($\Delta\lambda$=90 nm) of undiluted normal human urines (a, red) with undiluted bacteriuria samples (b, black) measured in 4 mm cuvette.

However, Figures 4.6 and 4.7 also show that irrespective of cuvette dimension (*i.e.* 4 mm or 10 mm), there is higher emission intensity for undiluted bacteriuria samples compared to undiluted normal samples when excited in the shorter UV region (250-300 nm). Further, taking the ratio of emission intensity between 280 nm and 320 nm excitation wavelengths for the samples, measured using 4 mm cuvettes, clearly differentiated the undiluted normal and bacteriuria samples [P = 6.6669 x 10^{-4} for

0.05% error]. Note that scanning speed of SFS for a single sample is approximately 1 minute.

4.3.6 Effect of dilution on the excitation/emission spectra of bacteriuria samples

The typical excitation/emission plots of bacteriuria samples for various dilutions (1:30, 1:300 and 1:1000) are presented in Figures 4.8 and 4.9. All the dilutions were made using double distilled water. It is evident from the Figures that the spectra of urine samples were profoundly changing with dilution. At 1:30 dilution, the bacteriuria sample 4 had strong emission peak around 270 nm excitation. At the same time sample 5, shown in Figure 4.9 had strong emission around 270 nm with 1:300 dilution. It is evident that with 1:30 dilution both samples showed higher group A fluorescence (explained as in Chapter 2) compared with the dilution at 1:1000.

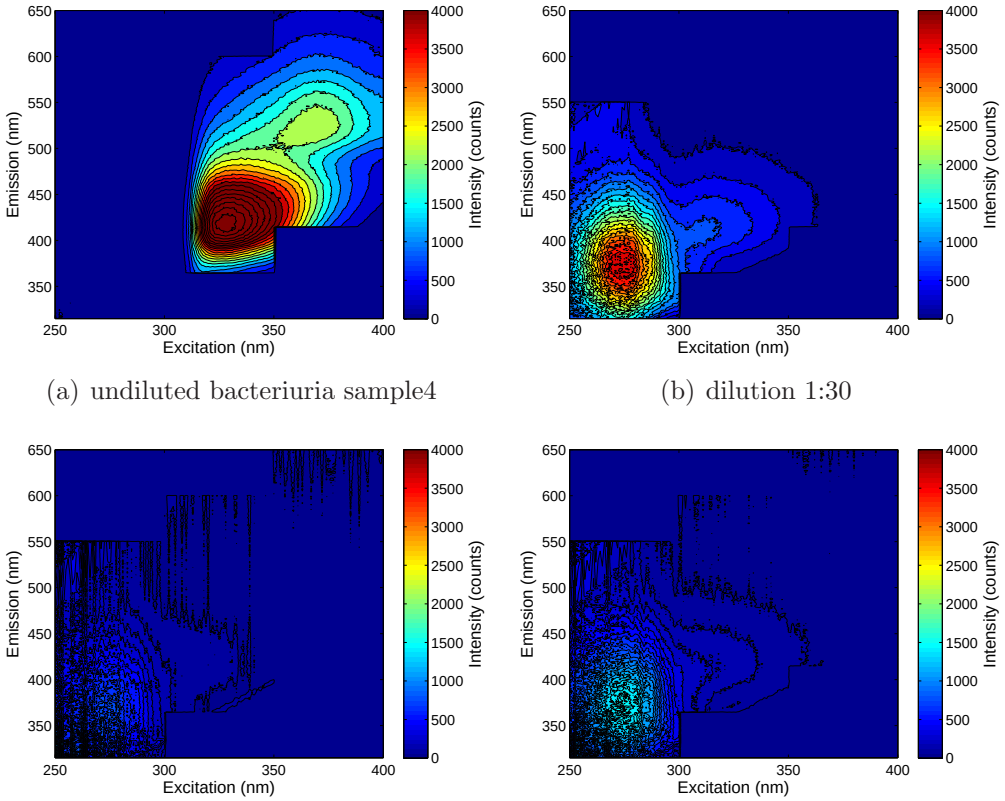

(a) undiluted bacteriuria sample4

(b) dilution 1:30

(c) dilution 1:300

(d) dilution 1:1000

Figure 4.8: Excitation/emission matrices of bacteriuria sample 4; (b),(c), (d) are at a dilution of 1:30, 1:300, 1:1000 respectively.

4.3.7 A comparison of the SFS of normal urines and bacteriuria samples for offset wavelengths $\Delta\lambda = 90$ nm and 30 nm at 1:30 dilution

We tested 25 normal and 25 bacteriuria samples using these parameters, *i.e.* the urine samples were centrifuged (10 min, 1100 rpm) and diluted 1:30 in double distilled water and the SFS was obtained using offset wavelengths $\Delta\lambda$ of 30 nm and 90 nm.

No clear difference was observed between the two groups of samples for $\Delta\lambda$ of 30 nm (Figure 4.10 a and b). However, a $\Delta\lambda$ of 90 nm showed a clear distinction between the two groups of diluted samples (Figure 4.10 c and d), with the ratio

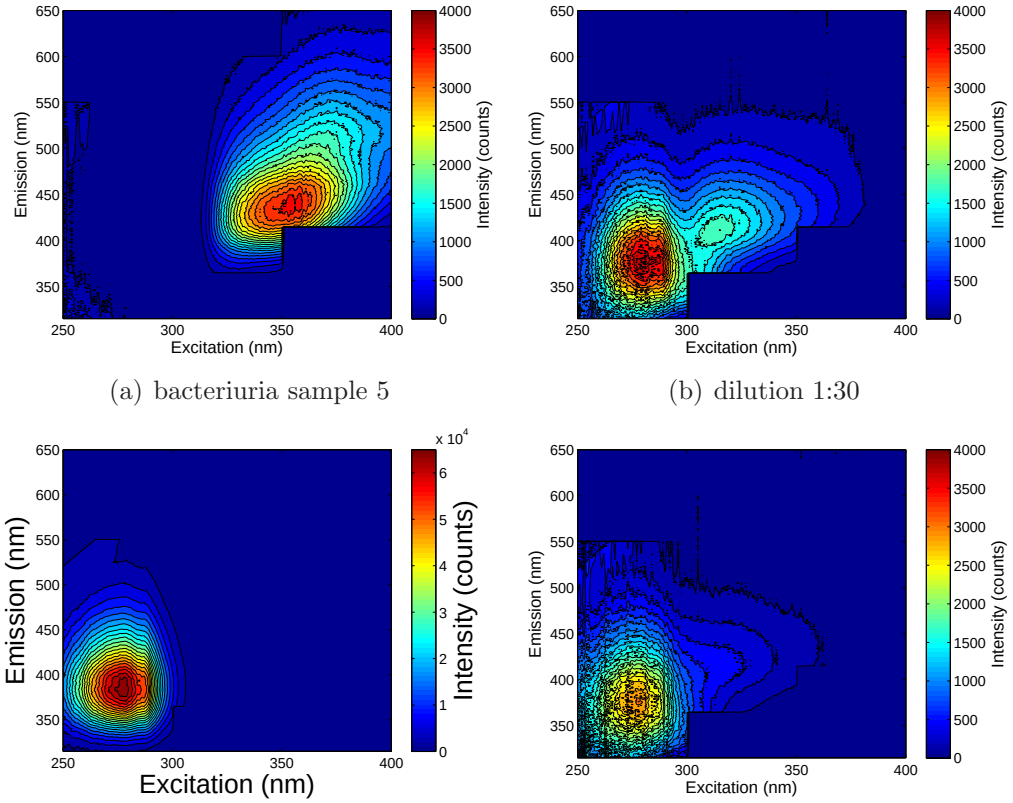

(a) bacteriuria sample 5

(b) dilution 1:30

(c) dilution 1:300

(d) dilution 1:1000

Figure 4.9: Excitation/emission matrices of bacteriuria sample 5; (b),(c), (d) are at a dilution of 1:30, 1:300, 1:1000 respectively. Please note: the scale in excitation/emission matrix of bacteriuria sample 1 is made different due to higher intensity in the shorter UV region.

of autofluorescence at 280 and 325 nm excitation between the groups showing a significant difference (P=0.0035 for 0.05% error).

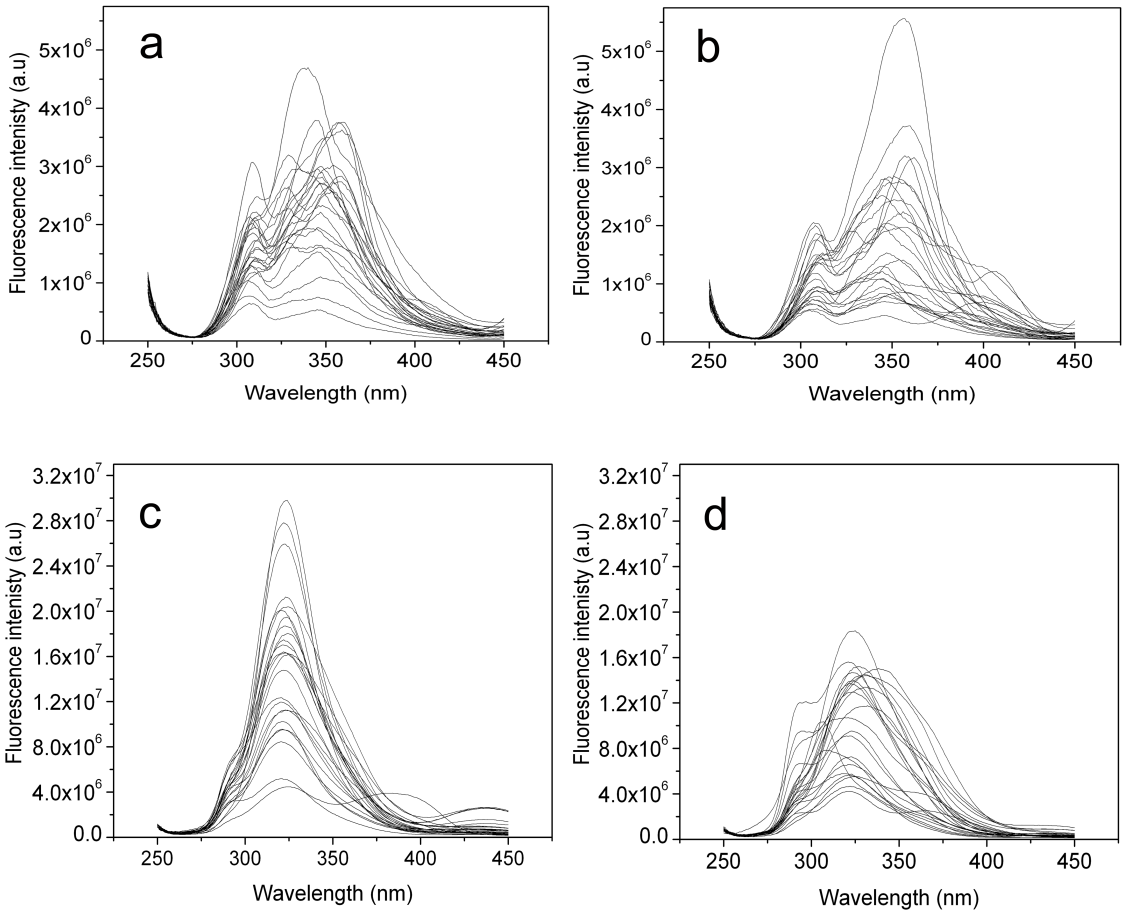

Figure 4.10: Comparison of SFS of diluted (1:30) normal human urines with diluted (1:30) bacteriuria samples measured using 10 mm cuvette. (a) and (c) SFS of diluted normal human urine with offset wavelengths $\Delta\lambda$=30 and $\Delta\lambda$=90 nm respectively; (b) and (d) SFS of diluted bacteriuria samples with offset wavelengths $\Delta\lambda$=30 and $\Delta\lambda$=90 nm respectively.

4.3.8 Effect of storage of the undiluted bacteriuria samples on their autofluorescence

Two undiluted bacteriuria samples were tested for the effect on their fluorescence spectra due to "aging". A comparison of excitation/emission matrix taken before and after storing at (4^0C) for 96 hours is shown in Figure 4.11.

There was no significant variation in the measured of fluorescent spectra of the

bacteriuria sample tested after 96 hours of storage at (4^0C).

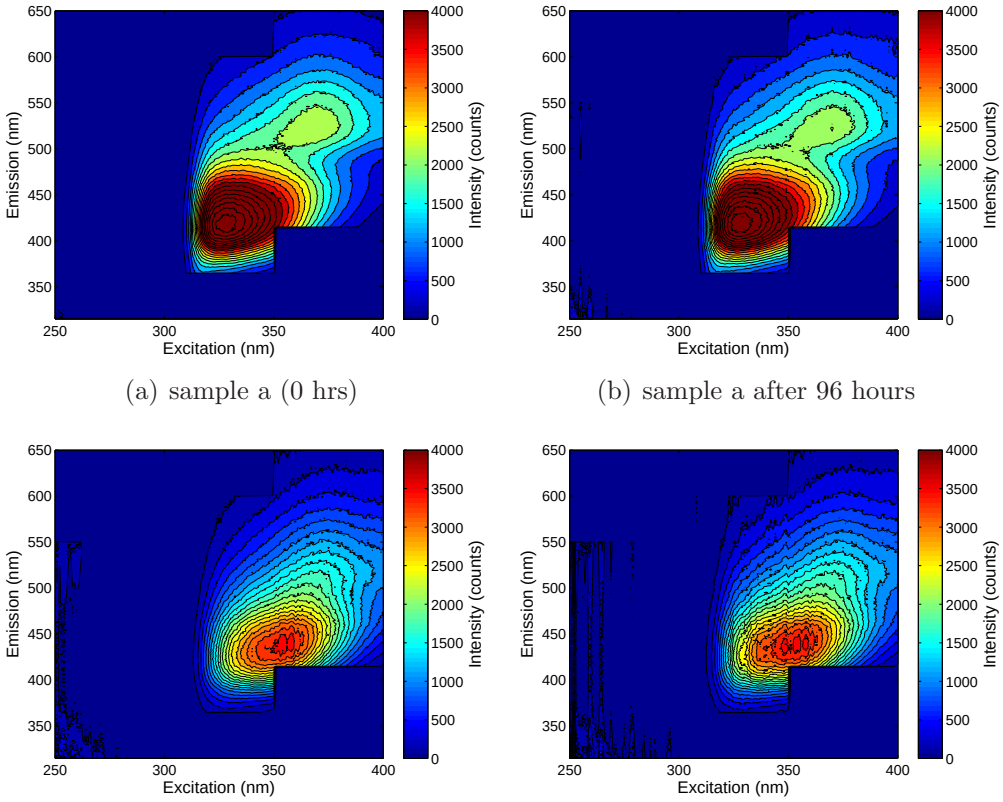

(a) sample a (0 hrs)

(b) sample a after 96 hours

(c) sample b (0 hrs)

(d) sample b after 96 hours

Figure 4.11: Illustration of the effect of storage of the undiluted bacteriuria samples on their autofluorescence.(a) and (b) are excitation emission matrix of sample a before and after 96 hour respectively. (c) and (d) are excitation emission matrix of sample b before and after 96 hour respectively.

4.3.9 Results of HPLC analysis for the concentration of indoxyl sulfate and tryptophan in urine samples

For measuring the concentration of indoxyl sulfate and tryptophan in normal urine and bacteriuria, HPLC measurements were performed on four normal human urines and four bacteriuria samples. The chromatograms of normal human urines and bacteriuria samples are shown in Figure 4.12. As seen from Tables 4.1 and 4.2, there is a slightly higher but not significant concentration of indoxyl sulfate in bacteriuria sam-

ples when compared to the normal urine samples. It is debatable whether this small concentration difference underpins the greater fluorescence observed for bacteriuria samples. HPLC results also show no significant differences in the concentration of tryptophan between the two sample groups.

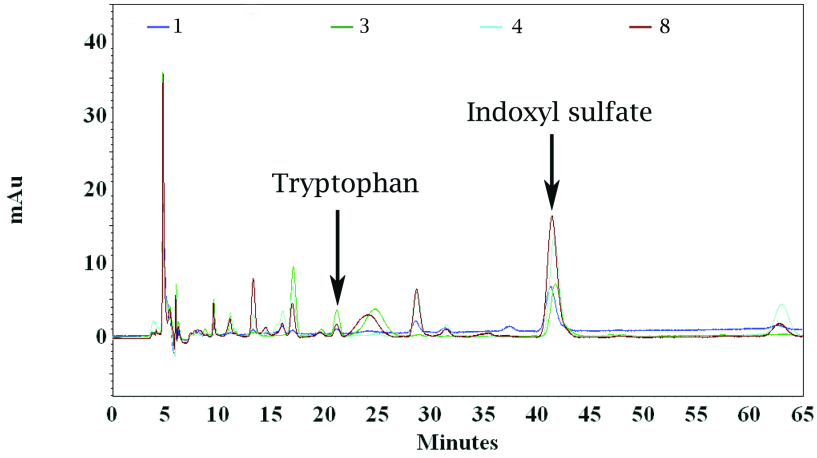

(a) Chromatogram of normal human urine samples

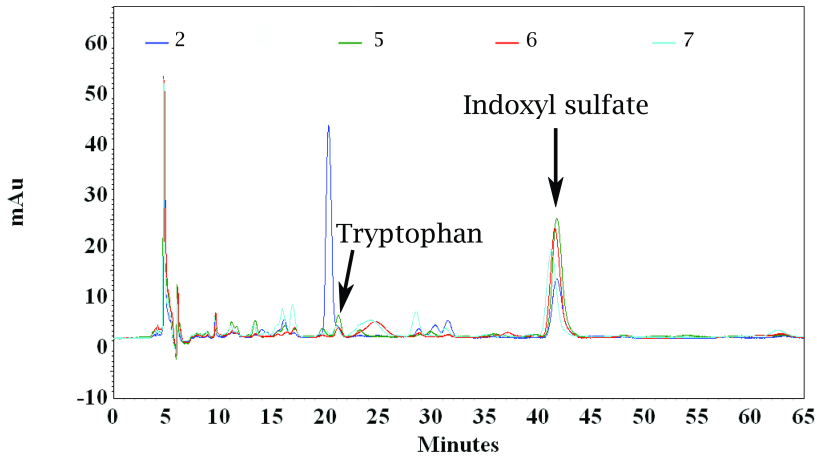

(b) Chromatogram of bacteriuria samples

Figure 4.12: Illustration of HPLC results (Chromatogram) of indoxyl sulfate and tryptophan in urine samples.

SL:No	Indoxyl sulfate concentration (μg)/(ml)	Tryptophan concentration (μg)/(ml)
1	76.021	4.18
3	121.625	9.12
4	101.28	8.64
8	159.36	8.0

Table 4.1: HPLC data for normal human urine samples

SL:No	Indoxyl sulfate concentration (μg)/(ml)	Tryptophan concentration (μg)/(ml)
2	150.354	No peak detected
5	154.43	12.6
6	170.2	7.2
7	156.94	8.0

Table 4.2: HPLC data for bacteriuria samples

4.4 Discussion

A majority of the earlier studies have focused on analysing diluted urine to avoid the concentration quenching effect due to the high concentration of fluorophores in urine [17, 18, 20]. However, dilution of urine can result in loss of information related to the fluorophores which are present in low quantities. In this study, spectra of undiluted urines were analysed because of two reasons: a) to develop a simpler testing protocol that eliminates the dilution step and b) to be able to analyse autofluorescence contributed by fluorophores which are present in low concentrations (for e.g. biopterin, neopterin, folic acid etc).

4.4.1 Fluorescence characteristics of undiluted bacteriuria samples

Tentative identification of peaks from excitation/emission matrix.

Figure 4.13 (a and b) shows two examples of excitation/emission matrix of bacteriuria samples. From the Figure 4.13 (a and b), four major peaks can be clearly observed. The information from Table 2.2 has been extrapolated to the Figure 4.13

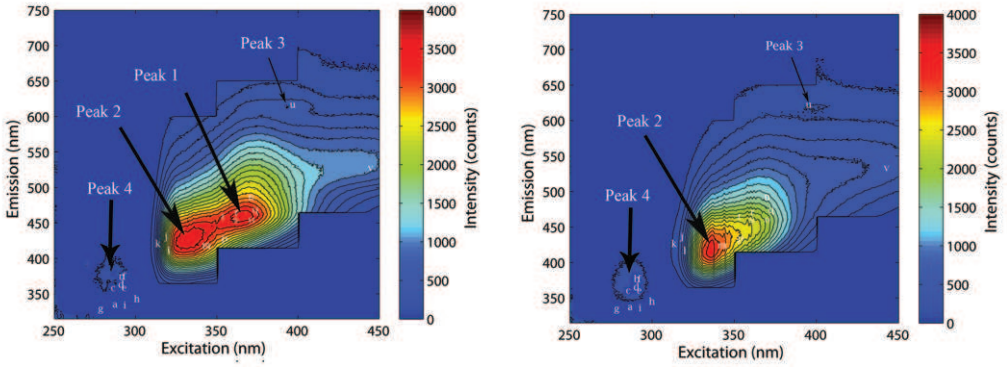

(a) Sample 1 (b) Sample 2

Figure 4.13: Identification of emission peaks in bacteriuria samples: (a) Melatonin, (b) Indoxyl sulphate, (c) Tryptophan, (d) Indolyl-3-acetate, (e) Skatol-5-sulphate, (f) Skatol-6-sulphate, (g) Metabolites of cathecholamines, (h) 5-Hydroxyindole-3-acetate, (i) 5-Hydroxytryptophan, (j) 4-Pyridoxic acid, (k)Xanthine, (l) 3-Hydroxyanthranilic acid, (m) 5-Hydroxyanthranilic acid, (n) Kynurenine, (o) Biopterin, (p) Neopterin, (q) 5-Hydroxykynurenine , (r) 3-Hydroxykynurenine , (s) Folic acid, (t) Xanthurenic acid, (u)Porphyrins, (v) Flavins. Note: The information from Table 2.2 has been extrapolated to the Figure 2.17 and 2.18 for inferring the contribution by different fluorophores.

(a and b) for inferring the contribution by different fluorophores. The possible contributors to the various peaks are given below.

1. Peak 1: 360/450 nm (excitation/emission) : This peak is mainly contributed by a number of endogenous fluorescent metabolites like Xanthurenic acid, Neopterin, 5-Hydroxyanthranilic acid, 4-pyridoxic acid, folic acid, 5-Hydroxy kynurenine, 3-Hydroxy kynurenine and biopterin.

2. Peak 2: 340 (+/- 5) /440 nm (excitation/emission) : This peak could be contributed by a number of endogenous fluorescent metabolites like 5-Hydroxyanthranilic acid, Xanthurenic acid, Neopterin, 4-pyridoxic acid.

3. Peak 3: 400/620 nm (excitation/emission) : Porphyrins could be responsible for this peak.

4. Peak 4: 270 /400 nm (excitation/emission) : The fluorophores which could possibly contribute most to the emission peak include indoxyl sulfate, tryptophan, indolyl-3-acetate and xanthine.

It is also apparent from the Figures 4.13 (a and b), that the autofluorescence of undiluted bacteriuria samples excited in 250 nm-300 nm range is very weak when compared to longer UV (300-450 nm) excitation.

Comparison of autofluorescence of undiluted normal urine with undiluted bacteriuria samples

EEMs are an accurate way to compare these two groups because they cover the broad spectral region of relevance. In the EEMs of undiluted human urine, it is practically impossible to attribute the fluorescence (emission) peak to a specific fluorophore because many fluorophores in urine possess similar spectral characteristics, and there are intervening effects that affect the spectra such as energy transfer, concentration quenching, inner filter effect etc [20]. Therefore the separation of the composite spectrum into the components corresponding to single fluorophores has not been attempted, and here, discussion focuses on the overall features of the mixture of all fluorophores present in urine.

The Figures 4.14, 4.15 and 4.16 show that undiluted normal urine samples have an emission peak around 440 ±15 nm when excited at 355 ±15 nm, whereas undiluted bacteriuria samples have a dominant emission peak around 425 ±10 nm when excited at much shorter wavelength (blue shift) i.e. at 330 ±20 nm excitation.

In addition, the bacteriuria samples showed a weak fluorescence emission peak emerging at 380 ±15 nm with 280 ±10 nm excitation which was not observed for the normal urine samples (Figures 4.14 and 4.15).

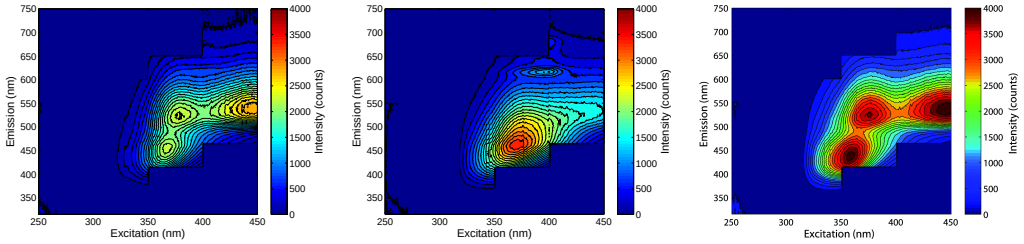

(a) Normal urine sample 1 (b) Normal urine sample 2 (c) Normal urine sample 3

Figure 4.14: Excitation/emission matrices of undiluted normal urine sample.

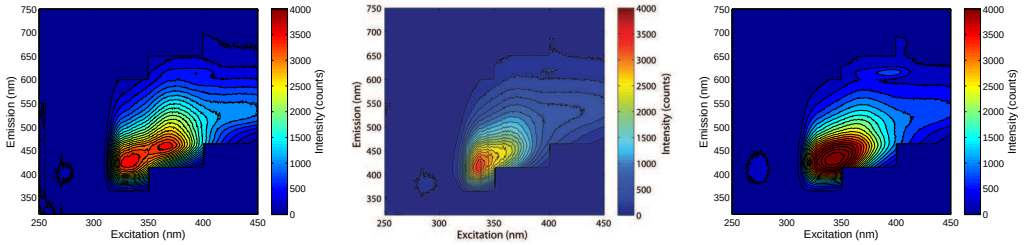

(a) Bacteriuria sample 1 (b) Bacteriuria sample 2 (c) Bacteriuria sample 3

Figure 4.15: Excitation/emission matrices of undiluted bacteriuria sample.

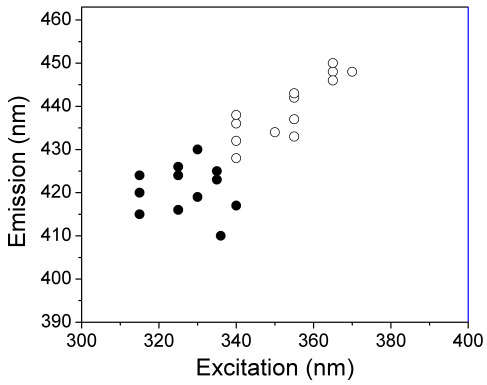

Figure 4.16: Localisation of highest excitation/emission peak of thirteen undiluted normal urine (○) and undiluted bacteriuria samples (●).

Comparison of synchronous fluorescence spectra (SFS) of undiluted normal human urines with bacteriuria samples using $\Delta\lambda$ 90 nm wavelength offset

The SFS technique provides more limited information than EEMs (located on an intersection of a 3D EEM plot with a single vertical plane). However SFS scans are much faster to perform than EEMs, and they can be effective for obtaining reasonably well separable data for several compounds in a mixture with a single scan [73]. Note that scanning speed of SFS for a single sample is approximately 1 minute.

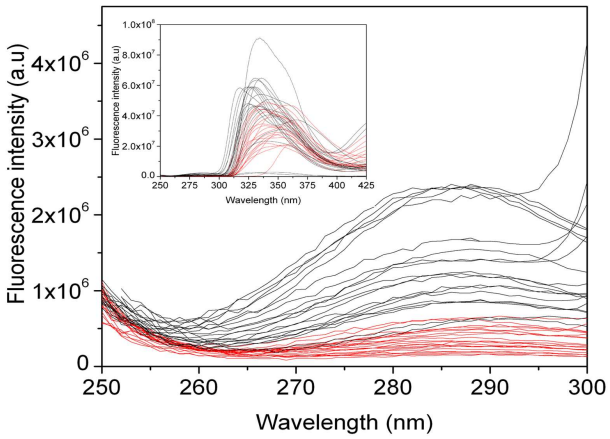

Figure 4.17: Comparison of SFS ($\Delta\lambda$=90 nm) of undiluted normal human urines with undiluted bacteriuria samples measured in 1 mm cuvette. The inset shows the SFS ($\Delta\lambda$=90 nm) of the same samples for 250 to 425 nm excitation. Each curve represents a different urine sample.

As the two peaks that differentiate between the normal and bacteriuria samples were emission at 425 ±10 nm and 380 ±10 nm, with 330 ±20 nm and 280 ±5 nm excitations respectively (Figures 4.14 and 4.15), a $\Delta\lambda$ of 90 nm (offset wavelength) was chosen for SFS to enable capturing the fluorescence in these regions of interest.

Figure 4.17 shows that undiluted bacteriuria samples have higher fluorescence intensity when excited at 280 ±10 nm, with an emission peak at around 375 ±10 nm,

as compared to undiluted normal urine samples. A 2 sample t test showed a statistically significant difference between the 2 groups (P = 9.4768e^{-}10 for 0.05%error). This result is also in agreement with the higher fluorescence intensity observed for 25 undiluted bacteriuria samples as compared with the 45 normal urine samples when excited at 290 nm (Figure 4.18(a and b)).

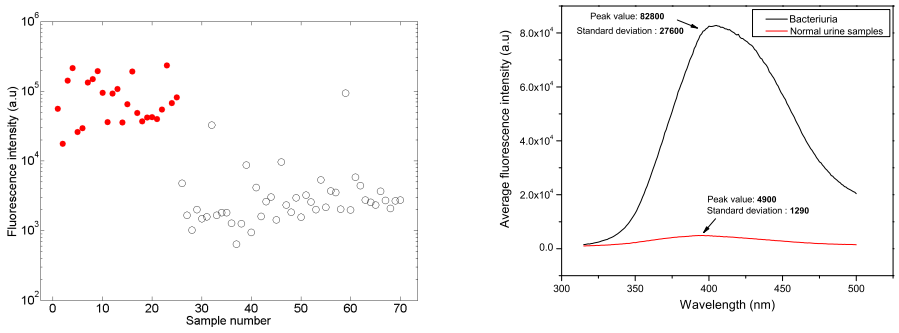

(a) (b)

Figure 4.18: (a) Comparison of maximum fluorescence intensity (emission intensity) for 45 undiluted normal human urines (•) and 25 undiluted bacteriuria samples (◦) at 290 nm excitation wavelength. P=2.14x10^{-12}, by Kolmogrov-Smirnov (KS) test; (b)Average emission spectra of autofluorescence of urine (25 bacteriuria and 45 normal) samples when excited at 290 nm.

The influence of inner filter effect on the EEMs and SFS (with offset $\Delta\lambda$ 90 nm) of undiluted normal human urine and undiluted bacteriuria samples

It is well known that the recorded fluorescence intensity may not be proportional to the fluorophore concentration due to a well-known phenomenon referred to as the inner filter effect [27]. This effect can be due to the absorption of excitation light by the sample (primary inner filter effect) or the reabsorption of emitted light (secondary inner filter effect) [27], or both. In order to understand spectral variations caused due to the inner filter effect, the urine samples were also analysed by using a shorter path length cuvette.

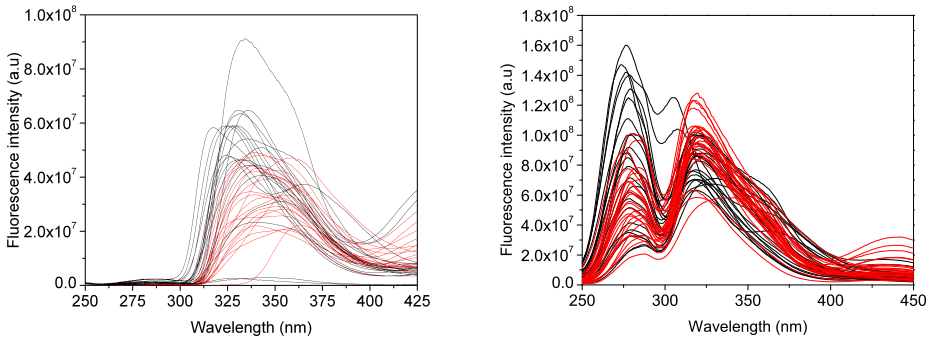

(a) Normal urine (b) Bacteriuria

Figure 4.19: Comparison of SFS ($\Delta\lambda$=90 nm) spectra of urine samples measured using 1mm and 4mm cuvettes (normal samples in red lines, bacteriuria in black lines).

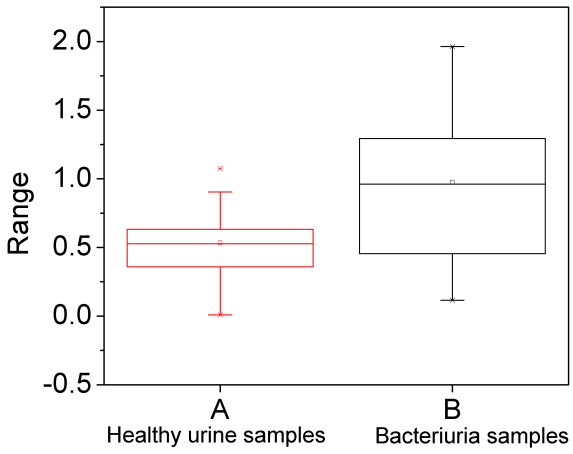

Figure 4.20: Box plot representing the ratio of emission intensity between 280 nm and 320 nm excitation wavelengths for undiluted normal human urines and undiluted bacteriuria samples (using 4 mm cuvettes).

A comparison of the SFS ($\Delta\lambda$=90 nm) of undiluted urines measured using a 10 mm and a 4 mm (Figure 4.19 (a and b)) cuvette clearly showed that the spectral patterns obtained with these cuvettes were different. With the 4 mm cuvette, both undiluted normal and bacteriuria samples showed higher emission intensity in the

shorter UV (250 -300 nm), relative to the emission in the 300-450 nm range (Figure 4.19 (b)). This feature was not observed for urine samples measured with 10 mm cuvette (Figure 4.19 (a)). This is due to higher inner filter effect in the 10 mm cuvette compared to 4 mm cuvette.

However, Figure 4.19 (a and b) also shows that irrespective of the cuvette dimension (i.e. 4 mm or 10 mm), there is higher emission intensity for undiluted bacteriuria samples compared to undiluted normal samples when excited in the shorter UV region (250-300 nm). Further, taking the ratio of emission intensity between 280 nm and 320 nm excitation wavelengths for the samples measured using 4 mm cuvettes clearly differentiated the undiluted normal and bacteriuria samples [P = 6.6x10^{-4} for 0.05% error, Figure 4.20].

Comparison of EEM of normal human urine with bacteriuria samples at various dilutions

1:30 Dilution

It is evident from the Figure 4.21 that both bacteriuria samples were showing higher intensity as compared with the normal samples in the shorter UV. This could be due to higher concentration of indoxyl sulfate in bacteriuria samples as compared with normal human urine [74, 75]. Another reason can be that the indoxyl sulfate at 1:10 dilution is free from concentration quenching and so would contribute more to the emission peak.

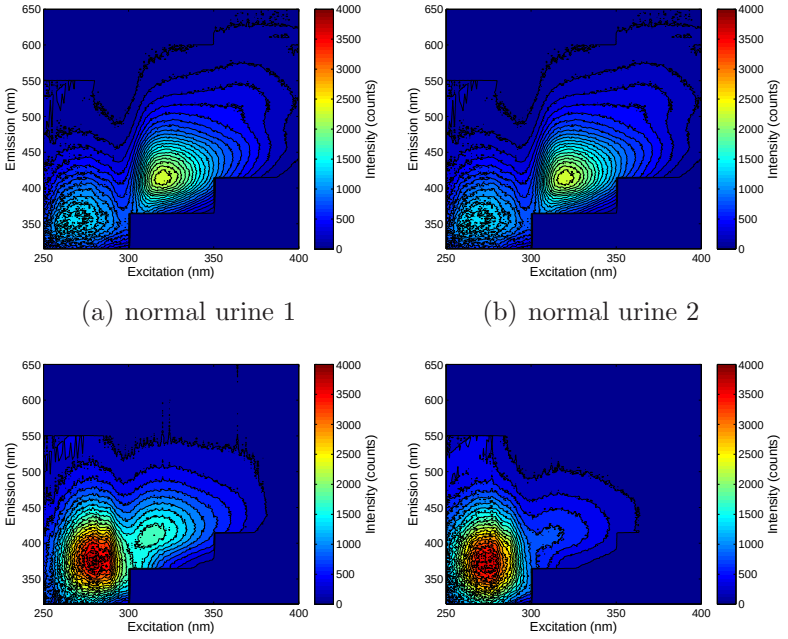

(a) normal urine 1 (b) normal urine 2

(c) Bacteriuria sample 1 (d) Bacteriuria sample 2

Figure 4.21: Excitation/emisson matrices at 1:30 dilution.

.

1:300 Dilution

The two normal urine samples had an almost similar spectral pattern and intensity at 1:300 dilution. Whereas the bacteriuria samples showed different features within themselves. No clear comparison could be made between the normal and bacteriuria samples.

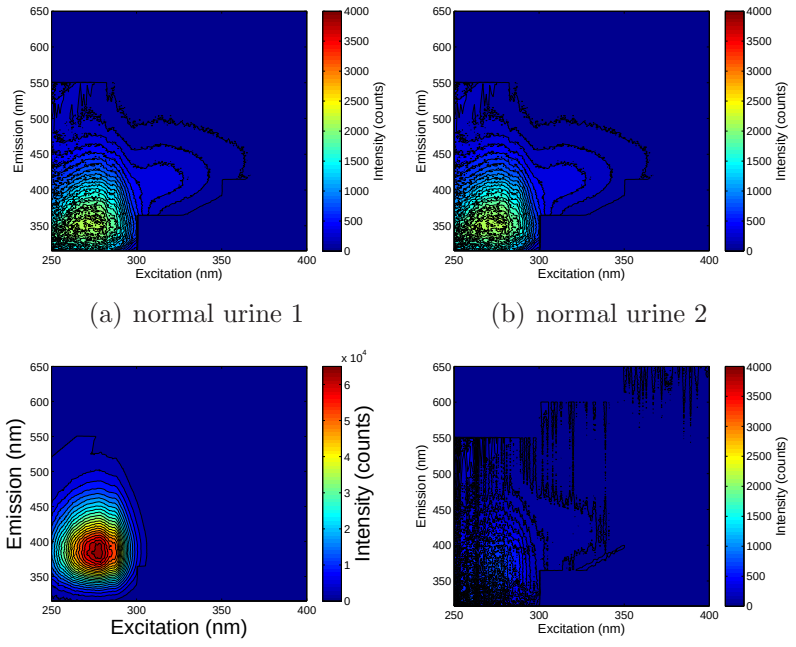

(a) normal urine 1 (b) normal urine 2

(c) Bacteriuria sample 1 (d) Bacteriuria sample 2

Figure 4.22: Excitation/emission matrices at 1:300 dilution. Please note: the scale in excitation/emission matrix of bacteriuria sample 1 is made different due to higher intensity in the shorter UV region.

1:1000 Dilution

It is observed from Figure 4.23, that the two normal human urine samples have similar emission intensity and features, but the two bacteriuria samples have different fluorescence intensity. At 1:1000 dilution normal human urine has higher intensity of blue fluorescence emission.

In conclusion, it is observed that normal human urine emission in the shorter UV increases with dilution, with emission of undiluted $<$ 1:30 $<$ 1:300 $<$ 1:1000. But in the case of bacteriuria samples, 1:30 and 1:300 dilutions were having higher intensity of emission in shorter UV.

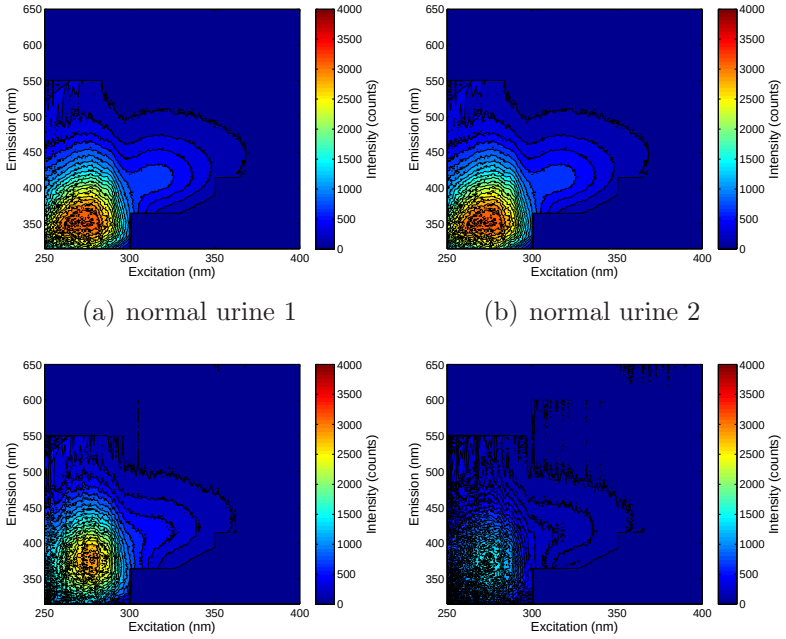

(a) normal urine 1 (b) normal urine 2

(c) Bacteriuria sample 1 (d) Bacteriuria sample 2

Figure 4.23: Excitation/emission matrices at 1:1000 dilution.

Effect of dilution of urine and offset $\Delta\lambda$ of 30 nm for synchronous fluorescence spectra (SFS)

An earlier study [18] advocated diluting the urine sample 1:30 as well as using a $\Delta\lambda$ of 30 nm to characterize a single UTI sample. 25 normal and 25 bacteriuria samples were tested using similar parameters, *i.e.* the urine samples were centrifuged (10 min, 1100 rpm) and diluted 1:30 in double distilled water and the SFS was obtained using a $\Delta\lambda$ of 30 nm.

Contrary to the findings of Dubayova *et al* [18], no clear difference was observed between the two groups of samples (Figure 4.24 a and b). However, an offset $\Delta\lambda$ of 90 nm showed a clear distinction between the two groups of diluted samples (Figure 4.24 c and d), with the ratio of autofluorescence at 280 nm and 325 nm excitation between the groups showing a significant difference (P=.0035 for 0.05% error).

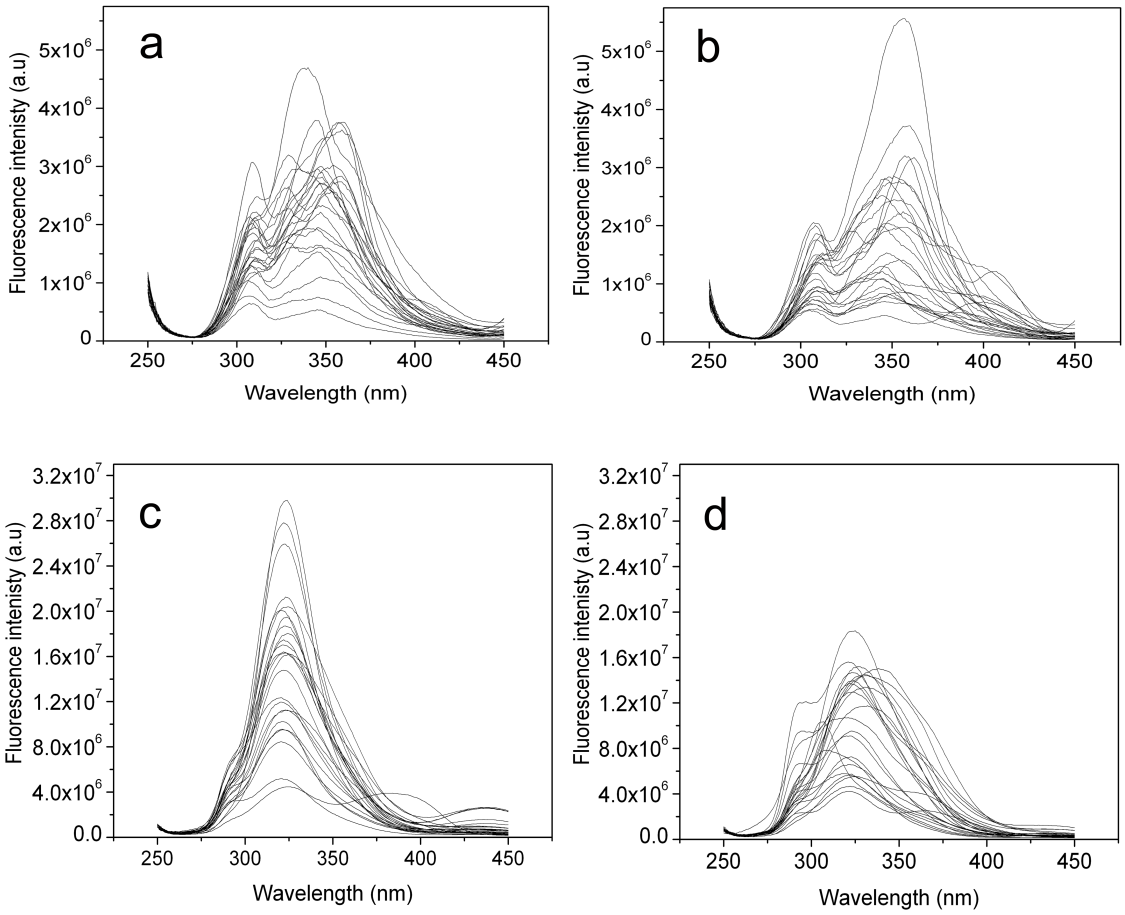

Figure 4.24: Comparison of SFS of diluted (1:30) normal human urines with diluted (1:30) bacteriuria samples measured using 10 mm cuvette. (a) and (c) SFS of diluted normal human urine with offset wavelengths $\Delta\lambda$=30 and $\Delta\lambda$=90 nm respectively; (b) and (d) SFS of diluted bacteriuria samples with offset wavelengths $\Delta\lambda$=30 and $\Delta\lambda$=90 nm respectively.

Comparison of the concentration of tryptophan and indoxyl sulfate in normal human urine and bacteriuria samples.

In order to shed some light on the identity of fluorophores responsible for the observed fluorescence intensity variations between UTI and normal urine, HPLC measurements was carried out. This is because the examination of fluorescence EEMs alone is generally not sufficient for chemical analysis of urine.

The fluorophores which can contribute most to the emission peak at 410 ±10 nm when excited at 280 ±5 nm include indoxyl sulfate, tryptophan, indolyl-3-acetate and xanthine (Table 2). The concentration of these fluorophores in urine may be linked to conditions such as UTI. Bacteria such as *E. coli* can reduce tryptophan to indole resulting in a variation of the concentration of tryptophan and its metabolites [76] which can alter the fluorescence. Increased levels of the enzyme indoleamine 2,3-dioxygenase (IDO) have been reported in infections and inflammatory conditions [77–80]. It is possible that there is a reduction in tryptophan and its metabolites in samples from bacteriuria cases, due to the increased levels of IDO. The reduction of tryptophan and its metabolites in urine could overcome the inner filter effect and possibly the quenching effect also [20] and hence show high fluorescence intensity at 290 nm excitation, not observed with normal urine samples.

In order to test this hypothesis, in the present study, the concentration of indoxyl sulfate and tryptophan in normal and bacteriuria samples, by HPLC was analyzed. As seen from Table 1, there is a slightly higher but not significant concentration of indoxyl sulfate in bacteriuria samples when compared to the normal urine samples. It is debatable whether this small concentration difference underpins the higher fluorescence observed for bacteriuria samples. HPLC results also show no significant differences in the concentration of tryptophan between the two sample groups.

Finally, other factors that could contribute to the differences in autofluorescence between normal and bacteriuria samples were also considered. It has been reported that in UTI, xanthine oxidase (XO) activity is above 1000 units/litre compared to its negligible quantities in sterile human urine [81]. XO catalyses the oxidation of hypoxanthine to xanthine and to uric acid. During this process, super oxides are also generated [82, 83]. Xanthine is excited at 270 ±10 nm with an emission peak around 350 nm [84]. It was suggest that the increased autofluorescence of bacteriuria

samples excited at shorter UV could be due to the variation in the concentration of xanthine, uric acid and the generation of super oxide in bacteriuria samples due to XO activity.

It is apparent from Table 2 that the fluorophores which could mainly contribute to emission at 425 ±10 nm at 330 ±20 nm excitation are 4-pyridoxic acid, 3-hydroxy-anthranilic acid, xanthurenic acid and neopterin. The possibility of 3-hydroxy-anthranilic acid and xanthurenic acid contributing to the differences observed in the fluorescence between the normal and bacteriuria samples is remote, in light of an earlier report that the mean excretion of 3-hydroxy-anthranilic acid and xanthurenic acid for normal and UTI patients are similar [85]. However, patients with bacterial urinary tract infections are known to have increased neopterin concentration in their urine, associated with protracted infection rather than with local activation of immune cascades and direct release of neopterin into the urinary tract [86]. Therefore the spectral blue shift observed in the emission region 425 ±10 nm with 330 ±20 nm excitation for the bacteriuria samples could be attributed to such increased neopterin concentration.

4.5 Summary

In this study, UV autofluorescence of UTI samples and normal human urine samples were analysed in detail. Even without dilution, pronounced spectral differences were observed in the EEMs in the shorter UV (250-300 nm) region, as well as a clear difference in the emission intensity at 290 nm for the two groups of urine samples. In this study it was shown that, SFS with an offset $\Delta\lambda = 90$ nm can be used effectively to differentiate between undiluted UTI and normal urine samples. The emission scan at 290 nm and SFS measurements with an offset $\Delta\lambda = 90$ nm will only take 1 minute for measuring a single sample, which is the fastest current diagnosis

technique for UTI.

The concentration of two key indole compounds (indoxyl sulfate and tryptophan) by using HPLC was tested, in an attempt to explain their role in urine autofluorescence. However, HPLC analysis did not reveal any significant difference in the concentration of tryptophan and indoxyl sulfate in the normal urine and UTI samples. It was suggest that multiple factors such as xanthine oxidise activity, tryptophanase and higher neopterin concentration could possibly contribute to the differences observed in the fluorescence spectra between the two groups of urine samples.

The results provide a proof of the concept for using the fluorescence spectrum of urine as a diagnostic tool to differentiate between normal and UTI urine, despite strong physiological variability between individual samples.

5

Autofluorescence of Human Adipose Derived Stem Cells

5.1 Introduction

In this Chapter, a preliminary study of autofluorescence of human adipose derived stem cells at 400 nm excitation wavelength has been described. Principal component analysis (PCA) was utilized to visualize the spectral pattern of stem cells undergoing differentiation in osteogenic medium. The aim of the study is to identify the potential of using autofluorescence measurement with a single excitation (400 nm) as a diagnostic tool for analyzing the osteogenic differentiation process.

5.1.1 Stem cells

Stem cells have the remarkable potential to develop into many different cell types in the body during early life and growth. Stem cells are distinguished from other cell types by two important characteristics. First, they are unspecialized cells capable of renewing themselves through cell division (self-regeneration). Second, under certain physiologic or experimental conditions, they can be induced to become tissue or organ-specific cells with special functions.

The ability to differentiate is the potential to develop into other specialised cell types. A totipotent stem cell (*e.g.* fertilized egg) can develop into all cell types including the embryonic membranes, Table 5.1. A pleuripotent stem cell can develop into cells from all three germinal layers (*e.g* cells from the inner cell mass). In addition, cells can also be oligopotent, bipotent or unipotent depending on their ability to develop into few, two or one other cell type (Table 5.1) [87].

Self-regeneration is the ability of stem cells to divide and produce more stem cells. During early development, the cell division is symmetrical *i.e.* each cell divides to gives rise to two daughter cells, each with the same potential. Later in development, the cell divides asymmetrically with one of the daughter cells produced being a stem cell and the other a more differentiated cell.

5.1.2 Adipose derived adult stem cells

The adipose tissue is a highly complex tissue, which consists of mature adipocytes, preadipocytes, fibroblasts, vascular smooth muscle cells, endothelial cells and resident monocytes/macrophages [88, 89]. The stromal-vascular cell fraction (SVF) of the adipose tissue compartment provides a rich source of pluripotent adipose tissue-derived stromal cells [90, 91]. They are ideal as a cell source in the field of regenerative medicine [92]. Adult adipose tissue has recently become recognised as an alternative and rich source of mesenchymal stem cells.

5.1.3 Differentiation

The phenotype of cells cultured and propagated as a cell line is often different from that of the predominant cell type in the originating tissue. This is due to several factors that regulate the geometry, growth and function in vivo, but that are absent from the in vitro microenvironment. *Differentiation* is the process leading to the expression of phenotypic properties characteristic of the functionally mature cell in

Differentiation potential	Number of cell types	Example of stem cell	Cell type resulting from differentiation
Totipotential	All	Zygote, blastomere	All cell types
Pleuripotential	All except cells of the embryonic membranes	Cultured human Embryonic stem cells	Cells from all three germ layers
Multipotential	Many	Hematopoietic cells	skeletal muscle, cardiac muscle, liver cells, all blood cells
Oligopotential	Few	Myeloid precursor	5 types of blood cells, (Monocytes, macrophages, eosinophils, neutrophils, erythrocytes)
Quadripotential	4	Mesenchymal progenitor cell	Cartilage cells, fat cells, stromal cells, bone-forming cells
Tripotential	3	Glial-restricted precursor	2 types of astrocytes, oligodendrocytes
Bipotential	2	Bipotential precursor from murine fetal liver	B cells macrophages
Unipotential	1	Mast cell precursor	Mast cells
Nullipotential	None	Terminally differentiated cell e.g. Red blood cell	No cell division

Table 5.1: Differentiating potential ranges from totipotent stem cells to nullipotent cells. Data taken from [87]

vivo [93].

Two models of stem cell differentiation

Stem cell differentiation has been explained by two models [94].

The first is the stochastic model of stem cell renewal [95]. In this model, stem cells in tissue units are postulated to exist in stable pools from which some differ-

entiate to form specialized tissue cells, whereas others remain as stem cells. The second, more recent model, is that of "transdifferentiation." Many laboratories have reported that when stem cells are transferred to a heterologous tissue site, they can begin to produce differentiated cells that are unique to the recipient tissue [3,4]. Transdifferentiation has been presented from the perspective that the stem cell itself changes fundamentally in different tissue environments [5]. Therefore, though plastic in some respects, stem cell differentiation might be restricted by local tissue factors to yield only the mature cell types of a stem cell's current tissue of residence.

5.1.4 Factors that control differentiation

- Cell interaction: Cell interaction can be divided into two main class, these are homotypic and heterotypic interactions. Homologous cell interactions which occurs at high density is called homotypic. Homotypic interaction generally involves gap junctional communication. As a result, metabolites, second messengers such as Ca^{2+}, or electric charges could be communicated between cells. The heterologous cell interactions are called heterotypic [93].

- Systemic or Exogenous factors: Exogenous factors which affect differentiation can be classified as physiological inducers and nonphysiological inducers. Hormones arising from a distant organ or tissue, Vitamins such as D3 and retinoic acid derived from diet and inorganic ions such as Ca^{2+} are some of the physiological inducers which are known to affect cell differentiation.

  On the other hand, nonphysiological inducers such as dimethyl sulfoxide (DMSO), hexamethylene bisacetamide (HMBA), mitomycin C *etc* are also known to affect cell differentiation [93].

- Cell-Matrix interactions: Cells are generally surrounded by complex mixtures of glycoproteins and proteoglycans that are highly specific for each tissue, and

even parts of tissue. literature has shown that artificial matrix can regulate gene expression in cells [93]. Collagen is a typical example which has been found to be very essential for the functional expression of many epithelial cells [93].

- Oxygen tension:

  Previous studies have shown that positioning the cells at the air-liquid interface enhances gas exchange, particularly facilitating oxygen uptake without raising the partial pressure and risking free radicals [93].

5.2 Importance of cell differentiation

Cellular differentiation plays a vital role in normal life. Differentiation occurs numerous times during the development of a multicellular organism as the organism changes from a simple zygote to a complex system of tissues and cell types. Differentiation is a common process in adult organism as well: adult stem cells divide and create fully-differentiated daughter cells during tissue repair and during normal cell turnover. Differentiation dramatically changes cell's size, shape, membrane potential, metabolic activity, and responsiveness to signals.

During development, for example, all cells first undergo rapid growth before settling down into specialized functions (jobs). Understanding of this process could lead to potential stem cell therapies as well as helping prevent developmental problems in the womb. MicroRNAs are viewed as a potential way to change differentiated adult cells back into pluripotent stem cells, which could then be used for therapeutic purposes, including wound healing and tissue regeneration.

Another area where cell differentiation is important is in cancer biology, where runaway growth causes disease. A thorough understanding of differentiation could

lead to better cancer treatments.

5.3 Osteogenic differentiation of adult stem cells

Bone is a tissue, constantly being remodeled in a dynamic process where osteoblasts are responsible for bone formation and osteoclasts for its resorption [96, 97]. The ability of mesenchymal stem cells (MSCs) to give rise to osteoblasts is well known [98]. Osteoblasts are specialized mesenchymal cells that undergo a process of maturation where genes like core-binding factor alpha1 (Cbfa1) and osterix (Osx) play a very important role [99].

From previous literature, it is known that, adipose derived stem cells (ADSCs) are observed to express genes and proteins associated with an osteoblasts phenotype. In addition, ADSCs also known to produce alkaline phosphatase, type 1 collagen, osteonectin, osteocalcin, bone sialo protein, RunX-1, BMP-2, BMP-4, BMP receptors I and II, PTH-receptor [98].

5.4 Autofluorescence of cells

Cells contain molecules which can fluoresce under suitable UV or visible wavelength. This fluorescence emission, arising from endogenous fluorophores, is an intrinsic property of cells and is called auto-fluorescence.

There are many endogenous fluorophores in cells and tissue. Some of the endogenous fluorophores are shown in the Figure 5.1. The most important endogenous fluorophores are molecules widely distributed in cells and tissues, such as proteins, NAD(P)H, flavins and lipopigments [100]. Most endogenous fluorophores are associated with the structural matrix of tissues or are involved in cellular metabolic processes [101]. The majority of cell auto-fluorescence originates from mitochondria and lysosomes [100]. The pyridine nucleotides and the flavins are major endogenous

fluorophores which are involved in the cellular energy metabolism. In the energy metabolism pathways, nicotinamide adenine dinucleotide NAD(P) act as a major electron acceptor, *i.e.* NADH act as a hydrogen transferring molecule in the respiratory chain [102]. The reduced form, NAD(P)H, is fluorescent and has an excitation maximum at 340 nm and emission maximum at approximately 450 nm. When NAD(P)H is bound to the proteins, the fluorescence quantum yield increases and both the excitation and emission maxima are blue-shifted [100]. The aromatic amino acids (e.g. tryptophan, tyrosine, phenylalanine), various porphyrins and lipopigments (e.g.ceroids, lipofuscin) that are the end-products of lipid metabolism are also known to be highly fluorescent and have excitation in the shorter UV region (200-300 nm) and emission near 350 nm [100, 101].

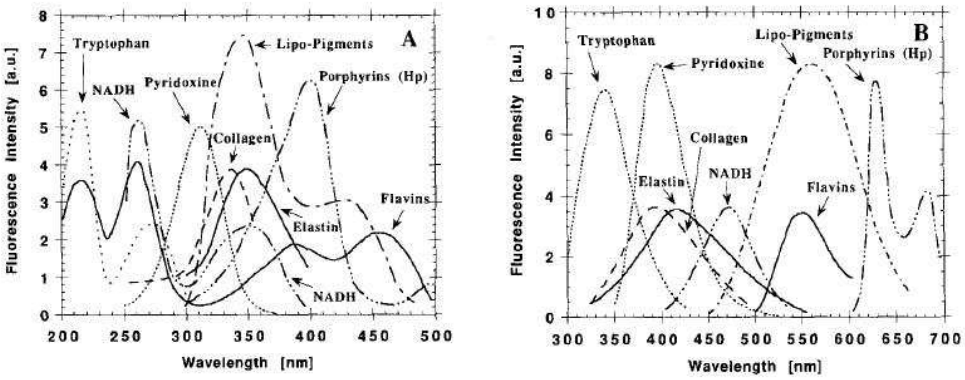

(a) (b)

Figure 5.1: Excitation (a) and emission spectra (b) of the principal endogenous fluorophores in cells. Data taken from Wagnieres *et al* [101].

5.5 Experimental Methodology

5.5.1 Establishing and preparing stem cells

Stem Pro Human Adipose Derived Stem Cells (ADSCs) were obtained from Invitrogen. These cells were isolated from human adipose tissue, collected during

liposuction procedures and cryopreserved from primary culture. Each vial of cells contained 1x 10^6 cells in freezing medium. These cells can differentiate into multiple mature cell phenotypes in vitro. These includes adipocytes, osteoblasts and chondrocytes.

Prior to each experiment, frozen cells were thawed under sterile conditions. The vials of cells were removed from liquid nitrogen storage, wiped with ethanol and the pressure was relieved by twisting the vials cap a quarter turn and retightened to avoid direct exposure of cells to air before thawing. Each vial was quickly thawed by swirling it in a 37 ^{0}C water bath and removing it when the last bit of ice has melted, typically less than 2 minutes. When thawed, cells were immediately transferred into a 50 ml sterile tube containing prewarmed complete medium , drop wise up to 10 ml. The supernatant was aspirated after centrifugation cells for 5 minutes at 1200 rpm. Cells were resuspended in Mesen Pro Rs medium and transferred into culture dishes (75 cm^2 culture flask, with seeding density about 5000 cells per cm ^{2}). Cells were incubated at 37^{0}C , 5%CO2 and 90% humidity to allow cells to adhere for several hours or overnight. The medium was replaced with fresh prewarmed complete Mesen Pro Rs medium and changed every 3-4 days.

5.5.2 Subculturing of cells

In order to maintain optimum and standardized conditions for cells during experiments, cells were subcultured before cells reached 60-80% confluency. The viability of cells was observed to be at least 90% for each subculturing. To avoid contamination, antibiotics-antimycotic containing pencillin, streptomycin and amphotericin B were added to medium. Subculturing was performed under aseptic conditions. Mesen Pro medium was aspirated from cells and the surface of cell layer was rinsed with Dulbeco Phosphate Buffer Saline (DPBS). For cell detachment, prewarmed

TrypLE (0.5ml/10 cm^2) was added and incubated at 37^0C for 7-9 minutes to achieve cell detachment of more than 90%. Prewarmed Mesen Pro medium (equivalent to twice the volume used for Tryp LE) was added and cells were transferred to a 15 ml conical tube and centrifuged at 1200 rpm for 5 minutes at room temperature. This is then followed by removing supernatant and resuspenstion of the cell pellet in a minimal volume of prewarmed medium. The viability of cells was determined using trypan blue exclusion test. The seeding density of cells was approximately 5000 cells/cm^2. Medium was replaced three to four days after seeding.

5.5.3 Characterization of cells using flow cytometery

Antigenic characteristics of adipose tissue derived stem cells were confirmed using antibodies conjugated with biomarkers such as CD45, CD31, CD90, CD105. Following subculturing, the pellet of centrifuged cells was suspended in a minimal volume of DPBS. Cells were fixed with 37% paraformaldehyde for 20 minutes at room temperature. Cells were washed with PBS to remove fixing solution and suspended with PBS. Fluorescent conjugated antibodies were added to cells to be analyzed by flow cytometer.

5.5.4 Autofluorescence microscopy

All images were obtained using Leica SP2 laser scanning confocal microscope, which had the emission scanning capabilities. The excitation wavelength used was 400 nm. The power of laser was set below 5 mw to avoid cell damage by light stimulation. Photomultiplier tube (PMT) was utilized to collect the emission signals. 40 x oil immersion objective was mainly utilized for imaging cells. Prior to autofluorescence microscopy, medium of cells was replenished with colorless Hank's Balance solution to avoid autofluorescence from the medium. All the images were processed using MATLAB or ImageJ.

5.5.5 Fluorescent dyes and subcellular marker

To confirm the identity of autofluorescent cellular structures, labeling dyes were used to stain the specimens. ER tracker Blue white DPX and Mitotracker deep red were used for staining the endoplasmic reticulum and mitochondria of ADSCs respectively. The final working concentration for each dye (100 nm) was achieved by prewarming in room temperature and subsequently diluting 1 mM stock solution using Hank's balanced salt solution (HBSS). Cell culture medium was removed and replaced with appropriate, prewarmed probe containing medium. Incubation was carried out for 20 minutes with ER tracker Blue white DPX dye and 15 minutes for Mitotracker deep red . The cells were then washed with HBSS and mounted on a single concave slide with 50μl of HBSS.

5.6 Results

5.6.1 Labeled stem cell mitochondria and endoplasmic reticulum using fluorescent dyes

Figure 5.2 shows the adipose derived adult stem cells, whose endoplasmic reticulum and mitochondria have been labelled using fluorescent dyes. The fluorescence dye used for staining endoplasmic reticulum was ER tracker green. The mitochondria were stained using Mitotracker deep red. The green regions of cells are endoplasmic reticulum and the red regions are mitochondria. It is evident from Figure 5.2 that, mitochondria are distributed near the nucleus (kind of perinuclear formation).

5.6.2 Colocalization of stem cell mitochondria autofluorescence at 400 nm

Figure 5.3 shows the autofluorescence of stem cells (green colour) at 400 nm excitation, overlayed with fluorescence from mitochondria (red colour) labeled with

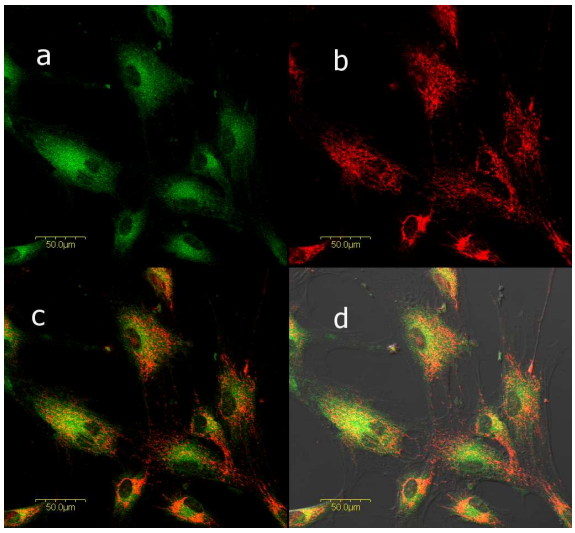

Figure 5.2: Labeled (a) endoplasmic reticulum (green), (b) mitochondria (red), (c) overlayed image a and b, (d) overlayed image with transmission for adipose derived adult stem cells.

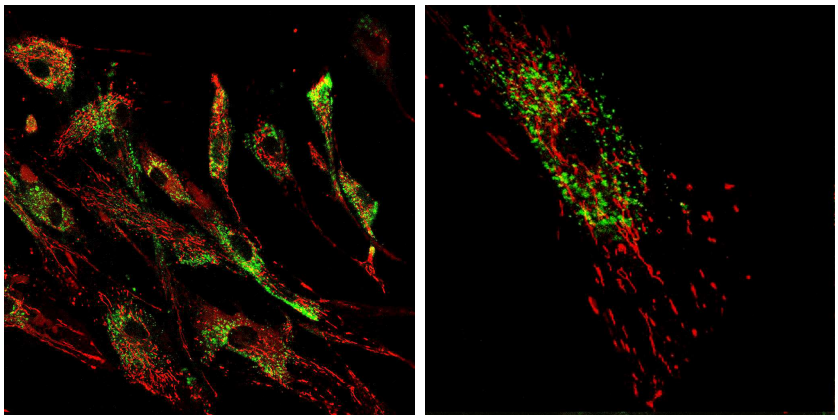

(a) (b)

Figure 5.3: Colocalization of stem cells autofluorescence at 400 nm and mitochondria. The red region is the mitochondria stained by Mitotracker and the green region is the autofluorescence at 400 nm. Note: first the autofluorescence is taken then cells were stained and imaged without changing the field of view.

Mitotracker deep red . It is evident from the Figure 5.3 that mitochondria of stem cells are not significantly contributing to the stem cells, autofluorescence at 400 nm excitation. It seems that lysosomes and endoplasmic reticulum are the possible

organelles showing fluorescence at 400 nm.

5.6.3 Stem cell autofluorescence at 400 nm with time

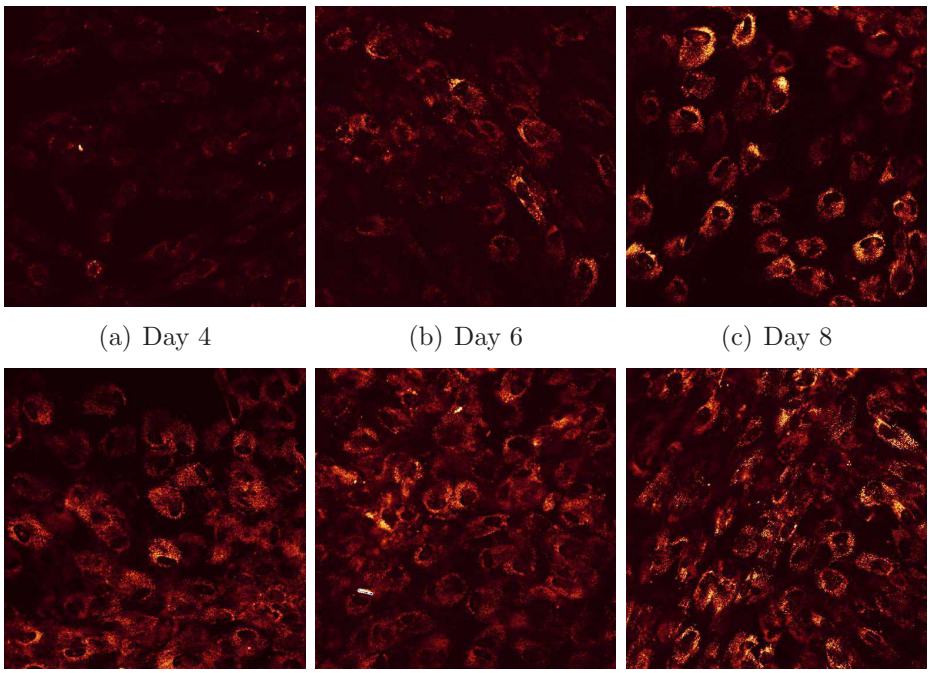

(a) Day 4 (b) Day 6 (c) Day 8

(d) Day 11 (e) Day 13 (f) Day 15

Figure 5.4: Autofluorescence of stem cells with time at 400 nm excitation wavelength. Note : emission spectra were taken from 420 to 560 nm with 20 nm step size.

Figure 5.4 shows the autofluorescence of stem cells at 400 nm excitation for different days. On the second day after seeding, autofluorescence of the cells was too weak to be detected by the confocal microscope. Only from day 4, autofluorescence of stem cells started to increase and there was enough signal to be detected by the confocal. It is evident from Figure 5.4 that there is more brightness in autofluorescence for stem cells with time. The cell confluence (density) was observed to be around 60% on day 4, Figure 5.5 a. By the 6th day the cell density reached 90%, Figure 5.5 b.

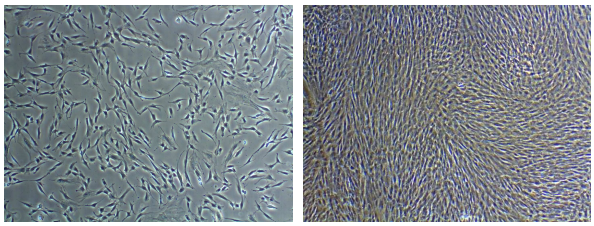

(a) (b)

Figure 5.5: Phase contrast image a and b, show the cell density (confluence) of stem cells on day 4 and day 6 respectively. Note from day 6 to day 15, the cell confluence was almost 100%.

5.6.4 PCA on stem cells, autofluorescence spectra for 400 nm excitation

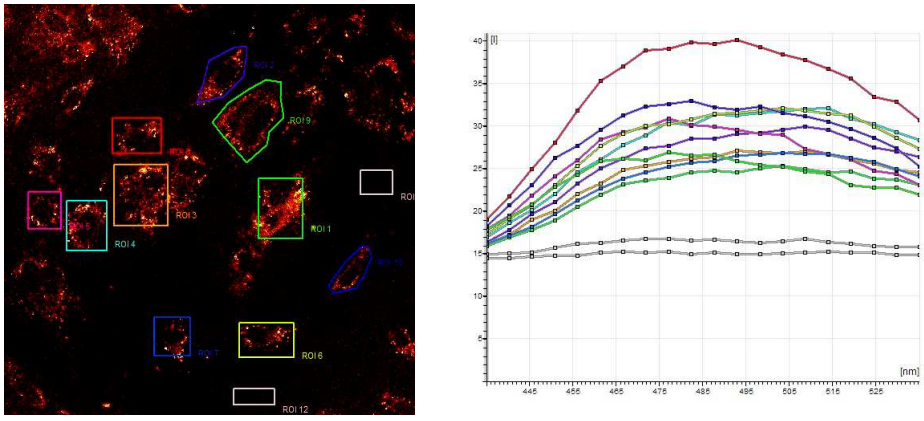

(a) (b)

Figure 5.6: a) Shows the extraction (selection) of emission spectra of individual cells randomly from a emission stack image. b) Illustrates the spectral data corresponding to the selected cells.

In order to understand and visualize the variation (pattern) of autofluorescence of stem cells at 400 nm with time, principal component analysis (PCA) was utilized. To perform PCA, the emission spectra of individual cells were picked first. A total number of 10 cells were measured from each image. This is illustrated in Figure 5.6 a and b. Three different regions of cells were imaged from each slide *i.e.* 30 cells were measured to be representative for each class of cells.

Figure 5.7 shows the projection of the cell classes into the PCA space (each dot in the plot represents a single cell). From Figure 5.7, it is evident that trajectories of spectral movement of the cell classes (the pattern of autofluorescence)at 400 nm changes with time. There is greater variance and spread with time. However, after 13th day the pattern of fluorescence moves towards the day 4 cells in space. This could be because the cells are not growing anymore.

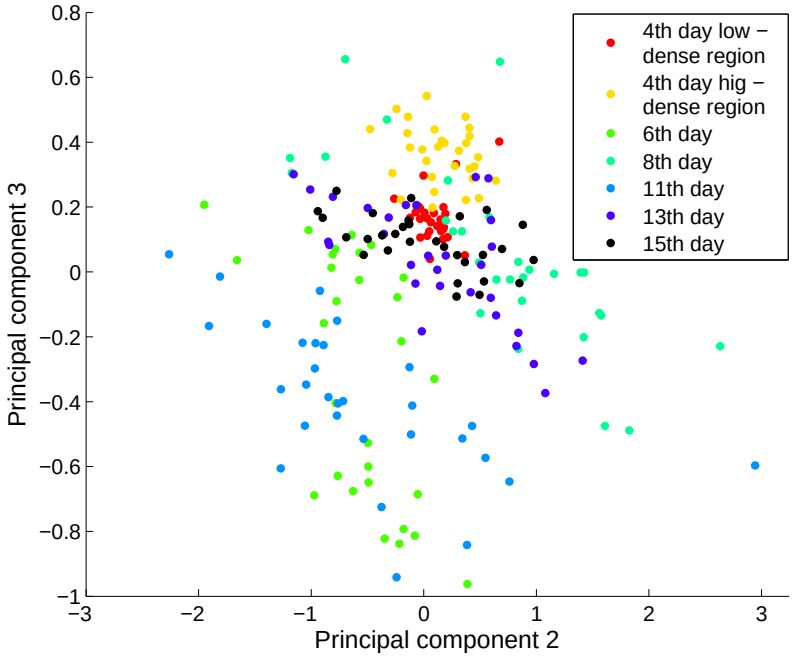

Figure 5.7: PCA of stem cell autofluorescence.

From the PCA analysis, it is also evident that there is fluorescence difference in the spectral pattern between high and low density for stem cells on day 4 (Figure 5.8).

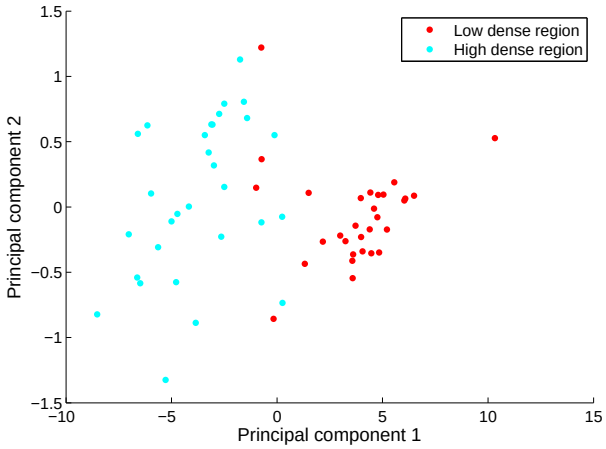

Figure 5.8: PCA illustrating the fluorescence difference between cells in high and low density regions (day 4).

5.6.5 Autofluorescence of stem cells undergoing differentiation medium, at 400 nm with time

Autofluorescence of stem cells differentiated in osteogenic medium cells were measured from 48 hrs. This was done for the cells to adapt to the new environment. The cell density of cells after 4 hrs (initial state) was around 40% (Figure 5.10 a). By the 2nd day the cell confluence has already become around 80-90%. Compared to the autofluorescence of stem cells at 400 nm excitation, stem cell differentiated in osteogenic medium also showed similar trend in increasing fluorescence with time, Figure 5.10.

5.6.6 PCA on autofluorescence spectra of stem cells undergoing differentiation in osteogenic medium at 400 nm excitation

In order to understand and visualize the variation (pattern) of autofluorescence for stem cells undergoing differentiation in osteogenic medium at 400 nm with time, principal component analysis (PCA) was utilized. Figure 5.11 shows the projection

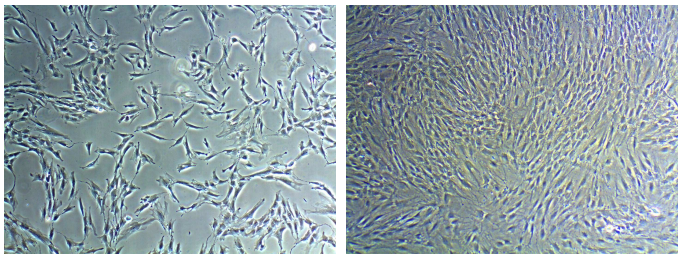

(a) (b)

Figure 5.9: Phase contrast images a and b, show the cell density (confluence) of stem cells on day 4 and day 6 respectively. Note from day 6 to day 15, the cell confluence was almost 100%.

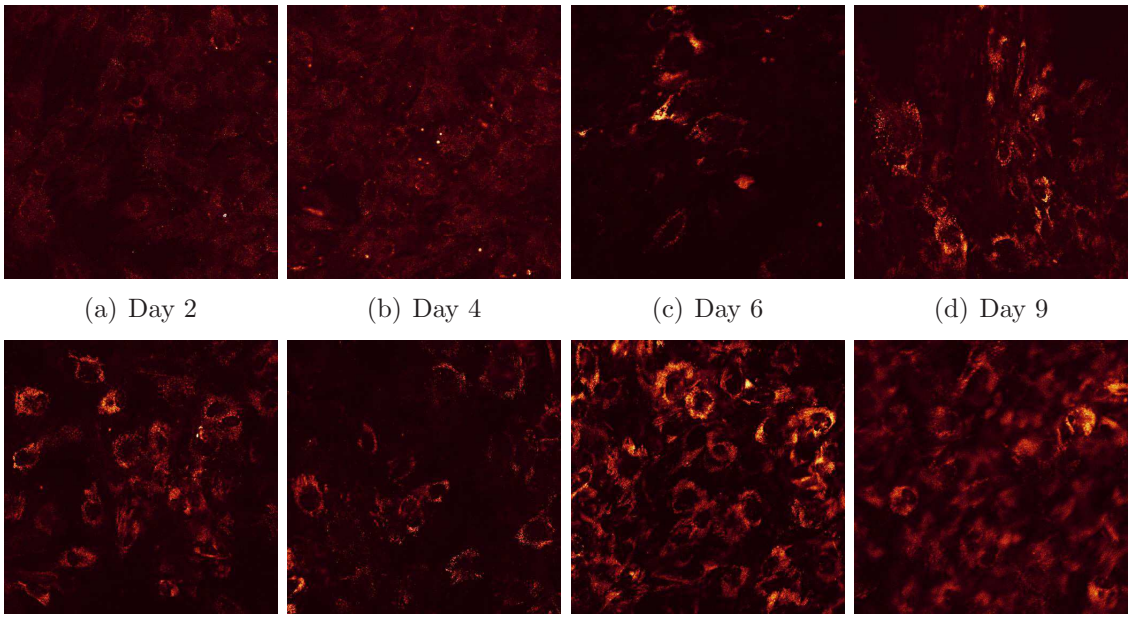

(a) Day 2 (b) Day 4 (c) Day 6 (d) Day 9

(e) Day 11 (f) Day 13 (g) Day 15 (h) Day 17

Figure 5.10: Autofluorescence of stem cells undergoing differentiation in osteogenic medium with time, at 400 nm excitation wavelength. Note : emission spectra were taken from 420 to 560 nm with 20 nm step size.

of the cell classes into the PCA space. The day 2 and day 4 cell pattern in 3D space has two different locations. However, when compared to the stem cells, spectra of stem cells undergoing differentiation in osteogenic medium in space was spreading away from the initial position.

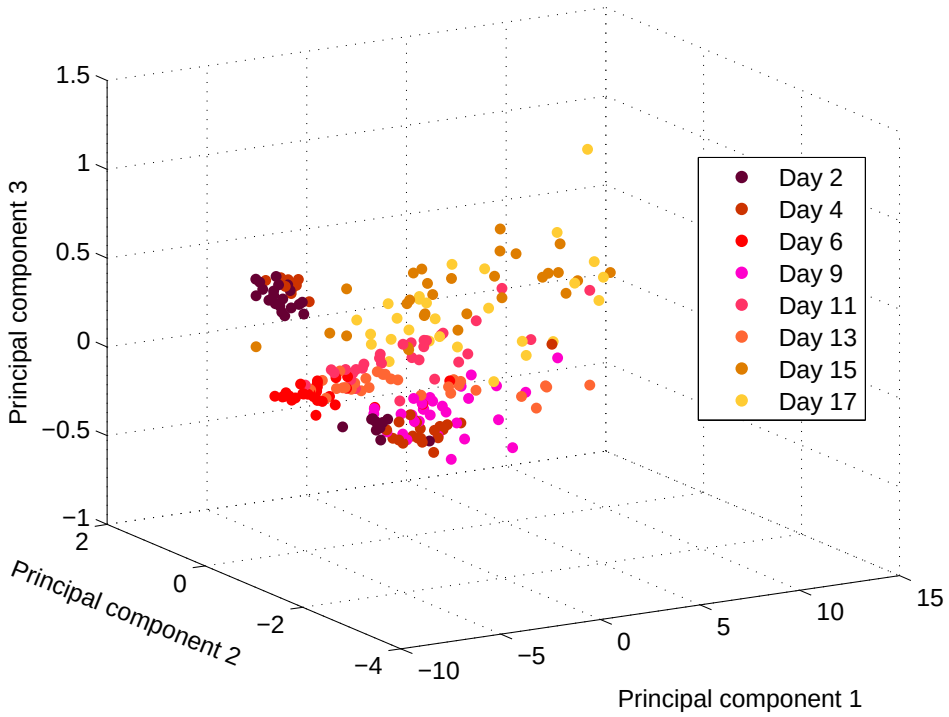

Figure 5.11: PCA of autofluorescence spectra for stem cells undergoing differentiation in osteogenic medium.

Figure 5.12 shows that irrespective of high and low density region of stem cells, within 60 hrs, stem cell and stem cell differentiated in osteogenic medium are separated clearly in 3D PCA space.

5.6.7 Tracking mitochondrial activity in stem cells with time

Figure 5.13 shows the stem cells stained by JC1 dye on the 2nd day and on the 8th day. Compared to stem cells on day 8, it is evident that stem cells on day 2 have less red emission. This indicates less activity of mitochondria for stem cells on day 2 compared to day 8. In other words, the day 8 cells were having higher mitochondrial activity (greater metabolism) compared to day 2 cells.

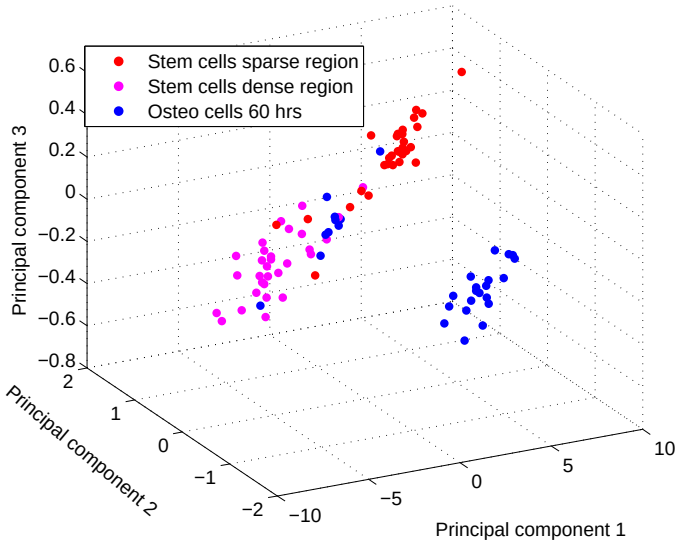

Figure 5.12: A comparison of stem cells and stem cells undergoing differentiation in osteogenic medium in 3D PCA space after 60 hrs.

5.6.8 Morphological changes in mitochondria of stem cell with time

In order to understand the morphological variations of mitochondria with time (in passage 3) in stem cells, Mitotracker deep red dye was used to stain the mitochondria of cell and cells were imaged using confocal microscope on different days (2nd and 8th day after seeding). Figure 5.14 shows the images of stem cells stained by Mitotracker deep red dye (specific to mitochondria) on day 2 and day 8. Figure 5.14 reveals that on both these days a similar perinuclear formation of mitochondria was observed.

5.6.9 Morphological changes in mitochondria of stem cells undergoing differentiation in osteogenic medium with time

In order to understand the morphological variations of mitochondria with time (in passage 3) for stem cells undergoing differentiation in osteogenic medium, Mito-

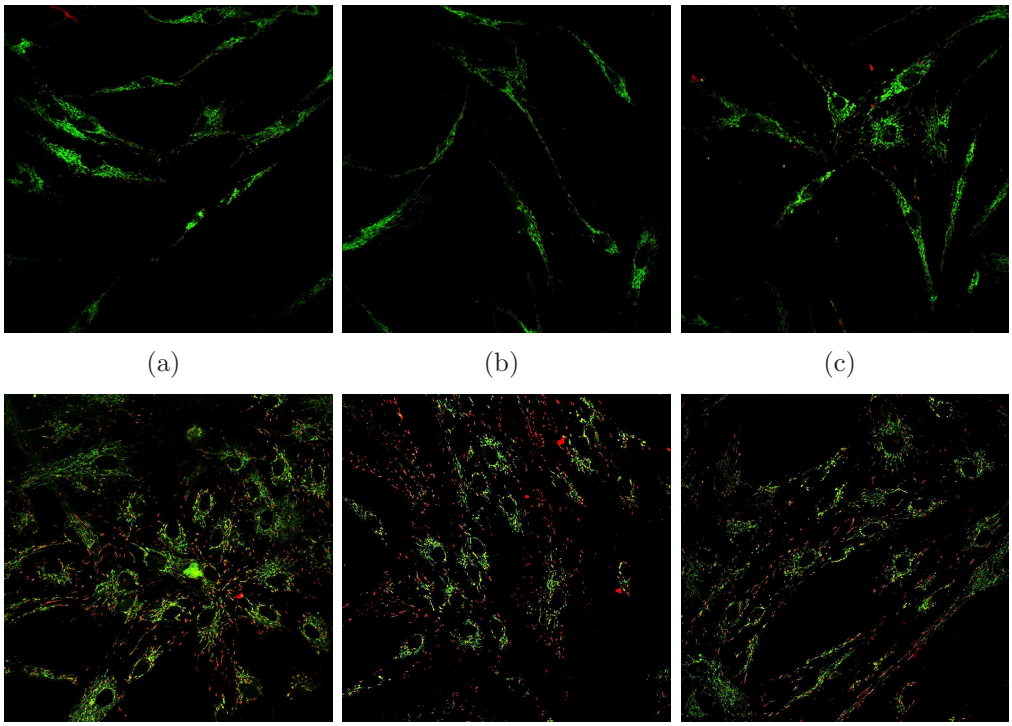

Figure 5.13: Comparison of mitochondrial activity of stem cells on day 2 and day 8 of passage 3, using JC1 dye. a, b and c were images taken on day 2 after seeding (Passage.3). d, e and f were images taken on day 8 (Passage.3). Note: greater red emission means higher activity in mitochondria.

tracker deep red dye was used to stain the mitochondria of cell and cells were imaged using confocal microscope on the 13th day (Figure 5.15). Compared to perinuclear formation of mitochondria in stem cells, the mitochondria of stem cells undergoing differentiation in osteogenic medium were having large and nod network like pattern.

5.7 Discussion

Currently, all the techniques for characterizing stem cells use chemicals, enzymes (bio-markers) and techniques such as PCR. All these characterization methods are invasive techniques. In this study, non invasive optical methods (measuring autofluorescence) have been utilized to test the potential for characterizing stem cells. The

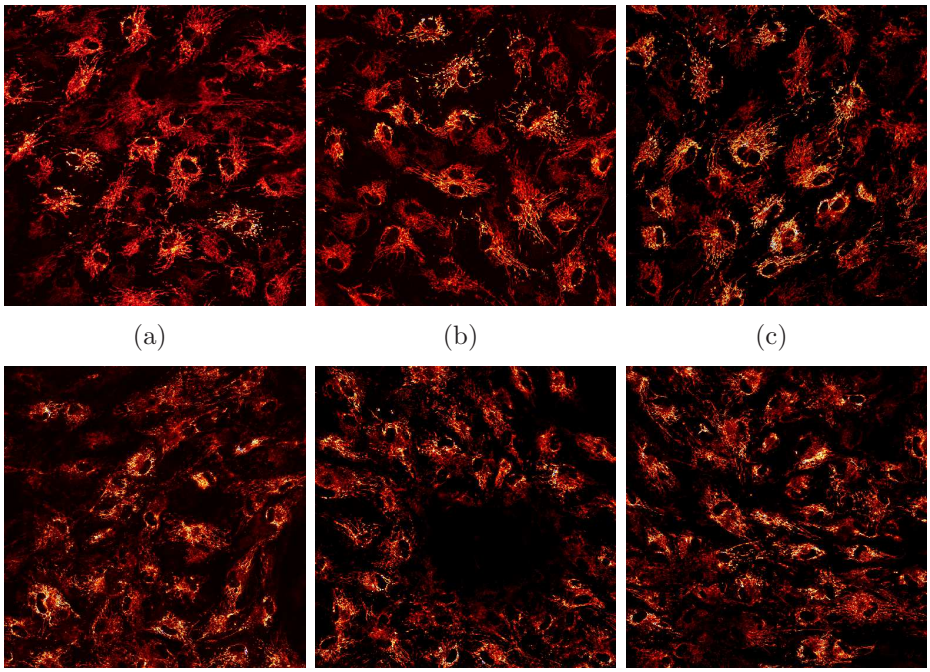

Figure 5.14: Images (40x objective) of stem cells stained by Mitotracker deep red dye. a, b and c were images taken on day 2 after seeding (Passage.3). d, e and f were images taken on day 8 (Passage.3). Note: Mitotracker deep red has excitation maximum at and emission maximum.

preliminary studies demonstrate that autofluorescence imaging of adult stem cells could provide vital information in understanding the cells metabolism and differentiation process.

A survey of the literature indicates that the fluorescence properties could be utilized to characterize cell metabolism [103, 104]. Reyes *et al* (2008), has demonstrated that pyridine nucleotide to flavoprotein ratio decreased upon transition from stem cells to differentiated cells [103]. In their study, 350 nm excitation has been utilised to excite pyridine nucleotides in the cells. In this study 400 nm excitation was chosen for two reasons. Firstly, it is speculated that exposure of cells to 350 nm (shorter UV) on to cells perhaps would be harmful compared to using 400 nm excitation (longer wavelength). Secondly, 400 nm excitation can itself give a lot of

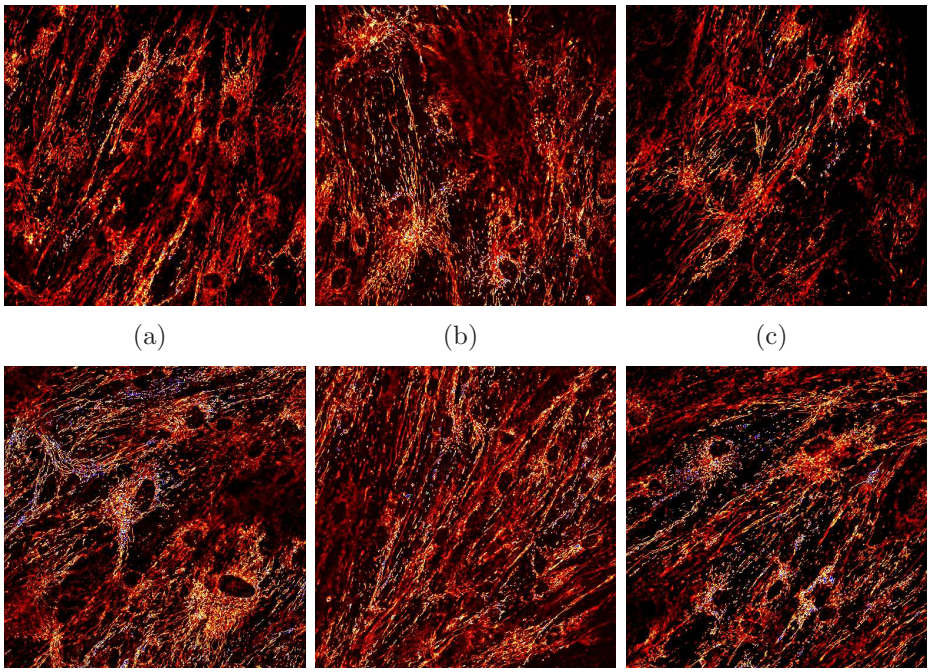

Figure 5.15: Images (40x objective) of stem cells undergoing differentiation in osteogenic medium stained by Mitotracker deep red dye. a, b and c are images taken on day 11 and d, e and f are images taken on day 13 (Passage.3). Note: Mitotracker deep red has excitation maximum at and emission maximum.

useful information about cell metabolism, as it can excite various fluorophores like flavo proteins, lipofuscin, porphyrin, elastin *etc*(Figure 5.1).

5.7.1 Colocalization of stem cell mitochondria autofluorescence at 400 nm

Originally, the expectation was that autofluorescence from stem cells at 400 nm would be mainly observed from mitochondrial compartments and lysosomes. However, the colocalization result of stem cell mitochondria autofluorescence at 400 nm shows (Figure 5.16 and Figure 5.16) that lysosomes could be more important contributors compared to mitochondria. This was not completely unexpected, since a similar observation was reported by Reyes *et al* [103]. At 400 nm excitation oxi-

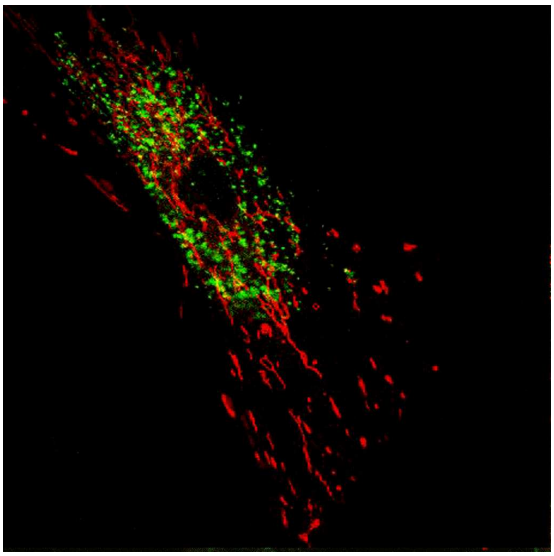

(a)

Figure 5.16: Colocalization of stem cells autofluorescence at 400 nm and mitochondria. The red region is the mitochondria stained by Mitotracker and the green region is the autofluorescence at 400 nm. Note: first the autofluorescence was measured, then the same cells were stained and imaged.

dized flavo proteins could be major contributors for the autofluorescence [103]. In addition, lipofuscin (lipofuscin is present dominantly in lysosomes) is also known to show higher fluorescence at 400 nm excitation.

5.7.2 Stem cell autofluorescence at 400 nm with time

First of all, the autofluorescence observed for the stem cells at 400 nm excitation in the first few days (day 1-3) was too weak to be detected by confocal microscope (Figure 5.4). With time, there was increase in autofluorescence. One of the most important properties of stem cell is their ability to slowly cycle, since stem cells are know to have a slower intrinsic metabolism [103]. In addition, some studies have postulated that stem cells depend on anaerobic glycolysis as compared to the more efficient mitochondrial oxidative metabolism (oxidative phosphorylation) [104]. The reason for reduced fluorescence observed in the stem cells could be possibly due to

the above mentioned reason *ie* slow metabolism.

A comparison of mitochondrial activity of stem cells (Figure 5.17 and Figure 5.13), on day 2 and day 8 clearly shows that on day 2, stem cell mitochondrial activity was very less. This result clearly substantiates the lower metabolic activity of stem cells. However, by day 8 the cell density and cell to cell contact increased. This could be the reason for higher mitochondrial activity observed in day 8 cells(Figure 5.17 b), which results in higher fluorescence intensity.

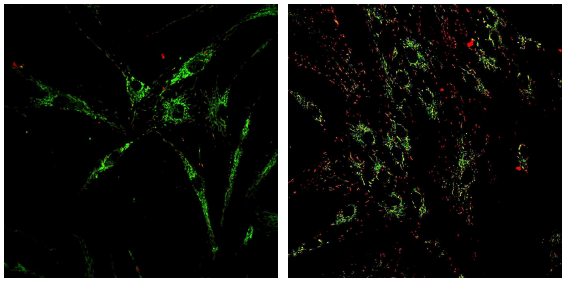

(a) (b)

Figure 5.17: Comparison of mitochondrial activity of stem cells on day 2 and day 8 of passage 3, using JC1 dye. (a) image taken on day 2 after seeding (Passage.3). (b) image taken on day 8 (Passage.3). Note: the greater the red emission means higher activity in mitochondria.

Usually stem cells are subcultured 3 to 4 days after passaging. However, in this study we decided to monitor the stem cells until 15 days without subculturing. This was done to observe the changes happening in cells with time. The PCA done on the stem cell spectra clearly showed that with time the 3D spatial localization of stem cells changes (Figure 5.18). This provides clear evidence that the cells were having metabolic changes with time. At this point there is limited data to find a concrete pattern of cell movement in the 3D space. This preliminary information could be still very useful in understanding cell growth.

It was interesting to observe the trajectory of stem cells in the 3D PCA space. From Figure 5.18, it is evident that by 13th day the cells were moving towards the

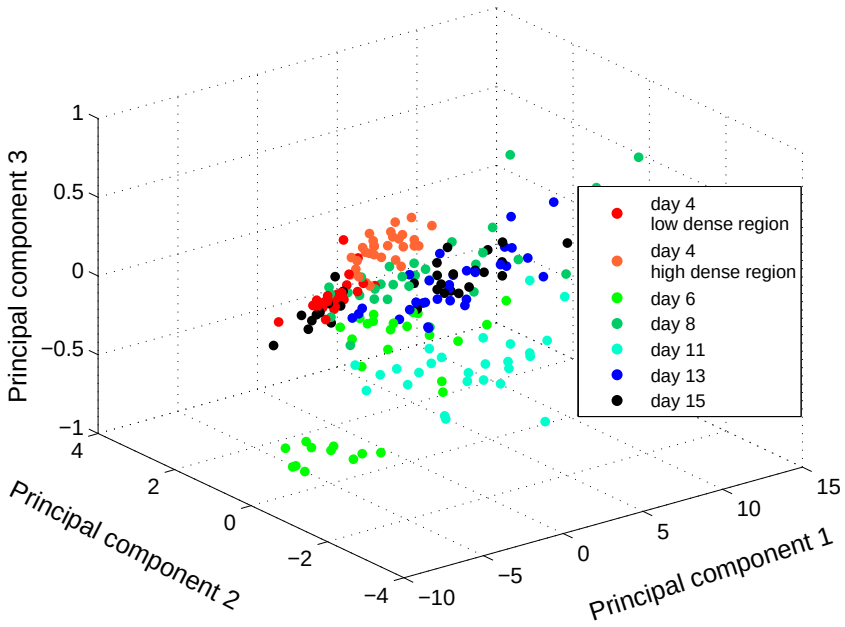

Figure 5.18: PCA of stem cell autofluorescence spectra with time.

position of the 2nd day cells. This may be because the cells would have stopped growing or proliferating (senescence) due to higher cell density. This could have resulted in reduced metabolism of cells after a certain period in their growth phase.

To understand and compare the metabolic parameters among different cell types, one should take into account the density-dependence, especially low density, single cells versus higher density and more confluent cells [103]. A comparison of high density cells and low density cells showed clear difference in the 3D PCA space (Figure 5.8). This result shows that cells in isolation and in groups have somewhat different metabolism. Similar observation was earlier made by Reyes *et al* using a redox fluorometric technique [103].

5.7.3 A comparison of stem cell and stem cells undergoing differentiation in osteogenic medium autofluorescence at 400 nm

Figure 5.19 shows the localisation of stem cells and stem cells undergoing differentiation in osteogenic medium in the 3D PCA space. Compared to stem cells, the stem cells undergoing differentiation in osteogenic medium were clearly separate in their spatial localization. The separation between stem cells and stem cells undergoing differentiation in osteogenic medium became more obvious after 6 days (Figure 5.19).

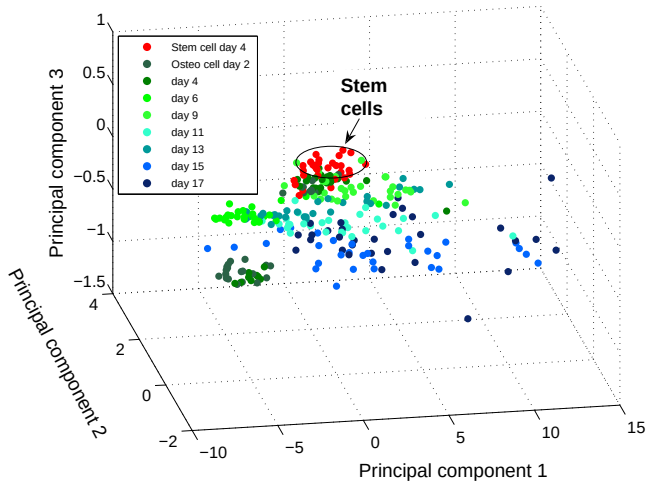

Figure 5.19: Illustration of autofluorescence spectra for stem cells undergoing differentiation in osteogenic medium and stem cells in 3D PCA space.

An important question in stem cell research is to address or analyze how fast a cell differentiates. Recent optical techniques such as redox fluorometry,two photon microscopy were used to characterize stem cells characterization [103,104]. However, they were only able to compare stem cells with stem cells undergoing differentiation in osteogenic medium after one week of differentiation. In this study, stem cells and differentiated cells within 60 hrs (Figure 5.20) were showing a clear difference in

fluorescence.

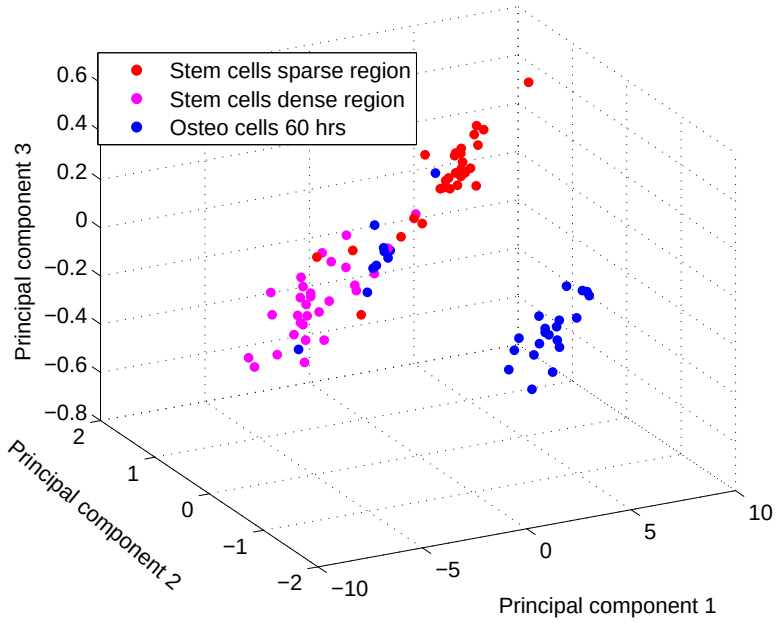

Figure 5.20: A comparison of stem cells and stem cells undergoing differentiation in osteogenic medium on 3D PCA space after 60 hrs.

One generally accepted property of stem cells that differs from their differentiated progenies is a lower metabolic rate accompanied by a lower adenosine triphosphate (ATP) content [105]. In addition, a shift from anaerobic glycolysis to the more efficient mitochondrial oxidative metabolism during differentiation has been demonstrated on human mesenchymal stem cells [104]. Reyes *et al*, have also demonstrated a decrease in NADH/FAD ratio (increased metabolism) in mesenchymal stem cells after osteogenic differentiation for one week [103].

During differentiation, osteogenic cells are known to secrete matrix proteins which are organized as an extracellular matrix (ECM)on which calcium phosphate is deposited as hydroxyapattite crystals [106, 107]. All these factors could possible contribute to the observed difference in fluorescence of stem cells and stem cells

undergoing differentiation in osteogenic medium.

Previous studies on osteogenic differentiation also has shown that the organization of mitochondria in the cells also changes during differentiation. Mitochondrial development is considered sometimes as a marker for differentiation. Since the role of mitochondria is crucial for cell metabolism, a comparison of mitochondria of stem cells and of differentiated cells was done in this study. The result clearly shows that during differentiation the mitochondria of cells become bigger, where as in the stem cells there is a kind of perinuclear formation of mitochondria .

5.8 Summary

In this study, autofluorescence of stem cells and stem cells undergoing differentiation in osteogenic medium at 400 nm excitation wavelength has been investigated. It was observed that the stem cells were having very low autofluorescence signals at 400 nm excitation, possibly due to reduced metabolism; with autofluorescence of cells increased with time. This result was supported by the reduced activity of mitochondria of stem cells observed using JC1 staining. From the colocalization experiment it was evident that at 400 nm excitation, mitochondrial compartments of stem cells showed less fluorescence. In addition, a comparison of mitochondria of stem cells and stem cells undergoing differentiation in osteogenic medium clearly showed that stem cells mitochondria have perinuclear formation. However, during differentiation the mitochondria in stem cell differentiated in osteogenic medium seems enlarged and were having a network appearance.

Principal component analysis (PCA) was utilized to visualize the overall trajectory in spectrum of stem cells undergoing differentiation in osteogenic medium. It was evident that with time the spectrum in the 3D PCA space was spreading away from the initial point, possibly reflecting the changes happening during differentia-

tion. Compared to the earlier studies, this is the first non invasive study to show the difference between stem cells and stem cells undergoing differentiation in osteogenic medium within 60 hrs. It is also significant to note that this was achieved using a single wavelength of light. In this study, a clear distinction between stem cells in dense and sparse region was also observed at 400 nm excitation.

These results show the potential of using autofluorescence measurement with a single excitation (400 nm) as a diagnostic tool for analyzing the osteogenic differentiation process.

6 Conclusion

6.1 Studies on autofluorescence of human urine samples

In the study of human urine autofluorescence, the main aim was to test the potential of autofluorescence for diagnosing urinary tract infection (UTI). This study is the first study ever to explore the applicability of autofluorescence as a technique to diagnose UTI. Various techniques including emission spectra, excitation/emission matrices and SFS were utilized to explore urine ?uorescence. It is worth reiterating that the method uses undiluted urine samples and requires no sample preparation.

Fluorescence characterization of undiluted human urine is fraught with difficulties because many fluorophores in urine possess similar spectral characteristics and the spectral characteristics could be affected by several factors such as energy transfer, concentration quenching and inner filter effect (high optical density).

Even without dilution, pronounced spectral differences were observed in the EEMs in the shorter UV (250-300 nm) region, as well as a clear difference in the emission intensity at 290 nm for the two groups of urine samples. SFS with an offset $\Delta\lambda = 90$ nm also showed that it can be used effectively to differentiate between

undiluted UTI- and normal- urine samples.

Using this fluorescence technique (SFS or emission scan at 290 nm excitation),), it takes approximately 2 minutes to complete the analysis of a sample. This is faster than any of the current diagnostic techniques for UTI, with the exception of dipsticks.

The concentration of two key indole compounds (indoxyl sulfate and tryptophan) by using HPLC was tested in this study, in an attempt to explain their role in urine autofluorescence. However, HPLC analysis did not reveal any significant difference in the concentration of tryptophan and indoxyl sulfate in the normal urine and UTI samples. It may be concluded that multiple factors such as xanthine oxidise activity, tryptophanase and higher neopterin concentration could possibly contribute to the differences observed in the fluorescence spectra between the two groups of urine samples.

As part of this work, the fluorescence of undiluted healthy human urine samples as well as the three major UV-excitable fluorophores in urine: tryptophan, indoxyl sulfate and 5-hydroxyindole-3-acetate was analysed, in order to understand the key fluorescence features in these complex biological fluids. The major factors that reduce the UV fluorescence, namely higher concentration of indoxyl sulfate producing the inner filter effect and concentration quenching and quenching of fluorophores by ammonium was identified. This work fills a gap in the existing literature concerning the factors influencing UV fluorescence of human urine and this understanding could contribute to harnessing autofluorescence as a diagnostic tool.

In this study it was also observed that storing the urine sample in the refrigerator (4^0C) for 96 hrs, did not affect its autofluorescence.

Limitations

The primary limitation of this study is the limited number and spectrum of samples used. Also, a majority of the samples in the UTI category were those with *Escherichia coli* as the causative agent. This was done because *Escherichia coli* is known to be the most common bacteria causing UTI (70% cases).

However, in addition to *Escherichia coli*, there are several other pathogen which can cause UTI, including fungi. This study was limited by the spectrum of disease, meaning that urine samples of UTI patients caused by various pathogens other than *Escherichia coli* was not studied in detail.

Future directions

The fluorescence technique used in the study should be further validated by analysing a larger set of urine samples and also urine samples of UTI caused by different types of pathogens. In addition, the fluorescence technique should be tested for sensitivity and specificity, by including samples from a wider spectrum of diseases of the urinary tract.

Further, this technique could be adapted to design a low cost, near patient or home diagnosis kit.

6.2 Studies on autofluorescence of adipose derived adult stem cell samples

In the study of autofluorescence of stem cells, the main aim was to test the potential of using autofluorescence measurement at 400 nm excitation wavelength as a diagnostic tool for characterizing stem cells. This study has demonstrated for the first time, a non invasive method to differentiate between stem cells and cells undergoing differentiation in osteogenic medium within 60 hrs. Currently polymerase chain reaction (PCR) is the only sensitive and fast means to check for cell differentiation. However, PCR technique is known to be an 'invasive' method. On the other hand, recently some optical techniques which are noninvasive, such as lifetime measurements and redox fluorometry have been used to study osteogenic differentiation. However, they showed a difference between undifferentiated and differentiated cells only after one week.

In this study, using autofluorescence together with PCA analysis, the overall trajectory in spectrum of stem cells undergoing differentiation in osteogenic medium with time was able to be visualized. A clear distinction between stem cells in the areas of dense and sparse cell populations was also observed at 400 nm excitation.

As a part of this study, mitochondrial features were also tracked during stem cell differentiation (in osteogenic medium). The results showed that during osteogenic differentiation the mitochondria were enlarged and had a network appearance as compared to their perinuclear appearance in undifferentiated stem cells.

From colocalization experiments in the study, it was evident that at 400 nm excitation, mitochondrial compartments of stem cells showed less fluorescence.

These results show the potential of using autofluorescence measurement with a single excitation (400 nm) as a diagnostic tool for analyzing the osteogenic differentiation process.

Limitations

A major limitation of this study was that the stem cells in the initial days were having too little autofluorescence to be measured by confocal photo multiplier tube (PMT), probably because these stem cells were quiescent (less metabolically active). This affected the analysis of stem cells during the initial days after passaging.

The study was also limited by the fact that the confocal microscope which was used to analyze the stem cells fluorescence did not have UV laser, UV diode sources or automated gratings (filters) for utilising mercury source (below 400 nm). This was crucial because most of the fluorophores such as NADH get excited in the shorter UV region, around 350 nm.

Future directions

In this study autofluorescence was utilised mainly to characterize osteogenic differentiation. The fluorescence method used in the study could be extended to study other differentiation processes such as adipogenic differentiation, chondrogenic differentiation etc.

Perhaps utilization of a high resolution camera such as electron multiplying charge coupled device (EMCCD) in the future future would enable the weak autofluorescence of stem cells to be detected.

BLANK PAGE

References

[1] A. C. Croce, S. Fiorani, D. Locatelli, R. Nano, M. Ceroni, F. Tancioni, E. Giombelli, E. Benericetti, and G. Bottiroli, "Diagnostic Potential of Autofluorescence for an Assisted Intraoperative Delineation of Glioblastoma Resection Margins," Photochemistry and Photobiology **77**(3), 309–318 (2003).

[2] M. Kraft, C. S. Betz, A. Leunig, and C. Arens, "Value of fluorescence endoscopy for the early diagnosis of laryngeal cancer and its precursor lesions," Head and Neck (2010).

[3] V. Duchac, J. Zavadil, J. Vrnov, T. Jirsek, J. tukavec, and L. Hork, "Peroperative optical autofluorescence biopsyverification of its diagnostic potential," Lasers in Medical Science pp. 1–9 (2010).

[4] "Half of Cost Burden of Urological Diseases Borne by Medicare," (2008).

[5] D. C. Miller, C. S. Saigal, and M. S. Litwin, "The Demographic Burden of Urologic Diseases in America," Urologic Clinics of North America **36**(1), 11–27 (2009).

[6] NIH, "Kidney and Urologic Diseases Statistics for the United States," (2010).

[7] W. Kravchenko, "Stem cells for hope," (2010).

[8] S. K. Strasinger, *Urinalysis and Body Fluids* (The Tabers Publisher, 2001).

[9] F. David Putnam, "Composition and concentrative properties of human urine," Tech. rep., NASA and Mcdonnell Douglas Astronoutics company-western division,Huntigton Beach,Calif, Langley Research Center (1971).

[10] S. G. Guminetsky and O. R. gaika, "Investigation of Absorption Spectra of The Main Human Urines Organic Components in Absence of Protein." SPIE **3904**, 579–589 (1999).

[11] T. Ohashi, Y. Kanamoto, S. Yamaguchi, Y. Eto, and K. Maekawa, "Abnormal excretion of autofluorescencet lipids in urine from patients with neuronal ceroid lipofuscinosis," Tohoku Journal of Experimental Medicine **148**(4), 335–339 (1986).

[12] M. Jaffe, "Zur Lehre von den Eigenschaften und der Abstammung der Harnpigmente," Virchows Archiv **47**(3), 405–427 (1869).

[13] B. T. Squires and J. H. Jeffree, "A simple ultra-violet fluorophotometer," Journal of Scientific Instruments **5**(9), 273–277 (1928). 0950-7671.

[14] H. M. Rabinowitz, "A Correlation of Fluorescence of Human Urine with Benign and Malignant Growth," Cancer Res **9**(11), 672–676 (1949).

[15] H. Mabuchi and H. Nakahashi, "Liquid-chromatographic profiling of endogenous fluorescent substances in sera and urine of uremic and normal subjects," Clin Chem **29**(4), 675–677 (1983).

[16] E. Marklov, H. Makovickov, and I. Krkorov, "Screening for defects in tryptophan metabolism," Journal of Chromatography A **870**(1-2), 289–293 (2000).

[17] M. J. P. Leiner, M. R. Hubmann, and O. S. Wolfbeis, "The Total Fluorescence of Human Urine," Analytica Chimica Acta. **198**, 13–23 (1987).

[18] K. Dubayova, J. Kusnir, and L. Podracka, "Diagnostic monitoring of urine by means of synchronous fluorescence spectrum," J Biochem Biophys Methods **55**(2), 111–9 (2003).

[19] E. J. Bukowski and F. V. Bright, "Minimizing urine autofluorescence under multi-photon excitation conditions," Appl Spectrosc **58**(9), 1101–5 (2004).

[20] J. Kusnir and L. Leskova, "Concentration Matrices - Solutions for Fluorescence Definition of Urine," Analytica letters **38**, 1559–1567 (2005).

[21] M. H. Mills, M. G. King, N. G. Keats, and R. A. McDonald, "Melatonin determination in human urine by high-performance liquid chromatography with fluorescence detection," Journal of Chromatography B: Biomedical Sciences and Applications **377**, 350–355 (1986).

[22] J. G. M. E. Claudia Bueno, "Spectroscopic Properties of 4-Pyridoxic Acid as a Function of pH and Solvent," Helvetica Chimica Acta **87**(4), 940–948 (2004).

[23] J. Qin, Y. Fung, D. Zhu, and B. Lin, "Native fluorescence detection of flavin derivatives by microchip capillary electrophoresis with laser-induced fluorescence intensified charge-coupled device detection," Journal of Chromatography A **1027**(1-2), 223–229 (2004).

[24] J. L. Chastain and D. B. McCormick, "Characterization of a new flavin metabolite from human urine," Biochimica et Biophysica Acta (BBA) - General Subjects **967**(1), 131–134 (1988).

[25] S. G. V. M. F. M. C. V. Antonie J. W. G. Visser, "Fluorescence Properties of Reduced Flavins and Flavoproteins," European Journal of Biochemistry **101**(1), 13–21 (1979).

[26] M. Kubista, "Experimental correction for the inner-filter effect in fluorescence spectra," Analyst (London) **119**(3) (1994).

[27] M. M. Puchalski, M. J. Morra, and R. Wandruszka, "Assessment of inner filter effect corrections in fluorimetry," Fresenius' Journal of Analytical Chemistry **340**(6), 341–344 (1991).

[28] J. W. Bridges and R. T. Williams, "The fluorescence of indoles and aniline derivatives," Biochem J **107**(2), 225–37 (1968).

[29] J. Lakowicz, *Principles of Fluorescence Spectroscopy*, 2nd ed. (Kluwer Academic/Plenum Publishers, New York, 1999).

[30] B. L. v. Duuren, "Solvent Effects in the Fluorescence of Indole and Substituted Indoles1," The Journal of Organic Chemistry **26**(8), 2954–2960 (1961).

[31] E. P. Kirby and R. F. Steiner, "Influence of solvent and temperature upon the fluorescence of indole derivatives," The Journal of Physical Chemistry **74**(26), 4480–4490 (1970).

[32] W. B. De Lauder and P. Wahl, "Effect of solvent upon the fluorescence decay of indole," Biochim Biophys Acta **243**(2), 153–63 (1971).

[33] J. Lipinski and H. Chojnacki, "Solvent effect on the spectroscopic properties of indole–semiempirical quantum chemical study," Spectrochimica Acta Part A: Molecular and Biomolecular Spectroscopy **51**(3), 381–386 (1995).

[34] G. T. Bryan, "Urinary Excretion of Indoxyl Sulfate (Indican) by Human Subjects Ingesting a Semisynthetic Diet Containing Variable Quantities of l-Tryptophan," Am J Clin Nutr **19**(2), 113–119 (1966).

[35] T. Niwa, "Uremic toxicity of indoxyl sulfate," Nagoya J Med Sci **72**(1-2), 1–11 (2010).

[36] T. Niwa, N. Takeda, A. Tatematsu, and K. Maeda, "Accumulation of indoxyl sulfate, an inhibitor of drug-binding, in uremic serum as demonstrated by internal-surface reversed-phase liquid chromatography," Clin Chem **34**(11), 2264–2267 (1988).

[37] T. Niwa and M. Ise, "Indoxyl sulfate, a circulating uremic toxin, stimulates the progression of glomerular sclerosis," J Lab Clin Med **124**(1), 96–104 (1994).

[38] L. Dou, N. Jourde-Chiche, V. Faure, C. Cerini, Y. Berland, F. Dignat-George, and P. Brunet, "The uremic solute indoxyl sulfate induces oxidative stress in endothelial cells," Journal of Thrombosis and Haemostasis **5**(6), 1302–1308 (2007).

[39] S. F. Dealler, P. M. Hawkey, and M. R. Millar, "Enzymatic degradation of urinary indoxyl sulfate by Providencia stuartii and Klebsiella pneumoniae causes the purple urine bag syndrome," J. Clin. Microbiol. **26**(10), 2152–2156 (1988).

[40] "Human Metabolome Database Version 2.5," (2005).

[41] G. J. Allesia M, *Manual of Fluorometric and Spectrophotometric Experiments* (Gordon and Breech Science Publishers S.A, 1985).

[42] J. Georges, "Deviations from Beer's law due to dimerization equilibria: theoretical comparison of absorbance, fluorescence and thermal lens measurements," Spectrochimica Acta Part A: Molecular and Biomolecular Spectroscopy **51**(6), 985–994 (1995).

[43] K. Y. Burshtein, A. A. Bagatur'yants, and M. V. Alfimov, "MO calculations on the absorption spectra of organic dimers The interaction energy between dipole moments of electronic transitions in monomers and the shape of absorption bands," Chemical Physics Letters **239**(1-3), 195–200 (1995).

[44] E. A. Permyakov, *Luminescent spectroscopy of proteins* (CRC Press, 1992).

[45] R. K. I. Tatischeff, "Influence of the environment on the excitation wavelength dependene of the fluorescence quantum yield of indole," Photochemistry and Photobiology **22**(6), 221–229 (1975).

[46] L. S. F. Leonard J. Andrews, "Fluorescence characteristics of indoles in non-polar solvents:lifetimes,quantum yields and polarization spectra," Photochemistry and Photobiology **19**(5), 353–360 (1974).

[47] A. H. Thomas, C. Lorente, A. L. Capparelli, M. R. Pokhrel, A. M. Braun, and E. Oliveros, "Fluorescence of pterin, 6-formylpterin, 6-carboxypterin and folic acid in aqueous solution: pH effects," Photochemical and Photobiological Sciences **1**(6), 421–426 (2002).

[48] J. Car, "Urinary tract infections in women: diagnosis and management in primary care," BMJ **332**(7533), 94–97 (2006).

[49] M. G. Morgan and H. McKenzie, "Controversies in the laboratory diagnosis of community-acquired urinary tract infection," European Journal of Clinical Microbiology and Infectious Diseases **12**(7), 491–504 (1993).

[50] R. Goodacre, E. M. Timmins, R. Burton, N. Kaderbhai, A. M. Woodward, D. B. Kell, and P. J. Rooney, "Rapid identification of urinary tract infection bacteria using hyperspectral whole-organism fingerprinting and artificial neural networks," Microbiology **144**(5), 1157–1170 (1998).

[51] J. Hacker, *Urinary tract infection: from basic science to clinical application*, pp. 1–8 (2000).

[52] G. K. M. Harding and A. R. Ronald, "The management of urinary infections; what have we learned in the past decade?" International Journal of Antimicrobial Agents **4**(2), 83–88 (1994).

[53] W. Stamm and S. R. Norrby, "Urinary Tract Infections: Disease Panorama and Challenges," The Journal of Infectious Diseases **183**(s1), S1–S4 (2001).

[54] Ramzan.M., Bakhsh.S., Salam.A., Khan.G.M, and M. Ghulam, "Risk Factors In Urinary Tract Infection," Gomal Journal of Medical Sciences **2**(1) (2004).

[55] S. D. Fihn, R. H. Latham, P. Roberts, K. Running, and W. E. Stamm, "Association Between Diaphragm Use and Urinary Tract Infection," JAMA **254**(2), 240–245 (1985).

[56] R. S. Remis, M. J. Gurwith, D. Gurwith, N. T. Hargrett-Bean, and P. M. Layde, "Risk factors for urinary tract infection," Am. J. Epidemiol. **126**(4), 685–694 (1987).

[57] W. E. Stamm and T. M. Hooton, "Management of Urinary Tract Infections in Adults," N Engl J Med **329**(18), 1328–1334 (1993).

[58] N. Roxon, "Healthier choices can reduce the risk of kidney disease." (2009).

[59] J. B. L. Lee and G. H. Neild, "Urinary tract infection," Medicine **35**(8), 423–428 (2007).

[60] R. Orenstein and E. Wong, "Urinary tract infections in adults," (1999).

[61] N. Hinata, T. Shirakawa, H. Okada, K. Shigemura, S. Kamidono, and A. Gotoh, "Quantitative detection of Escherichia coli from urine of patients with bacteriuria by real-time PCR," Mol Diagn **8**(3), 179–84 (2004).

[62] M. Basu, S. Seggerson, J. Henshaw, J. Jiang, R. del A Cordona, C. Lefave, P. J. Boyle, A. Miller, M. Pugia, and S. Basu, "Nano-biosensor development for bacterial detection during human kidney infection: Use of glycoconjugate-specific antibody-bound gold NanoWire arrays (GNWA)," Glycoconjugate Journal **21**(8), 487–496 (2004).

[63] M. J. Pugia, R. G. Sommer, H.-H. Kuo, P. F. Corey, D. L. Gopual, and J. A. Lott, "Near-patient testing for infection using urinalysis and immunochromatography strips," Clinical Chemistry and Laboratory Medicine **42**(3), 340 (2004).

[64] S. Zomer, C. Guillo, R. G. Brereton, and M. Hanna-Brown, "Toxicological classification of urine samples using pattern recognition techniques and capillary electrophoresis," Anal Bioanal Chem **378**(8), 2008–20 (2004).

[65] R. V. Sultana, S. Zalstein, P. Cameron, and D. Campbell, "Dipstick urinalysis and the accuracy of the clinical diagnosis of urinary tract infection," Journal of Emergency Medicine **20**(1), 13–19 (2001).

[66] J. C. d. Santos, L. P. Weber, and L. R. R. Perez, "Evaluation of urinalysis parameters to predict urinary-tract infection," Brazilian Journal of Infectious Diseases **11**, 479–481 (2007).

[67] N. M. Carroll, P. Adamson, and N. Okhravi, "Elimination of Bacterial DNA from Taq DNA Polymerases by Restriction Endonuclease Digestion," J. Clin. Microbiol. **37**(10), 3402–3404 (1999).

[68] B. R. Berridge, J. D. Fuller, J. de Azavedo, D. E. Low, H. Bercovier, and P. F. Frelier, "Development of Specific Nested Oligonucleotide PCR Primers for the Streptococcus iniae 16S-23S Ribosomal DNA Intergenic Spacer," J. Clin. Microbiol. **36**(9), 2778–2781 (1998).

[69] K. Chen, H. Neimark, P. Rumore, and C. R. Steinman, "Broad range DNA probes for detecting and amplifying eubacterial nucleic acids," FEMS Microbiology Letters **57**(1), 19–24 (1989).

[70] K. Shigemura, T. Shirakawa, H. Okada, K. Tanaka, S. Kamidono, S. Arakawa, and A. Gotoh, "Rapid detection and differentiation of Gram-negative and Gram-positive pathogenic bacteria in urine using TaqMan probe," Clinical and Experimental Medicine **4**(4), 196–201 (2005).

[71] J. Lu, S. Gao, Y. Yang, X. Lu, and G. Chen, "Study on characteristic intrinsic fluorescence spectra of urine from ovarian cancer patients," in *Optics in Health Care and Biomedical Optics III*, vol. 6826, pp. 68,262O–7 (SPIE).

[72] A. G. Anwer, P. M. Sandeep, E. M. Goldys, and S. Vemulpad, "Distinctive autofluorescence of urine samples from individuals with bacteriuria compared with normals," Clinica Chimica Acta **401**(1-2), 73–75 (2009).

[73] E. Sikorska, T. Grecki, I. V. Khmelinskii, M. Sikorski, and D. De Keukeleire, "Monitoring beer during storage by fluorescence spectroscopy," Food Chemistry **96**(4), 632–639 (2006).

[74] I. K. Wang, D.-R. Ho, H.-Y. Chang, C.-L. Lin, and F.-R. Chuang, "Purple Urine Bag Syndrome in a Hemodialysis Patient," Internal Medicine **44**(8), 859–861 (2005).

[75] D. Bar-Or, L. T. Rael, R. Bar-Or, M. L. Craun, J. Statz, and R. E. Garrett, "Mass spectrometry analysis of urine and catheter of a patient with purple urinary bag syndrome," Clinica Chimica Acta **378**(1-2), 216–218 (2007).

[76] J. L. Botsford and R. D. Demoss, "Escherichia coli Tryptophanase in the Enteric Environment," J. Bacteriol. **109**(1), 74–80 (1972).

[77] W. Daubener, C. Hucke, K. Seidel, U. Hadding, and C. R. MacKenzie, "Interleukin-1 Inhibits Gamma Interferon-Induced Bacteriostasis in Human Uroepithelial Cells," Infect. Immun. **67**(11), 5615–5620 (1999).

[78] O. Takikawa, "Biochemical and medical aspects of the indoleamine 2,3-dioxygenase-initiated l-tryptophan metabolism," Biochemical and Biophysical Research Communications **338**(1), 12–19 (2005).

[79] U. Grohmann, F. Fallarino, and P. Puccetti, "Tolerance, DCs and tryptophan: much ado about IDO," Trends in Immunology **24**(5), 242–248 (2003).

[80] A. Matin, I. M. Streete, I. M. Jamie, R. J. W. Truscott, and J. F. Jamie, "A fluorescence-based assay for indoleamine 2,3-dioxygenase," Analytical Biochemistry **349**(1), 96–102 (2006).

[81] S. Giler, E. F. Henig, I. Urca, O. Sperling, and A. de Vries, "Urine xanthine oxidase activity in urinary tract infection," J Clin Pathol **31**(5), 444–446 (1978).

[82] T. Ardan, J. Kovaceva, and J. Cejkov, "Comparative histochemical and immunohistochemical study on xanthine oxidoreductase/xanthine oxidase in mammalian corneal epithelium," Acta Histochemica **106**(1), 69–75 (2004).

[83] A. Pieroni, V. Janiak, C. M. Drr, S. Ldeke, E. Trachsel, and M. Heinrich, "in vitro antioxidant activity of non-cultivated vegetables of ethnic Albanians in southern Italy," Phytotherapy Research **16**(5), 467–473 (2002).

[84] M. K. Shukla and P. C. Mishra, "Electronic spectra and structures of some biologically important xanthines," Journal of Molecular Structure **324**(3), 241–249 (1994).

[85] A.-H. Najim A, "The Role of Some Tryptophan Metabolites in Certain Diseases of the Genito-Urinary System1," British Journal of Urology **46**(3), 337–341 (1974).

[86] H. Denz, D. Fuchs, A. Hausen, H. Huber, D. Nachbaur, G. Reibnegger, J. Thaler, E. R. Werner, and H. Wachter, "Value of urinary neopterin in the differential diagnosis of bacterial and viral infections," Journal of Molecular Medicine **68**(4), 218–222 (1990).

[87] G. K. Preeti, "What Are Stem Cells," (2004).

[88] S. P. Weisberg, D. McCann, M. Desai, M. Rosenbaum, R. L. Leibel, and A. W. Ferrante, "Obesity is associated with macrophage accumulation in adipose tissue," The Journal of Clinical Investigation **112**(12), 1796–1808 (2003).

[89] H. Xu, G. T. Barnes, Q. Yang, G. Tan, D. Yang, C. J. Chou, J. Sole, A. Nichols, J. S. Ross, L. A. Tartaglia, and H. Chen, "Chronic inflammation in fat plays a crucial role in the development of obesity-related insulin resistance," The Journal of Clinical Investigation **112**(12), 1821–1830 (2003).

[90] P. A. Zuk, M. Zhu, P. Ashjian, D. A. De Ugarte, J. I. Huang, H. Mizuno, Z. C. Alfonso, J. K. Fraser, P. Benhaim, and M. H. Hedrick, "Human Adipose

Tissue Is a Source of Multipotent Stem Cells," Mol. Biol. Cell **13**(12), 4279–4295 (2002).

[91] A. J. Katz, A. Tholpady, S. S. Tholpady, H. Shang, and R. C. Ogle, "Cell Surface and Transcriptional Characterization of Human Adipose-Derived Adherent Stromal (hADAS) Cells," STEM CELLS **23**(3), 412–423 (2005).

[92] A. Schaffler and C. Bchler, "Concise Review: Adipose Tissue-Derived Stromal CellsBasic and Clinical Implications for Novel Cell-Based Therapies," STEM CELLS **25**(4), 818–827 (2007).

[93] R. I. Freshney, "Culture of Animal Cells: A Manual of Basic Technique," (2005).

[94] J. L. Sherley, "Adult stem cell differentiation: what does it mean?" in *[Engineering in Medicine and Biology, 2002. 24th Annual Conference and the Annual Fall Meeting of the Biomedical Engineering Society] EMBS/BMES Conference, 2002. Proceedings of the Second Joint*, vol. 1, pp. 741–742 vol.1.

[95] M. Loeffler and I. Roeder, "Tissue stem cells: definition, plasticity, heterogeneity, self-organization and models - a conceptual approach," Cells Tissues Organs **171**, 8 – 26 (2002).

[96] A. G. Robling, A. B. Castillo, and C. H. Turner, "Biomechanical and molecular regulation of bone remodeling," Annual Review of Biomedical Engineering **8**(1), 455–498 (2006).

[97] P. J. Marie, *Osteoblasts and Bone Formation*, vol. Volume 5, pp. 445–473 (Elsevier, 1998).

[98] B. M. Strem, K. C. Hicok, M. Zhu, I. Wulur, Z. Alfonso, R. E. Schreiber, J. K. Fraser, and M. H. Hedrick, "Multipotential differentiation of adipose tissue-derived stem cells," Keio J Med **54**(3), 132–41 (2005).

[99] C. L. Joana, C. Helena, and E. F. Joo, "Osteoblasts and bone formation," ACTA REUM PORT **32**(2), 103–10 (2007).

[100] M. Monici and M. R. El-Gewely, *Cell and tissue autofluorescence research and diagnostic applications*, vol. Volume 11, pp. 227–256 (Elsevier, 2005).

[101] W. Lai, Y. Xu, D. Y. Fung, and Y. Xiong, "Development of a lateral-flow assay for rapid screening of the performance-enhancing sympathomimetic drug clenbuterol used in animal production; food safety assessments," Asia Pac J Clin Nutr **16 Suppl 1**, 106–10 (2007).

[102] Andersson, Baechi, Hoechl, and Richter, "Autofluorescence of living cells," Journal of Microscopy **191**(1), 1–7 (1998).

[103] J. M. G. Reyes, S. Fermanian, F. Yang, S.-Y. Zhou, S. Herretes, D. B. Murphy, J. H. Elisseeff, and R. S. Chuck, "Metabolic Changes in Mesenchymal Stem Cells in Osteogenic Medium Measured by Autofluorescence Spectroscopy," Stem Cells **24**(5), 1213–1217 (2006).

[104] H.-W. Guo, C.-T. Chen, Y.-H. Wei, O. K. Lee, V. Gukassyan, F.-J. Kao, and H.-W. Wang, "Reduced nicotinamide adenine dinucleotide fluorescence lifetime separates human mesenchymal stem cells from differentiated progenies," Journal of Biomedical Optics **13**(5), 050,505–3 (2008).

[105] T. Lonergan, B. Bavister, and C. Brenner, "Mitochondria in stem cells," Mitochondrion **7**(5), 289–296 (2007).

[106] M. W. Long, J. A. Robinson, E. A. Ashcraft, and K. G. Mann, "Regulation of human bone marrow-derived osteoprogenitor cells by osteogenic growth factors," The Journal of Clinical Investigation **95**(2), 881–887 (1995).

[107] F. Lecanda, L. V. Avioli, and S.-L. Cheng, "Regulation of bone matrix protein expression and induction of differentiation of human osteoblasts and human bone marrow stromal cells by bone morphogenetic protein-2," Journal of Cellular Biochemistry **67**(3), 386–398 (1997).

[108] G. G. Stokes, "On the Change of Refrangibility of Light," Philosophical Transactions of the Royal Society of London **142**, 463–562 (1852).

[109] P. Nick, "Electric Ladyland the First Museum of Fluorescent Art," (1999).

[110] R. Williams and J. Bridges, "Fluorescence of solutions: A review," J clin Path **17**(4), 371–394 (1964).

[111] R. Daniel, "Atomic I/O letters column," (2011).

[112] F. Yang and L. Moss, "The molecular structure of green fluorescent protein," **14**, 1246–51 (1996).

[113] Roberto, "Green fluorescent protein history and perspectives," (2009).

[114] Olympus, "Laser scanning confocal microscopy," (2004).

[115] M. Kasha, "Characterization of electronic transitions in complex molecules," Discussions of the Faraday Society **9**, 14–19 (1950).

[116] H. Nishikiori, N. Tanaka, K. Takagi, and T. Fujii, "Solvent effect on fluorescence spectra of a spirooxazine," Research on Chemical Intermediates **29**(5), 485–493 (2003).

[117] J. A. Gally and G. M. Edelman, "The effect of temperature on the fluorescence of some aromatic amino acids and proteins," Biochimica et Biophysica Acta **60**(3), 499–509 (1962).

[118] W. R. Ware and B. A. Baldwin, "Effect of Temperature on Fluorescence Quantum Yields in Solution," The Journal of Chemical Physics **43**(4), 1194–1197 (1965).

[119] G. Guilbault, *Practical Fluorescence*, p. 28, 2nd ed. (Marcel Dekker Inc, New York, 1990).

[120] B. Clarke, T. Frost, and M. Russel, "UV spectroscopy techniques instrumentation data handling," (1993).

[121] "Fluorometric Facts: A Practical Guide to Flow Measurement," (1990).

BLANK PAGE

A

Fluorescence: Theoretical Considerations and Instrumentation

In this section, an overview of basic theory of fluorescence and the main fluorescence measuring devices (instrumentation) used for the purpose of the research study will be discussed. In addition, various factors which effect fluorescence measurement and some considerations and spectral corrections required to obtain accurate data are also discussed in this section.

A.1 Fluorescence

Fluorescence is the emission of light from a compound (fluorophore) when excited by light. Fluorescence emission takes place in about 10^{-8} second [29]. The phenomenon of fluorescence has been known for hundred of years. In the year 1852, that George Gabriel Stokes first explained this phenomenon [108]. The name fluorescence was derived from the mineral fluorite (calcium difluoride). The fluorescence of some minerals under UV excitation is shown in Figure A.1 [109]

Fluorescence has been studied by Physicists and Photochemists for over a century. However, in recent years there is a remarkable growth in the use of fluores-

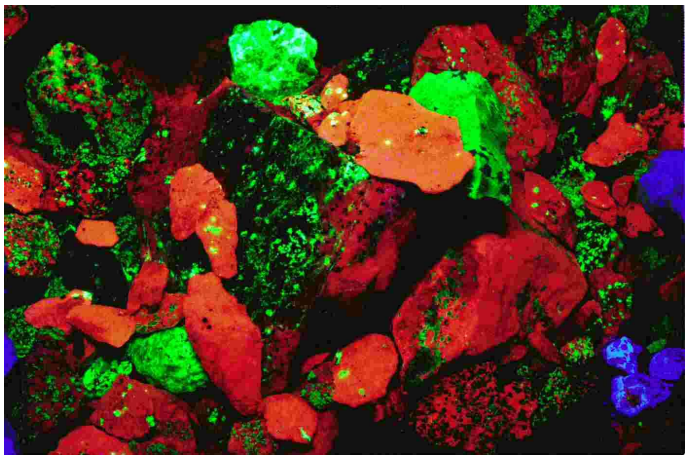

Figure A.1: Fluorescence of minerals under UV light [109]

cence in many fields including biological sciences. Fluorescence spectroscopy and time-resolved fluorescence are considered to be primary research tools in biochemistry and biophysics [29]. Fluorescence is a highly sensitive analytical tool which can be used to measure fluorophore concentrations as low as 10^{-8} to 10^{-10} g/ml (0.01 to 0.0001 μg/ml) whereas few substances can be estimated colorimetrically below 10^{-7}g/ml (0-1 μg/ml) [110]

The first commercial spectrofluorimeter (Aminco-Bowman spectrophotofluorometer) which was used to measure fluorescence, was designed by Dr. R. L. Bowman in the year 1955. Due to the significance and advanced capability of fluorescence measurements, fluorescence is currently a dominant methodology which is extensively used in various technologies, including genomics, proteomics, bioengineering etc.

The wide applications of fluorescence phenomenon range from popular fluorescence tube lighting to DNA detection.

A.2 The Phenomenon of Fluorescence

Certain compounds when illuminated with light absorb specific wavelengths of light and the wavelengths absorbed are characteristic of the particular compound being tested. The extent to which the light of these wavelengths is absorbed constitutes the absorption spectrum of the compound. As a result of the absorption of light some of the molecules of the compound become excited because certain electrons in the molecule are raised to a higher energy level.

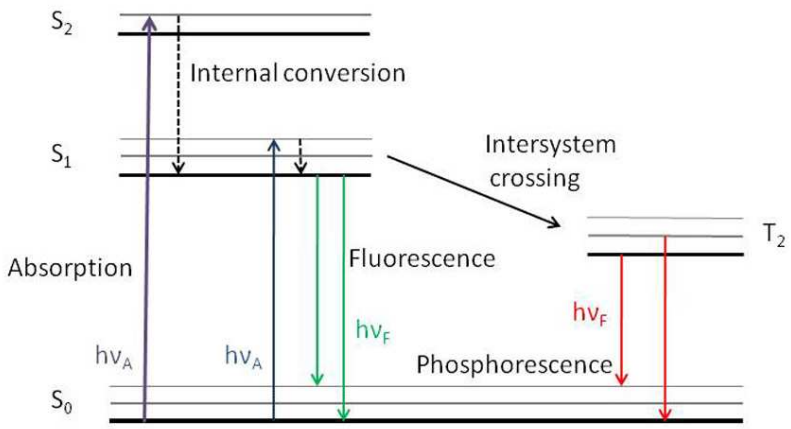

Figure A.2: Jablonski diagram [29]

The energy levels of a molecule are represented in Figure A.2 by horizontal lines and the directions of the energy transitions by vertical lines. On absorption of light, the molecule is raised from the ground state S_0 to the excited state S_1 or S_2 as indicated by the vertical arrow A. Sometimes the molecules in the higher vibrational states rapidly relax to lowest vibrational state (S_1) without emission. This process

is known as internal conversion [29].

On the other hand, the molecule may return to the ground state, emitting some of its absorbed energy as light, referred to as fluorescence, as indicated by the vertical green lines. An electronic transition due to light absorption is almost instantaneous (10^{-15} second), whereas the lifetime of the excited state is about 10^{-8} second, and therefore, the whole process of light absorption and fluorescence emission takes place in about 10^{-8} second [29]. It is to be noted that, some of the absorbed energy is lost partly by collisions with other molecules and partly by other means, so that less energy is emitted as fluorescence than it is delivered via excitation.

Molecules in the S1 state can also undergo intersystem crossing to the first triplet state T1. The phenomenon of phosphorescence occurs when there is emission from the T1 state. The phosphorescence emission rates tend to be relatively low as the process requires a reversal of the spin of electron to form the ground state, which is generally forbidden. Compared to fluorescence, phosphorescence phenomenon takes longer time [29].

A.2.1 Fluorescent compounds

Fluorescence is typically observed in aromatic molecules [29]. Quinine is a typical example of a fluorescencent compound. As shown in the Figure A.3a, a faint blue colour is generally observed for tonic water in light (450 nm). This is due to the presence of quinine. Quinine, discovered by Sir John Frederick William Herschel in 1845 is also the first known fluorophore. The structure of quinine is shown in Figure A.3b.

The green or red-orange glow sometimes seen in antifreeze is due to the presence of fluorescein or rhodamine. Fluorescent polynuclear aromatic hydrocarbons, such as anthracene and perylene are used for environmental monitoring of oil pollution.

(a) a

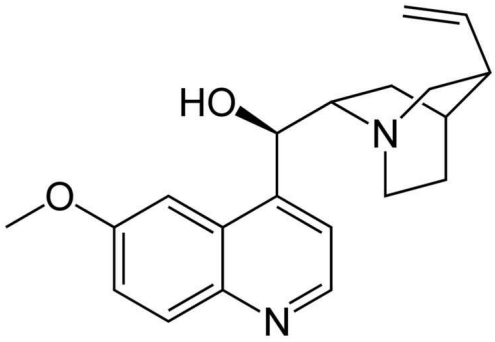

(b) b

Figure A.3: (a) Fluorescence of tonic water [111]; (b) Structure of quinine

Green fluorescent protein, GFP (Figure A.4), is a spontaneously fluorescent protein isolated from coelenterates, such as the Pacific jellyfish, *Aequoria victoria* [112]. The enormous flexibility of GFP, as a noninvasive marker in living cells has given rise to numerous other applications such as a cell lineage tracer, reporter of gene expression and as a potential measure of protein-protein interactions. Some of the intrinsically fluorescent compounds in physiological fluids are mentioned in Chapter 2.

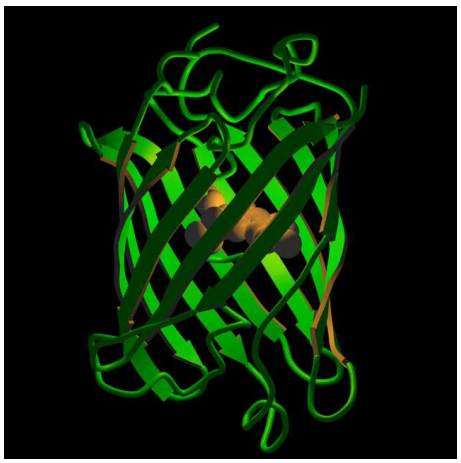

Figure A.4: Structure of GFP [113]

A.2.2 Fluorescence emission characteristics

The phenomenon of fluorescence displays a number of general characteristics. Some of the significant ones are described in this section.

Stokes shift

In the year 1852, Sir G.G. Stokes stated that fluorescence emission occurs at longer emission wavelengths or at lower energies [108]. In other words, the difference between excitation and emission spectra is known as Stokes shift Figure A.5

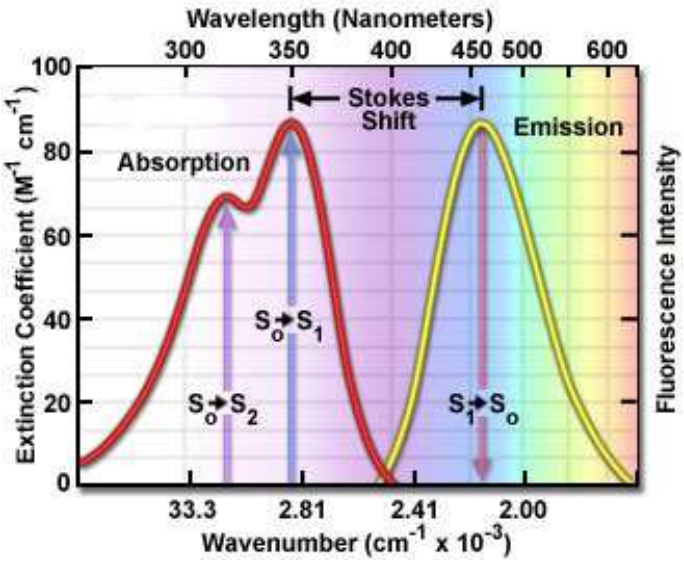

Figure A.5: Illustration of Stokes shift [114]

Emission spectra

Another general property of fluorescence is that the same fluorescence emission spectrum is generally observed irrespective of the excitation wavelength. This property of fluorescence was explained by Michael Kasha in the year 1950 (Kasha's rule [115]). In addition, Vavilov reported in 1926 that quantum yields were generally independent of excitation wavelength.

Upon excitation into higher electronic and vibrational levels, the excess energy is quickly dissipated, leaving the fluorophore in the lowest vibrational level of S_1. This relaxation occurs in about 10^{-12} second, and is presumably a result of a strong overlap among numerous states of nearly equal energy. Because of this rapid relaxation, emission spectra are usually independent of the excitation wavelength.

For some compounds the excitation and emission spectra look symmetrical. This is because they follow the mirror image rule. The reason behind the symmetric nature of these spectra is due to the similar transitions being involved in both absorption and emission. However, there are exceptional cases like quinine where the excitation spectra and emission spectra look different (Figure A.5).

A.2.3 Fluorescence lifetime and quantum yield

Fluorescence lifetime is the average time the molecules spend in the excited state before returning to its ground state.

$$\tau = 1/(\Gamma + K_{nr}) \tag{A.1}$$

where, Γ=emissive rate of fluorophores (rate constant).

K_{nr}= rate of non radiative decay.

The lifetime of the fluorophore in the absence of nonradiative processes is called the intrinsic or natural lifetime, and is given by

$$\tau_n = 1/\Gamma \tag{A.2}$$

Fluorescence lifetimes for dipole allowed transitions are usually $\sim$10 ns. The decay of fluorescence intensity as a function of time can be represented as an exponential function.

$$F(t) = F_0 e(-t)/\tau \tag{A.3}$$

where, F(t)= fluorescence intensity at time t.

F_o= initial fluorescence intensity

$^{\tau}$= fluorescence lifetime.

The quantum yield Q, is a measure of the emission efficiency of the fluorophore and is expressed as the ratio of number of emitted photons to absorbed photons by the fluorophore. The rate constants Γ and K_{nr} both depopulate the excited state. The fraction of fluorophores that decay through emission, and hence the quantum yield, is given by

$$Q = \Gamma/(\Gamma + K_{nr}) \tag{A.4}$$

The relation between fluorescence lifetime and quantum yield can be expressed as

$$\tau_n = \Gamma/Q \tag{A.5}$$

A.3 Factors affecting fluorescence intensity

There are various factors which can affect the fluorescence intensity. The most important of these are:

1. **Solvent** Solvents may have large and unpredictable effects on both the intensity as well as the wavelength of fluorescence. Fluorescence intensity variations can occur as a result of alterations in the relative energy of the electronic states or as a result of quenching phenomena. The wavelength shift can occur via Lippert mechanism which predicts the longer wavelength shift seen

in polar solvents. Figure A.6 shows a typical example of solvent effect for spironaphthoxazine(SNO)in protic solvents. The emission spectra are seen to shift dramatically to longer wavelengths as the solvent polarity is increased (ethylacetate) [116].

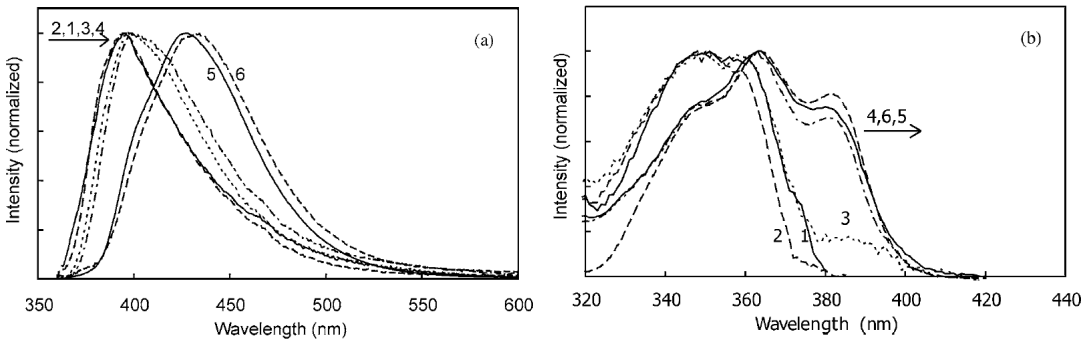

(a) a (b) b

Figure A.6: Fluorescence (a) and excitation (b) spectra of spironaphthoxazine (SNO) in protic solvents: (1) benzene, (2) diethyl ether, (3) ethylacetate, (4) methylacetate (5) acetone and (6) acetonitrile. Excitation wavelength for the fluorescence spectra and emission wavelength for the excitation spectra are 350 and 450 nm, respectively.

2. **pH**

   A large number of fluorescent compounds contain ionizable groups. It is known that ionic forms of compounds often have different fluorescence characteristics from the unionised forms. Thus there is considerable pH effect on the fluorescence.

3. **Raman scattering**

   Raman scattering is a common phenomenon observed in a gas, liquid or solid, due to the inelastic scattering of photon. Raman scattering can occur with a change in vibrational, rotational or electronic energy of a molecule.

   However, Raman spectra, unlike fluorescence spectra, have no absolute excitation and emission wavelengths and can arise from any wavelength of incident

light. If Raman line of the solvent happens to coincide with the fluorescence maximum of the compound being estimated, it could interfere considerably with the fluorescence measurement. However, Raman scattering is usually weak and may interfere only at high dilutions of the fluorescent substance.

4. **Quenching**

When one compound reduces or abolish the fluorescence of another compound, it is said to quench the fluorescence. Some of the major quenching mechanisms are listed below:

(a) Inner filter effect

The recorded fluorescence intensity may not be proportional to the fluorophore concentration due to a well known phenomenon known as the inner filter effect. This can be due to high absorption of excitation light by the sample (primary inner filter effect) and by reabsorption of emitted light (secondary inner filter effect) [27]. These effects may decrease the intensity of the excitation at the point of observation, or decrease the observed fluorescence by absorption of the fluorescence. The relative importance of each process depends upon the optical densities of the sample at the excitation and emission wavelengths. The typical example of concentration quenching is illustrated in Figure A.7. In addition, there is higher probability of aggregate formation in samples of higher concentration which can also affect fluorescence intensity.

(b) **Quenching by energy degradation**

The energy degradation of the excited state by the quencher can occur in several ways, for example, by conversion of the excited molecule into the triplet state, by electron transfer, or by energy transfer.

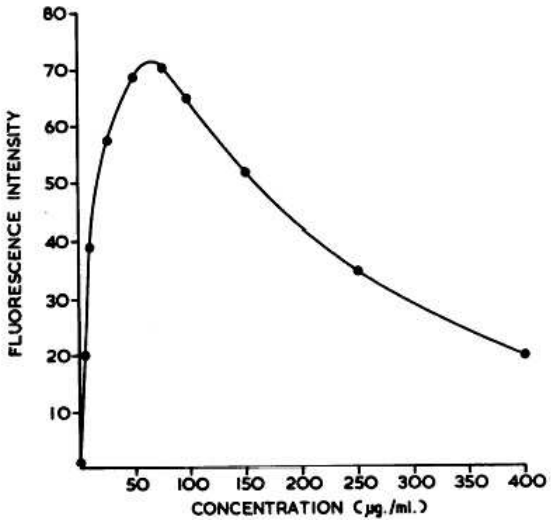

Figure A.7: Concentration quenching plot of phenol in water [110]

(c) Quenching by chemical change

If a fluorescent compound undergoes a chemical change as a result of the presence of a second compound it could be converted into a non-fluorescent product. Note even pH can change the chemical nature of a fluorescent compound to be non-fluorescent compund.

5. **Temperature**

The temperature dependence of the fluorescence quantum yield and lifetime has been studied extensively in the past. A typical example of the effect of temperature on two fluorophores is shown in Figure A.8. Some studies have mentioned that radiative transitions has slight dependency with temperature [118]. In addition, there have also been studies which suggest that higher temperature can result in increased collisional interaction and thus increase the chance of quenching [119].

6. **Viscosity**

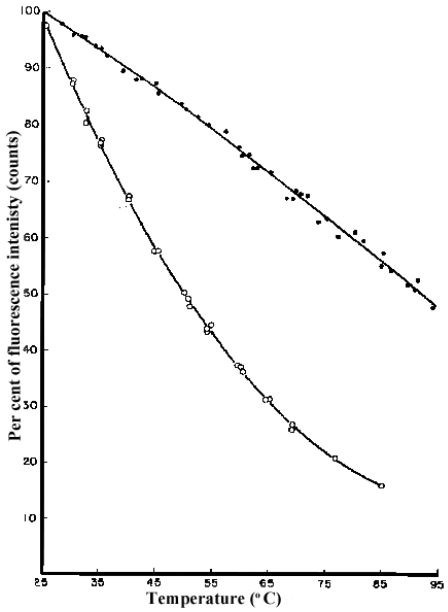

Figure A.8: The intensity of fluorescence at the wavelength of maximal emission of water solutions of tryptophan (4 μg/ml) and tyrosine (20 μg/ml), as a function of temperature. Intensity values are expressed as percentages, the value at 2 being taken as 100 %. The wavelength of the exciting light was 280 mμ. Light emitted at 350 mμ was measured for the tryptophan and at 303 mμ for the tyrosine solution($\circ$) tryptophan; ($\bullet$) tryosine [117].

Increase in viscosity is known to increase fluorescence due to reduced collision between molecules [120].

7. **Phto-decomposition**

Higher intensity of excitation light or certain wavelength (UV) can break down fluorescence molecules. Fluorescence readings decrease as the molecules are destroyed. The rate of destruction varies depending upon environmental factors, including temperature. Fluorescein, for example, is destroyed rapidly in sunlight. Rhodamine WT, however, is adequately stable for field studies [121]. It should be noted that photo-decomposition does not always lead to loss of fluorescence and in some cases it leads to the enhancement of fluorescence.

A.4 Instruments for detecting and measuring fluorescence

A.4.1 Spectrofluorometry

In my PhD study, the urine fluorescence spectra were mainly analysed using a spectrofluorometer (Figure A.9). Spectrofluorometers are generally designed to detect and quantify fluorophores. A schematic diagram of the spectrofluorometer is illustrated in Figure A.10. It consists of six main parts namely the light source, excitation monochromator, sample chamber, emission monochromator, data acquisition and optics controller and an output data display. Basically, the light from an excitation source passes through a monochromator, and strikes the sample. The fluorescent light emitted from the molecules passes through a emission monochromator and reaches a detector, which is usually placed at 90 degree to the incident light beam to minimize the risk of transmitted or reflected incident light reaching the detector. The general characteristics of selected components are described below for better understanding the capabilities and limitations of spectroflurometers.

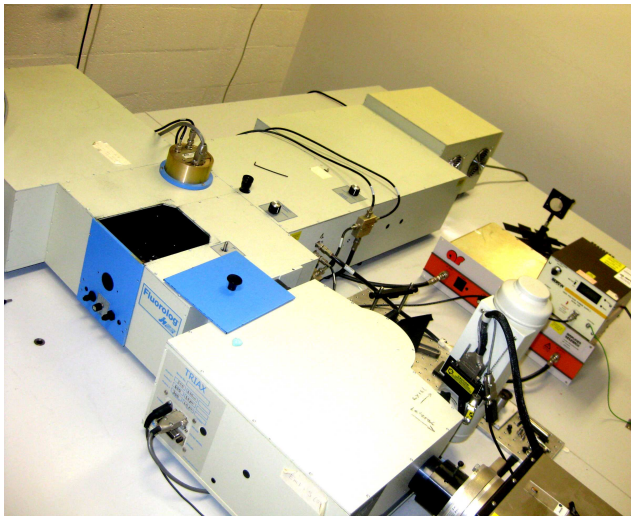

Figure A.9: Spectroflurometer (Flurolog Tau system)

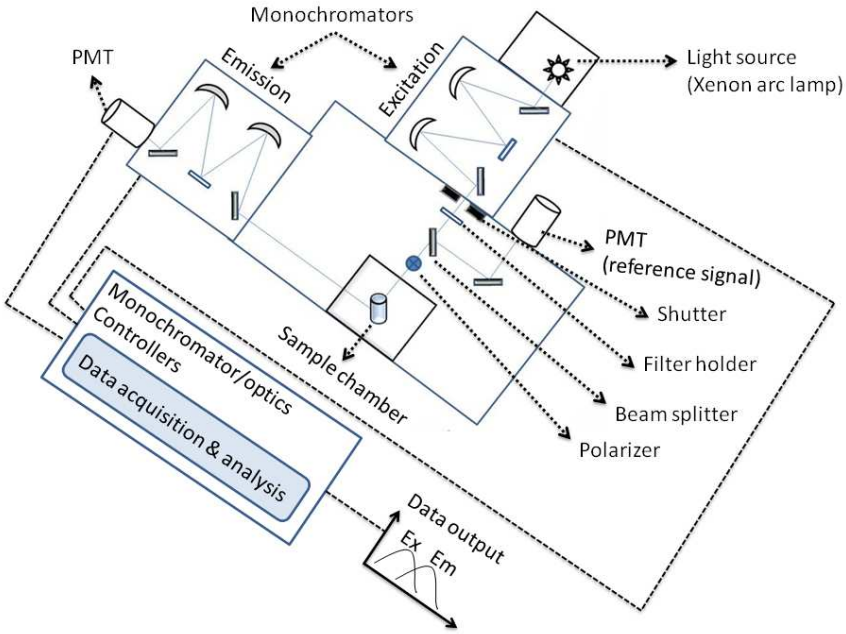

Figure A.10: Schematic diagram of spectroflurometer

Light source

There are different types of light sources used for spectroflurometer, these include high pressure and low pressure mercury lamps, mercury-xenon arc lamps, quartz-tungsten halogen lamps, and solid-state light sources such as Light-Emitting Diodes (LEDs) and laser diodes or lasers. However, for the spectrofluromter xenon arc lamp was chosen as excitation source (Figure A.10). This is because, xenon arc lamps are considered the most versatile light sources emitting light over a broad range, from UV (250 nm) to near infrared (700 nm), with high intensity. Xenon arc lamps predominantly emit a continuum of light over a broad band as a result of the recombination of electrons with ionized xenon atoms. The spectrum of a xenon lamp is however not uniform, as illustrated in (Figure A.11). Such wavelength-dependent output of the lamp will cause distortion of the excitation spectra of samples that absorb light in the visible and ultraviolet region. The excitation spectrum hence

needs proper correction, which is performed by dividing the intensity of the sample by reference intensity. The reference intensity, proportional to the lamp intensity, is measured with a quantum counter. In the Fluorolog-Tau-3 system, there is a reference detector (R), which measures the lamp signal directly and in order to obtain correction of the excitation scan, the emission detector signal is simply ratioed to the reference signal.

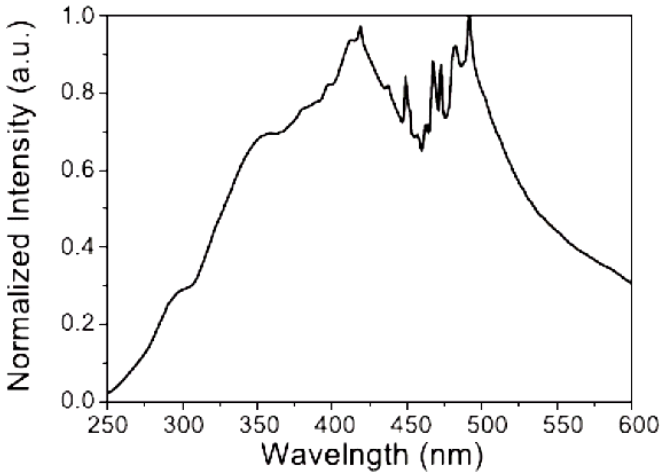

Figure A.11: Spectra of xenon lamp

Monochromators

Monochromators are used to disperse light into various colours or wavelenths. Light dispersing element may be any or combinations of the following: filters, gratings, prisms, and slits. Diffraction gratings are more commonly used in most spectrofluorometers. The dispersion by a typical grating is shown in Figure A.12. The gratings consist of a series of parallel grooves engraved on a reflecting surface. Grooves of 1200 lines per mm are considered to provide good performance (higher dispersion implying larger separation of the wavelengths) in the ultraviolet and visible wavelength region. When a beam of light hits the grating surface, it diffracts the light.

The wavelength at which the light is diffracted, λ, is dependent upon the angle of incidence, Θ, and the distance separating the grooves, d.

$$n\lambda = 2dsin\Theta \tag{A.6}$$

Here, n represents the order of the spectrum produced. A diffraction grating produces a number of overlapping spectra at angles determined by the value of n. The spectrum thus produced is termed first order, second order or third order depending on whether the value of n is 1, 2 or 3 respectively. Hence, at any given angle, a grating reflects radiation of λ and also $\lambda/2$, $\lambda/3$ and so on. Out of these a single order only, typically the first order is selected. The higher orders and the unwanted radiation, which otherwise appears as stray light, is usually removed with 'order-sorting filters' that are inserted into the beam at appropriate wavelengths to absorb light from higher-order reflections.

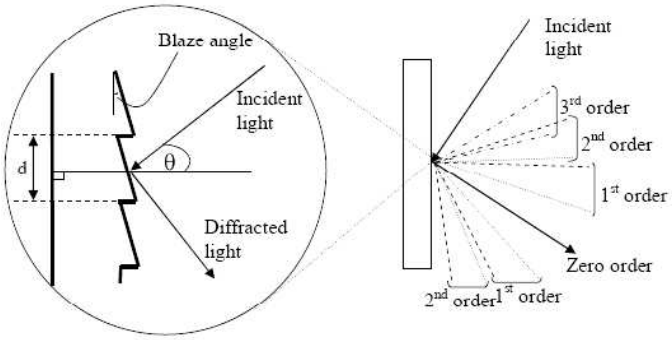

Figure A.12: Dispersion of gratings

A monochromator is best described by spectral dispersion, stray light levels and efficiency. The dispersion is normally given in nanometers per millimeter where the slit width, generally variable, is given in millimeters. Better quality monochromators are characterized by low stray light. Higher efficiency is desired in monochromators for the possibility of detecting low levels of light. Since, the light intensity through a

monochromator is approximately proportional to square of the slit width; larger slit widths provide increased signal levels. Smaller slit widths however trade intensity for better spectral resolution. Besides the slit width, the properties of the grating, particularly the number of grooves per mm, sets the ultimate limit for the resolution. The resolving power R, of the grating is defined in its simplest form as:

$$R = \lambda/\Delta\lambda = nN \tag{A.7}$$

where $\Delta\lambda$ is the separation between two spectral peaks that can just barely be detected as separate with the instrument, n is the diffraction order and N is the total number of grooves on the entire grating surface. As an example, a 110 mm wide grating with 1800 grooves/mm, used in first order diffraction, has a theoretical resolving power of 198,000 that implies a wavelength resolution of 0.003 nm at 500 nm wavelength.

Photomultiplier tubes (PMTs)

Photomultiplier tubes (PMTs) are used to detect the fluorescence signals at a wide wavelength range (200 nm to 900 nm) with high sensitivity. PMTs have become a popular choice as detectors for almost all the modern fluorometers. A PMT is capable of detecting individual photons. Each photoelectron results in a burst of around million electrons, which can be detected as individual pulses. Hence, PMTs can be operated in photon counting mode or as a current source where the current is proportional to the light intensity. In the photon counting mode, the individual anode pulses due to each photon are detected and counted. In the current source (analog) mode, the individual pulses are averaged giving average anode current. The stability of a PMT in photon counting mode can be increased by operating the PMT at a high constant voltage. At such high PMT voltage, the photon counting

efficiency is significantly unchanged even with small drifts in the voltage. Hence, photon counting detection is normally used when signal levels are low and when it is necessary to average repetitive wavelengths scans to increase the signal-to-noise ratio. During the experiments, the PMT is used in photon counting mode with high voltage of 950V.

Performance checks and correction files

One needs to be aware of the instrumentation limitations, pay substantial attention to experimental details and control the various factors that could affect reliable spectral data. A check of the steady-state system calibration before each day of use was carried out. Scans of the xenon-lamp output and the Raman scatter band of water are considered sufficient to verify system calibration and throughput. These scans were conducted and the system calibration adjusted where needed during the experiments. The Fluorolog-Tau-3 is an auto calibrating spectrofluorometer. This means that the system initializes its monochromators drives, locates the zero of each drive, and assigns a wavelength value to the low limit of each drive from a calibration file. It is important to recognize that fluorescence intensities are proportional to the concentration over only a limited range of optical densities of the sample, which is usually affected by the fluorophore content. Attenuation of fluorescence starts occurring at higher optical densities in the sample typically > 0.05, a phenomenon known as the inner filter effect. However, this problem did not exist due to the fact that the solid samples with monolayer of fluorophores usually have very low optical densities. Another artifact to note during fluorescence measurements is the effect due to Raman scattering. When a beam of light is incident upon a sample, photons are absorbed by the material and scattered. Raman scattering is the radiation caused by molecular vibration and rotation, which always occurs at

a constant wavenumber difference from the incident light. The spectral width of the Raman peak is determined by the resolution of the monochromators. Raman peak is significant when analyzing samples with low fluorescence and is relatively less pronounced for highly fluorescence samples.

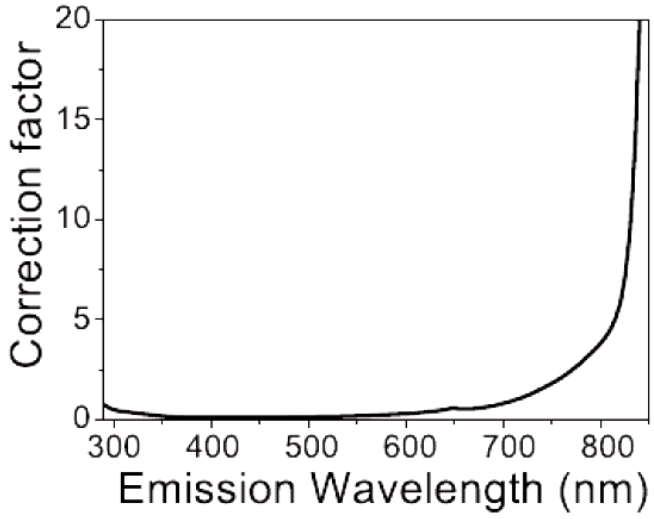

Figure A.13: Emission correction file for the Fluorolog Tau 3 system.

The spectral output of a broadband light source (xenon lamp, Figure A.11) is normally non-uniform and the monochromators and detectors have wavelength dependent efficiency. The polarization and anisotropy of the emitted light can also affect the measured fluorescence intensities. Hence, proper correction for both the excitation and emission spectra are essential. The excitation correction was conducted by dividing the excitation spectra with reference signal, which is the lamp signal, as discussed earlier. For correction of emission spectra, a correction file was generated through an experiment using a standard lamp. This correction file was stored in the computer and where the light source and optics of the system remained unchanged, the correction file was used to generate standard emission spectra. Figure A.13 shows a correction file for the Fluorolog system. This file was included

whilst undertaking experiments as correction file for the emission spectra. This corrected the spectra automatically and produced the final result. Where the data was taken without including the correction file, the corrected emission spectra was calculated as per the following equation:

$$Corrected\ spectra = Measured\ emission\ spectra * Emission\ correction\ spectra$$

A.4.2 Confocal microscopy

In order to study autofluorescence of stem cells, laser scanning confocal microscopy has been utilised. This is because confocal microscopy provides quantitative, spatial and temporal visualization of fluorescence in the cell samples.

In confocal microscopy, a single point of the specimen is illuminated with a focused beam and the pin hole allows it to create optical sections that are approximately 0.5 μ thick as compared to 2-3 μ in conventional microscopy. The key to the confocal approach is the use of spatial filtering to eliminate out-of-focus light in specimens that are thicker than the plane of focus. This is illustrated by the schematic diagram Figure A.14.

Confocal microscopy has several advantages over conventional optical microscopy, including controllable depth of field, the elimination of image degrading out-of-focus information, and the ability to collect serial optical sections from thick specimens. There has been a tremendous explosion in the popularity of confocal microscopy in recent years, due in part to the relative ease with which extremely high-quality images can be obtained from specimens prepared for conventional optical microscopy, and in its great number of applications in many areas of current research interest.

Figure A.15 shows the laser scanning confocal microscope from Leica Microsystem with spectral and fluorescence life time imaging (FLIM) capabilities, which was used for experiments. In the following sections some of the essential components of

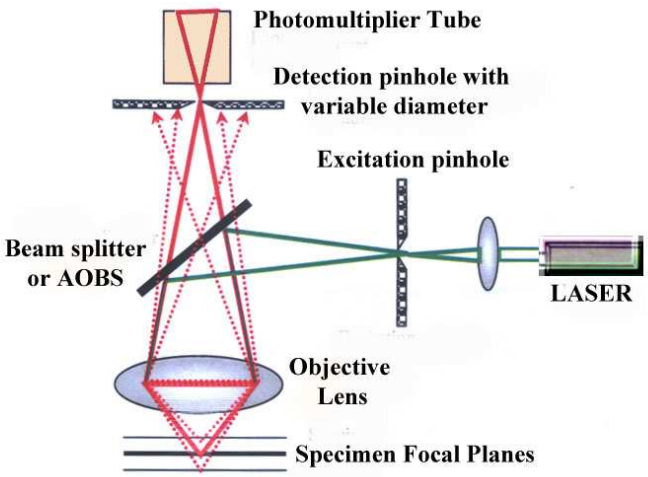

Figure A.14: Schematic of confocal microscopy illustrating confocal light pathways.

a microscopy will be described.

Excitation light sources

Tungsten-halogen and short arc lamps have been commonly used as excitation light sources in the traditional wide-field microscopy. Presently, with the advancement in laser technology and due to the advent of the confocal microscopy, lasers are commonly used as light source in microscopy. Lasers commonly employed in laser scanning confocal microscopy are high-intensity monochormatic light sources which can be focused to a very small spot with a high level of brightness. Lasers can be used in continuous wave (CW) or pulsed mode of operation.

Pulsed lasers are finding greater applications in fluorescence microscopy, especially in two-photon excitation microscopy and FLIM. The Leica confocal microscope used has a number of lasers as excitation light source. The various laser excitation

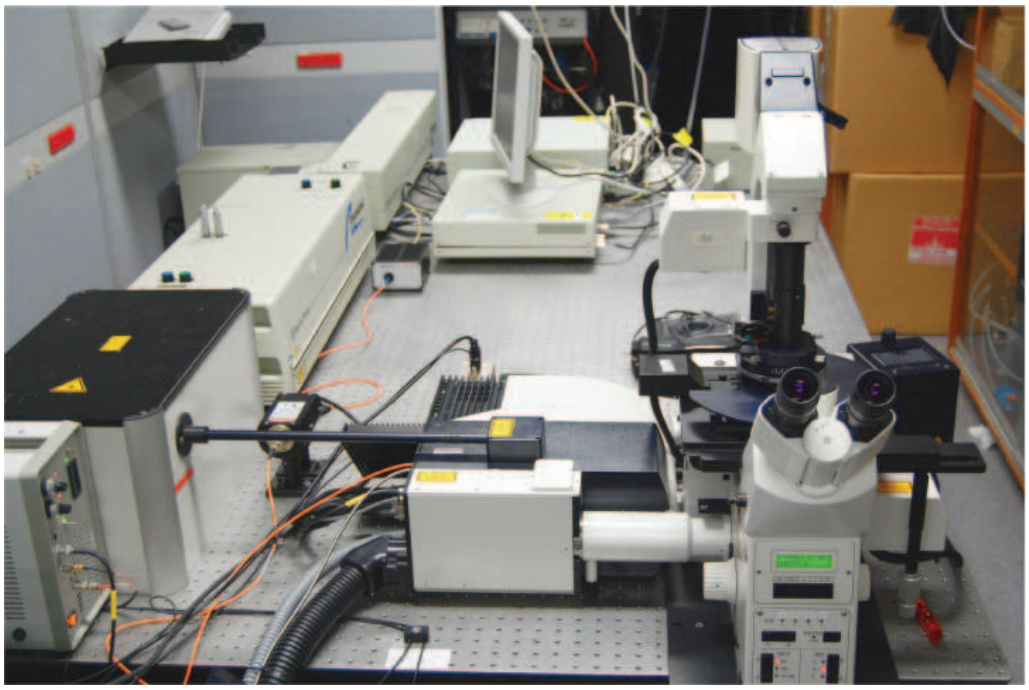

Figure A.15: Leica TCS SP2 confocal system.

sources were 405 nm (HeNe blue pulse laser diode), 488 and 514 nm (Ar ion laser). The two main laser excitation wavelengths used for analyzing the autofluorescence of stem cells were 405 nm and 488 nm.

Wavelength selection devices

There are various wavelength selection devices used in microscopy. These include, monochromators, tunable lasers, various band -pass optical filters, dichroic mirrors, acousto optical tunable filters (AOTF), liquid crystal tunable filters (LCTF) and acousto optic beam splitters (AOBS). Filters are used to select a certain part of the electromagnetic spectrum for transmission, while preventing the rest of the electromagnetic spectrum from passing through the filter.

Instead of using a conventional beam splitter, the Leica TCS SP2 system uses the acoustic optic beam splitter (Figure A.16), for various wavelength (exciting)

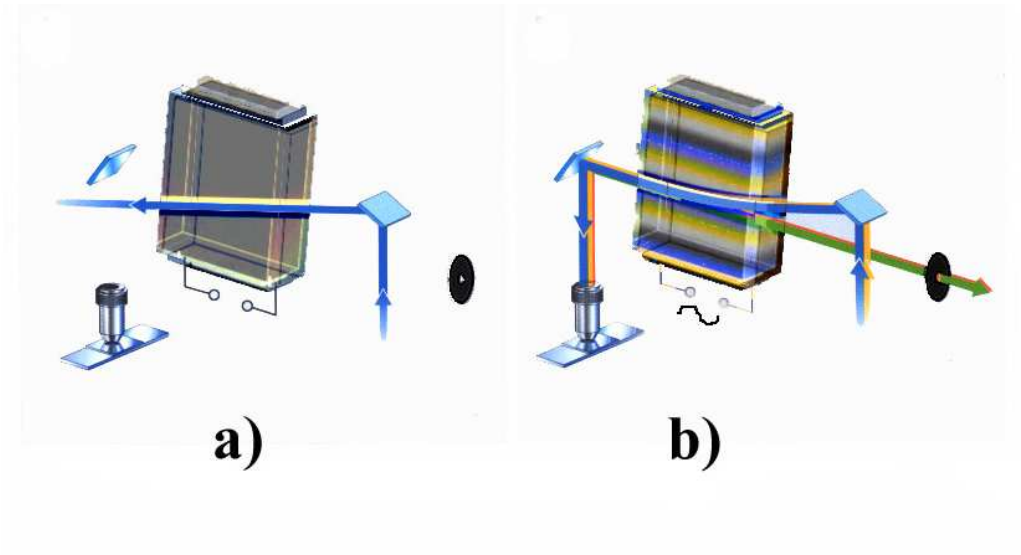

Figure A.16: Illustration of acoustic optic beam splitter working principle. (a) without ultrasonic field; (b) with ultrasonic field

selections. The AOBS is a transparent optical crystal to which an ultrasonic field is applied (Figure A.16 a). The light which penetrates the optical crystal is deflected depending on its wavelength and the wavelength of the ultrasonic field (Figure A.16 b). When compared to conventional beam splitter, AOBS system provides marked increase of signal yield through improved adaptability, selectivity and higher transparency. In addition, other advantages of AOBS are rapid wavelength switching, recording of spectral scans to determine emission maxima without superimposed filter characteristics.

Objective lenses

A number of objectives with varying magnification are used in fluorescence microscopy. These objective lenses have different performance depending on whether they are used as air, water, oil or glycerine immersion. In microscopy, the numerical

aperture of an optical system such as an objective lens is defined by:

$$NA = nsin\theta \tag{A.8}$$

where n is the index of refraction of the medium in which the lens is working (1.0 for air, 1.33 for pure water, and up to 1.56 for oils), and θ is the half angle of the maximum cone of light that can enter or exit the lens. NA is important because it indicates the resolving power of a lens. The size of the finest detail that can be resolved is propotional to λ/NA, where λ is the wavelength of light. The lens with high numerical aperture will collect more light and generally provide a brighter image. However, with large numerical aperture the field of view will be narrower. In this study mainly 100x and 40x oil immersion objectives have been utilized. For measuring autofluorescence of stem cells (Chapter 4), 40x objective has been mostly utilized to get more number of samples in a field of view so as to get more statistically reliable data.

Detectors

Light detectors in fluorescence microscopy allow the real time visualization and recording of low levels of fluorescence emitted by specimen. Various detectors used in fluorescence microscopy range from photomultiplier tubes (PMT), which are used for quantitative measurements, to imaging detectors like CCDs, which allow rapid acquisition of two-dimensional images of fluorescence. Since the efficiency of detection of emission is dependent on various factors such as efficiency of the optics associated with light collection and detection path, efficiency of the objective, and incident laser power , the final fluorescence signal reaching the detectors may have low intensity. Additionally, in confocal microscopy, fluorescence emission is directed through a pinhole aperture positioned near the image plane, thus reducing the amount of light available for image formation. As a result, the exceedingly low light levels most

often encountered in confocal microscopy require the use of highly sensitive photon detectors, which have no spatial discrimination, but are able to respond very quickly with a high level of sensitivity to a continuous flux of varying light intensity. Photomultipliers which contain a photosensitive surface that captures incident photons and produce a stream of photoelectrons to generate and amplified electric charge, are the popular detector choice in many commercial confocal microscopes.

A.5 Summary

In this section, some basic information about fluorescence and its significant role in various applications are discussed. This was done because in the present study, fluorescence principles have been utilized to diagnose samples such as urine and stem cells.

In addition, various factors which effect fluorescence measurements, some fluorescence theoretical considerations and various instruments for measuring fluorescence in this study are also described.